INVESTIGATION OF PARAMETERS OF LASER SHOCK PEENING ON TURBINE BLADE PROFILE BY DED PROCESS

MTech Thesis

By

RUSHIKESH ANIL MALI
Roll No.: 2302103020

DEPARTMENT OF MECHANICAL ENGINEERING
INDIAN INSTITUTE OF TECHNOLOGY INDORE
May 2025

INVESTIGATION OF PARAMETRS OF LASER SHOCK PEENING ON TURBINE BLADE PROFILE BY DED PROCESS

A THESIS

Submitted in partial fulfillment of the
requirements for the award of the degree
of
Master of Technology

by
RUSHIKESH ANIL MALI
Roll No.: 2302103020

DEPARTMENT OF MECHANICAL ENGINEERING
INDIAN INSTITUTE OF TECHNOLOGY INDORE
May 2025

INDIAN INSTITUTE OF TECHNOLOGY INDORE

CANDIDATE'S DECLARATION

I hereby certify that the work which is being presented in the thesis entitled "**INVESTIGATION OF PARAMETRS OF LASER SHOCK PEENING ON TURBINE BLADE PROFILE BY DED PROCESS"** in the partial fulfillment of the requirements for the award of the degree of **M.tech** and submitted in the **DEPARTMENT OF Mechanical Engineering, Indian Institute of Technology Indore**, is an authentic record of my own work carried out during the time period of July 2023 to May 2025 under the supervision of Dr. Girish Verma , Assistant Professor, Department of Mechanical Engineering, Indian Institute of Technology, Indore and Dr. C. P. Paul , Head of EDMD , Raja Ramanna Centre for Advanced Technology, Indore.

The matter presented in this thesis has not been submitted by me for the award of any other degree of this or any other institute.

Ramali 27-05-2025

Signature of the student
(Rushikesh Anil Mali)

This is to certify that the above statement made by the candidate is correct to the best of my/our knowledge.

Girish 28/05/25

Signature of the Supervisor of
MTech. thesis #1
(Dr. Girish Verma)

28/05/2025

Signature of the Supervisor of
MTech. thesis #2
(Dr. C. P. Paul)

Rushikesh Anil Mali has successfully given his MTech. Oral Examination held on **9 May 2025.**

Girish 28/05/25

Signature of the Supervisor of M.Tech.
Thesis #1 (with date)

28/05/2025

Signature of the Supervisor of
M.Tech Thesis #2(with date)

Convener, DPGC
Date:29-5-25

ACKNOWLEDGEMENTS

First of all, I want to convey my sincere gratitude to my supervisors, Dr. Girish Verma, Assistant Professor Department of Mechanical Engineering, Indian Institute of Technology, Indore, Dr. I.A Palani, Professor, Department of Mechanical Engineering, Indian Institute of Technology, Indore and Dr. C. P. Paul, Head of EDMS, Raja Ramanna Centre for Advanced Technology, Indore. for providing me with the opportunity to work on this M. Tech Thesis work under their esteemed supervision.

I sincerely thank our Director Sir, Prof. Suhas S. Joshi for his encouragement during M. Tech. classes and thesis work. I also wholeheartedly thank our HOD Sir and coarse co-ordinator of M. Tech program for their valuable supports in every stage of my thesis work. I also thank all the faculty members, specially DPGC convener and PSPC members for their fruitful technical interactions during the progress of my M. Tech. thesis work.

I am deeply indebted to all the research scholars of our laboratory specially Dr. Anshu Sahu, Dr. Vipin Goyal and Mr. Rajendra Goud whose guidance and mentorship have been pivotal in my learning journey. Their insightful feedback and unwavering support have been instrumental in helping me throughout this M. Tech Thesis work. Further, I would like to extend my gratitude to other group members and staff members of other laboratories for the supportive environment and valuable suggestions.

I would like to express my heartfelt gratitude to my friends, Himanshu Sharma and Abneesh Kumar, Kaustubh Sarode for their unwavering support and insightful discussions throughout this journey. Finally, I am eternally grateful to my family for their continuous encouragement, and moral support.

DEDICATED TO MY BELOVED PARENTS

Abstract

Ti-6Al-4V is a widely used titanium alloy known for its exceptional strength-to-weight ratio, excellent corrosion resistance, good biocompatibility, and superior high-temperature performance. These attributes make it a preferred material in diverse industries, including aerospace, biomedical, automotive, and marine sectors. With increasing demand for complex and high-performance components, additive manufacturing (AM) techniques such as Direct Energy Deposition (DED) have gained significant attention. DED is an advanced AM process that uses a high-energy laser beam and a coaxial powder delivery system to fabricate components layer by layer. This process offers high material utilization and is well-suited for fabricating large, complex geometries or repairing existing components. However, the quality and mechanical performance of DED-fabricated parts are highly sensitive to process parameters such as laser power, scanning speed, and powder feed rate. Improper selection can lead to high residual stresses, poor surface finish, and sub-optimal mechanical properties due to rapid thermal cycling. In this study, an effort has been made to optimize key DED process parameters for Ti-6Al-4V. A statistical approach based on First Variable at time was employed to investigate the effect of these parameters. Multi-objective optimization was done using Desirability Function Analysis (DFA) to determine the optimal combination of input parameters. Under optimized conditions, Ti-6Al-4V wall structures were fabricated and tested for tensile strength and microhardness. To further enhance performance, Laser Shock Peening (LSP) was applied as a post-processing technique. LSP is a high-energy surface treatment process that imparts beneficial compressive residual stresses and improves fatigue life. The influence of LSP parameters such as laser pulse energy, scanning speed, and overlap ratio was studied with respect to surface roughness, microhardness, and residual stress distribution. Results indicated that LSP significantly improved the surface and mechanical properties of the DED-fabricated Ti-6Al-4V components, making them more suitable for aerospace and turbine engine applications.

TABLE OF CONTENTS

List of Figures

List of Tables

Chapter 1: Introduction

1.1 Introduction to Additive Manufacturing

Additive Manufacturing (AM), called as 3D printing, is a transformative approach to industrial production that enables the creation of complex geometries directly from digital models by successively adding material layer by layer. Unlike conventional subtractive manufacturing processes, AM offers significant advantages such as reduced material waste, increased design flexibility, rapid prototyping capabilities, and the ability to fabricate lightweight structures with internal features that are otherwise difficult or impossible to achieve through traditional methods. [1]

Over the past decade, AM has evolved from a prototyping tool into a robust manufacturing technology used in critical industries such as aerospace, biomedical, automotive, and energy sectors [2]. Various AM techniques have been developed, each with distinct material compatibility, resolution, and mechanical performance characteristics. Among these, metal additive manufacturing processes like Directed Energy Deposition (DED), Wire Arc Additive Manufacturing (WAAM) and Powder Bed Fusion (PBF) have gained prominence for fabricating functional metallic components with high mechanical integrity [3].

The increasing industrial demand for lightweight and high-strength components, combined with the flexibility of AM to integrate complex design features, has significantly expanded its adoption in engineering applications. However, challenges remain in terms of surface finish, dimensional accuracy, residual stress, and anisotropic mechanical properties, often necessitating the use of post-processing techniques to meet application-specific requirements [4]. Research continues to optimize AM process parameters and explore hybrid approaches that combine AM with surface treatment technologies to enhance part performance and reliability.

1.1.1 Classification of Additive Manufacturing

Additive Manufacturing (AM) can be divided into different ways based on various factors such as the material used, the mechanism of layer deposition, and the application. Here some classifications of AM:

1. Material- based classification: AM based on polymer, metal, ceramic, and composite material.
2. Mechanism- based classification: Material Extrusion, Direct Energy Deposition, Powder Bed Fusion , Material Jetting, vat Polymerization, Binder Jetting and sheet lamination.
3. Application-based classification: Rapid Prototyping (RP), Tooling, medical, Aerospace, Automotive, and Architecture.

1.1.2 Mechanism based classification.

According to the ISO/ASTM 52900 standard, Additive Manufacturing (AM) processes are classified into seven distinct categories based on the method of material deposition and fusion. These categories encompass a wide range of technologies that differ in terms of feedstock type, energy source, application areas, and achievable material properties.[1]

1. **Vat Photopolymerization:** Polymerization process employs a tank of liquid photopolymer resin, selectively cured by an ultraviolet (UV) light source to build solid layers. Typical methods involve Stereolithography (SLA) and Digital Light Processing (DLP). It has high resolution and smooth surface finish, and is primarily used for prototypes, dental models, and jewelry. Materials are normally brittle and not appropriate for load-bearing applications.
2. **Material Jetting:** Material jetting works by depositing tiny droplets of build material (usually photopolymers) through a nozzle and curing

them with UV light. It supports multi-material and full-color printing with excellent surface finish. The process is best for aesthetic or conceptual models but is limited by the mechanical properties of the materials and higher equipment cost.

3. **Binder Jetting:** In Binder Jetting, a liquid binder is selectively deposited onto a powder bed (metal, ceramic, or sand) to bond particles layer by layer. After printing, parts typically require sintering or infiltration. It is suitable for large-scale components and casting molds, but the green parts are fragile before post-processing.
4. **Material Extrusion:** Material extrusion involves heating and extruding thermoplastic material through a nozzle to build objects layer by layer. The most common technique is Fused Deposition Modeling (FDM). It's affordable and widely used for prototyping and functional parts, though it often results in lower resolution and visible layer lines.
5. **Powder Bed Fusion (PBF):** PBF employs a laser or electron beam to selectively melt metal or polymer powder in a bed. Methods are Selective Laser Melting (SLM) and Electron Beam Melting (EBM). It makes high-strength, complex structures for aerospace and biomedical uses. It has high equipment cost and needs support removal and post-processing.
6. **Directed Energy Deposition (DED):** DED involves melting material (usually metal powder or wire) as it is deposited using a focused energy source like a laser, electron beam, or plasma arc. It is ideal for repairing or adding features to existing parts and for fabricating large components. Though flexible and high in deposition rate, it typically yields rough surface finishes.
7. **Sheet Lamination:** Sheet lamination joins sheets of material (paper, polymer, or metal) using adhesives or ultrasonic welding, and cuts them into shape layer by layer. It is fast and cost-effective for producing large parts or concept models. Limitations include lower mechanical strength and restricted material options compared to other AM processes.

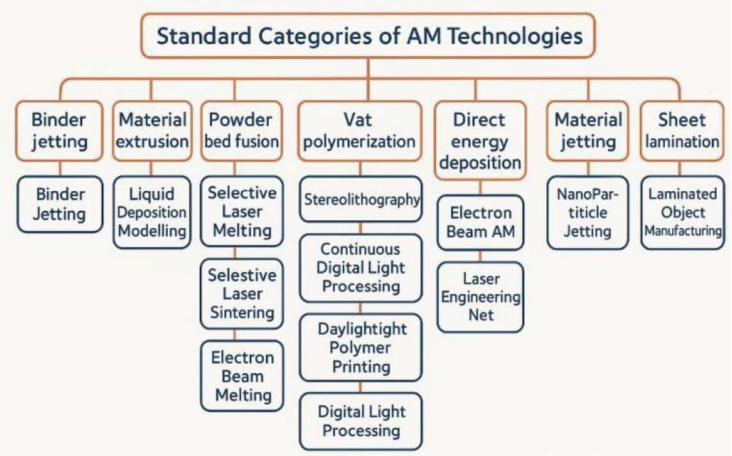

Fig 1.1 Flow chart of different Additive Manufacturing [38]

1.1.3 Direct Energy Deposition (DED)

Direct Energy Deposition (DED) is an additive manufacturing (AM) process for metals that uses intense heat energy to melt the material being deposited. In contrast to powder bed fusion methods that add parts layer-by-layer to a bed of powder, DED constructs parts by adding material directly into a melt pool created by a high-energy source like a laser, electron beam, or plasma arc.[2] It is typically performed with a multi-axis robot arm or CNC-controlled gantry system, enabling the production of intricate geometries, large-scale parts, and component repairs.[3] DED is widely used in the aerospace, defense, energy, and biomedical industries due to its ability to repair high-value components, produce functionally graded materials, and fabricate near-net-shape parts with relatively high deposition rates. However, challenges such as poor surface finish, residual stresses, and lower dimensional accuracy compared to powder bed systems still remain, often requiring post-processing techniques to enhance part quality.[4]

Powder-fed DED systems employ a nozzle or multiple nozzles to feed metal powder into the melt pool created by the energy source, typically a high-power

laser. The powder particles are carried by an inert carrier gas (like argon) and are melted upon or just before reaching the substrate.[5] This configuration allows for precise control over material feed rates and enables multi-material deposition by switching powders during the process, making it suitable for creating functionally graded materials and alloy development. Powder-fed DED offers good resolution and material flexibility but suffers from lower material efficiency due to powder loss and requires complex powder recovery systems. Furthermore, handling fine metal powders raises safety and health concerns, and the equipment cost can be significant due to the need for shielding gas, powder delivery systems, and advanced optics.[4]

Wire-fed DED, on the other hand, uses metal wire as the feedstock, which is fed directly into the melt pool created by the thermal energy source. The wire-based approach has several advantages, including near-100% material utilization, easier handling, and a safer working environment compared to powder-based systems. Wire-fed DED processes are often used with plasma arc or laser as the energy source and are especially effective for large part fabrication and structural repairs. Due to their high deposition rates and lower operational costs, wire-fed systems are increasingly used in industries such as shipbuilding, automotive, and construction. However, wire-fed DED systems may offer less precision compared to powder-fed ones and are generally limited in terms of material variety and geometric complexity.[3]

Together, powder-fed and wire-fed DED represent the two major material delivery approaches in the DED process, each with distinct advantages and limitations. The choice between the two depends on the specific application requirements, such as part size, complexity, material properties, and economic considerations. Ongoing advancements in process control, hybrid manufacturing integration, and real-time monitoring are continuously improving the reliability and adoption of DED technologies in modern manufacturing.[2]

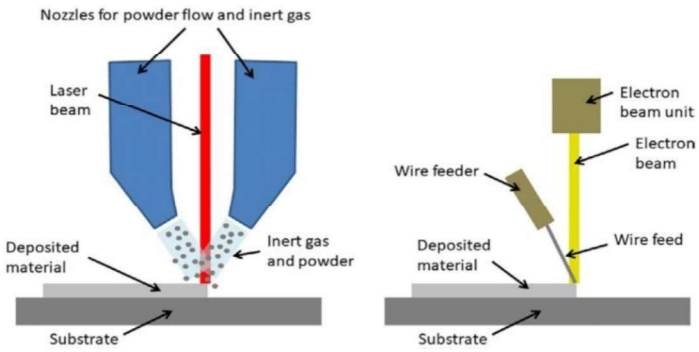

Fig 1.2 Types of Direct Energy Deposition[1],[2]

1.2 Different Post Processing Techniques of Additively Manufactured parts

Nearly all additive manufactured parts required post processing to achieve the required properties, like surface finish, geometric accuracies, microstructure and mechanical properties. Post-processing is an indispensable phase in the additive manufacturing (AM) workflow, directly influencing the final quality, functionality, and performance of fabricated components. Although AM offers substantial benefits—including design flexibility, material efficiency, and rapid prototyping—parts manufactured directly by AM techniques often suffer from inherent defects such as high surface roughness, residual stresses, porosity, dimensional inaccuracies, and microstructural inhomogeneities. These issues can adversely affect mechanical properties, wear and corrosion resistance, and long-term durability, particularly in critical sectors such as aerospace, biomedical, automotive, and energy.[4] Consequently, post-processing is essential to refine geometrical accuracy, improve surface finish, reduce internal voids, relieve thermal stress, and tailor microstructure and surface characteristics to meet stringent application demands. The choice of post-processing technique depends on the specific AM process (e.g., DED, SLM, WAAM), the material used, and the intended service requirements of the part.

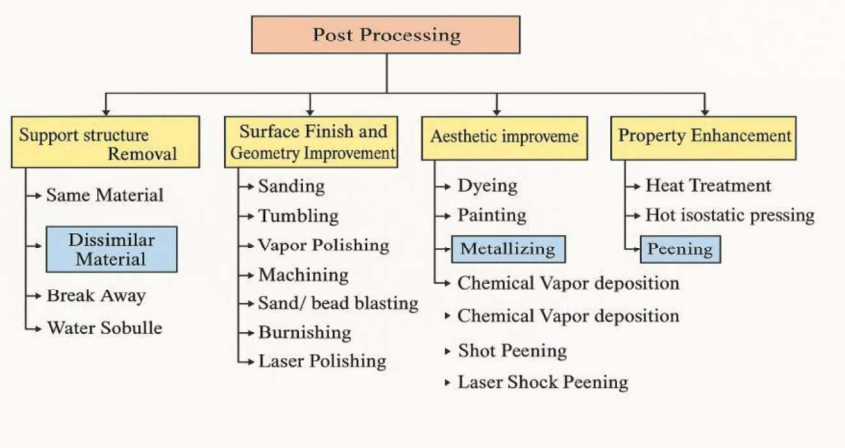

Fig 1.3 Flow chart of Different Post Processing after AM

Among the most commonly applied post-processing methods is heat treatment, which is used to mitigate residual thermal stresses, promote microstructural homogenization, and improve the mechanical integrity of AM parts. Depending on the alloy system such as Ti6Al4V, aluminum alloys, or stainless steels appropriate thermal cycles like annealing, aging, or solution treatment are applied to enhance ductility, tensile strength, and fatigue performance.[2] One of the most important densification methods is Hot Isostatic Pressing (HIP), where high temperature and isostatic pressure in an inert environment are utilized to remove internal porosity and reach near-theoretical density. HIP is especially suitable for parts manufactured through powder bed fusion processes such as Selective Laser Melting (SLM) or Electron Beam Melting (EBM), which greatly improve fatigue life, structural integrity, and reliability—qualities essential for high-performance applications in aerospace and biomedical applications.

Surface finishing is equally crucial due to the inherently rough surfaces produced by layer-by-layer deposition. Common methods such as abrasive blasting, grinding, mechanical polishing, and chemical etching are employed to improve surface texture and reduce roughness. For more advanced applications, mechanical and electrochemical surface treatments like shot

peening, electropolishing, and particularly Laser Shock Peening (LSP) are employed.

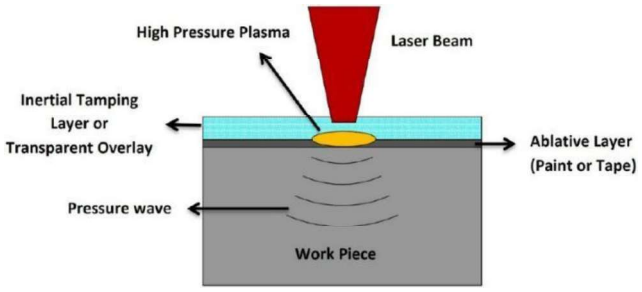

Fig 1.4 Schematic of LSP Process[39]

LSP has emerged as a powerful laser-based post-processing technique for AM parts, especially those produced by Direct Energy Deposition (DED), due to its ability to induce deep compressive residual stresses, enhance surface hardness, and significantly improve fatigue resistance without material removal. [6] Additionally, laser remelting and laser surface alloying are increasingly used to recondition the surface microstructure, eliminate pores, and refine grain size, thereby improving the tribological and corrosion behavior of AM components.[7]

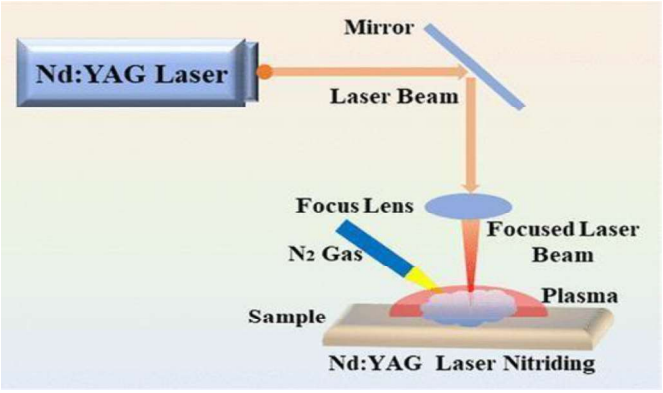

Fig 1.5 Schematic of Laser Nitriding Process

Subtractive post-processing methods such as CNC machining are often essential for achieving the required dimensional accuracy and surface finish, especially in precision-critical regions such as mating faces, sealing surfaces, and threaded holes. In parts requiring high surface integrity or functional gradients, thermal-chemical post-processing techniques like carburizing,

boriding, or laser nitriding are applied. For example, laser nitriding of aluminum or titanium-based AM parts forms a ceramic-like surface with superior hardness, wear resistance, and corrosion resistance—features particularly beneficial in marine and biomedical environments.[8] These laser-assisted surface engineering techniques offer localized control, minimal thermal distortion, and high precision, making them ideal for AM component post-treatment.

Non-destructive testing (NDT) is another integral aspect of post-processing, enabling quality assurance without compromising component integrity. Techniques such as ultrasonic testing, X-ray computed tomography (CT), magnetic particle inspection, and dye penetrant testing are employed to detect subsurface defects, verify structural soundness, and ensure conformance to design standards. Furthermore, surface coatings such as thermal barrier coatings (TBCs), anti-corrosion paints, and bio-functional layers like hydroxyapatite are often applied based on application needs. These coatings not only improve performance under harsh environmental conditions but also extend the functional life of the AM parts.

In conclusion, post-processing is a vital and value-adding phase in the AM process chain. It transforms as-built parts—often geometrically complex but mechanically imperfect—into high-performance, application-ready components. With the advancement of hybrid manufacturing, laser-based surface enhancement, and intelligent process monitoring, post-processing continues to evolve as a key enabler for the broader industrial adoption of additive manufacturing technologies. A well-designed post-processing strategy is essential for bridging the gap between AM's design potential and its performance reliability in real-world applications.

1.3 Conventional Shock Peening Techniques and Their Types

Conventional shock peening techniques are mechanical surface treatment methods employed to enhance the fatigue life, hardness, and resistance to stress corrosion cracking of metallic components. These techniques function by introducing beneficial compressive residual stresses on the surface layers of materials through the application of high-intensity, rapid mechanical shocks. Unlike traditional surface treatments such as heat treatment or case hardening, shock peening does not involve thermal processes but relies on mechanical energy to alter surface properties. The energy from the shock impact creates localized plastic deformation, which in turn induces compressive stresses that retard crack initiation and propagation, especially under cyclic loading conditions.

There are several types of conventional shock peening techniques, each differing in the nature of the shock application. Shot peening is the most widely used method, where small spherical media (steel, ceramic, or glass beads) are propelled at high velocities onto the surface using compressed air or centrifugal wheels. The repeated impacts cause surface plastic deformation, leading to strain hardening and the formation of compressive residual stress. Another variant is needle peening, which involves high-frequency impact of hardened needles or pins onto the surface, often used in weld zones and hard-to-reach areas. Hammer peening, either manually or pneumatically driven, is employed to treat welded joints, particularly to reduce tensile residual stresses. Water jet peening (also known as cavitation peening) utilizes high-pressure water jets to generate shock waves that create similar effects without introducing foreign media or particles.

Each technique offers unique advantages and is selected based on application requirements, material type, and desired surface characteristics. For instance, shot peening is ideal for complex geometries and mass production, while water jet peening is beneficial where cleanliness and surface integrity are paramount. Despite their effectiveness, conventional shock peening methods have certain

limitations, such as limited control over depth of penetration and residual stress uniformity. These challenges have led to the development of advanced methods such as laser shock peening, which offers improved precision and repeatability for high-performance applications.[9]

1.3.1 Shot Peening

Shot peening is a widely employed mechanical surface treatment It is applied to enhance the durability of metal components by increasing their resistance to fatigue, wear, and stress corrosion. In this process, small spherical media typically steel, ceramic, or glass beads—are blasted at high velocities onto a material surface using compressed air or centrifugal wheels. Each impact acts as a tiny hammer, plastically deforming the surface and introducing beneficial compressive residual stresses that inhibit the initiation and propagation of fatigue cracks.[10] These compressive stresses are particularly effective in counteracting tensile stresses induced during service conditions, such as those in aerospace, automotive, and power plant components.

Shot peening is adaptable to a variety of materials and geometries, making it a preferred choice for enhancing the durability of gears, springs, turbine blades, and welded joints. The process parameters—such as shot size, hardness, velocity, and coverage—must be carefully controlled to ensure optimal surface modification without over-peening, which could lead to surface damage.[11] Advanced variations, like micro-shot peening and ultrasonic peening, have emerged for treating fine components and complex geometries. Ultrasonic peening utilizes high-frequency vibrations to drive pins into the material surface, resulting in deeper and more uniform compressive stresses with minimal surface roughness, particularly useful for weld zone enhancement and fatigue crack retardation. Another related technique, hammer peening, involves mechanical or pneumatic hammers to impart localized impacts manually or semi-automatically, commonly used in welded structures to relieve tensile residual stresses and improve fatigue life (Kumar et al., 2021). As non-thermal, mechanically driven processes, these peening methods provide flexible,

effective solutions for extending component life in cyclic and corrosive environments.

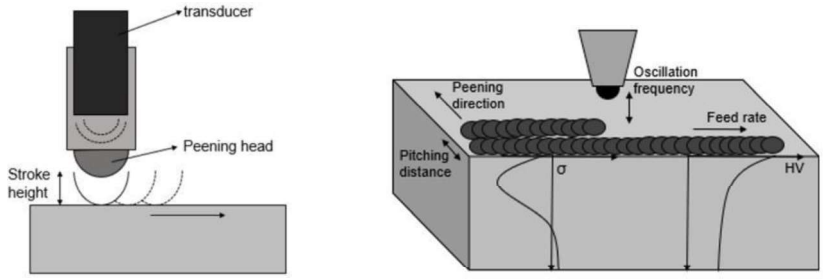

Fig 1.6 Schematic of ultrasonic hammer peening process [11]

1.3.2 Water Jet Peening

Water Jet Peening (WJP) is a surface treatment technique that enhances the fatigue life and corrosion resistance of metallic components by inducing compressive residual stresses without using solid media. Unlike conventional shot peening, WJP uses high-pressure water jets, typically in the range of 30–300 MPa, to create cavitation bubbles on the surface of the material. The collapse of these bubbles near the surface generates intense shock waves that plastically deform the surface layer, introducing beneficial compressive stresses.[12] This process is especially advantageous in applications where contamination from peening media must be avoided, such as in the nuclear, aerospace, and medical industries.

Water Jet Peening offers several benefits over conventional mechanical peening methods. It avoids media entrapment or surface contamination, making it suitable for components like steam generator tubes, turbine blades, and weld zones in nuclear reactors. Moreover, the absence of solid particles minimizes damage to complex geometries and sensitive materials, making it a safer and cleaner alternative. Studies have shown that WJP-treated surfaces exhibit improved resistance to stress corrosion cracking, particularly in

austenitic stainless steels, due to the induced compressive stress and surface work hardening. [13] However, the effectiveness of WJP largely depends on parameters such as nozzle geometry, water pressure, and stand-off distance, which must be carefully optimized for each application.

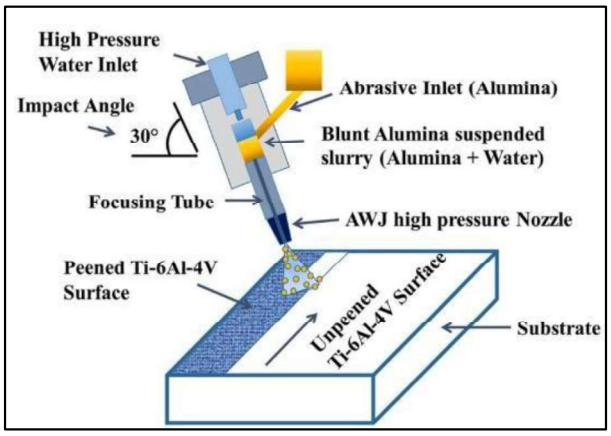

Fig 1.7 Schematic representation of Abrasive Water Jet peening [13]

1.4 Laser Shock Peening

Laser Shock Peening (LSP) is a sophisticated surface treatment method that employs high-energy laser pulses to improve the mechanical performance of metallic parts, particularly their fatigue strength, wear resistance, and stress corrosion cracking resistance. In LSP, a high-intensity laser (typically in the nanosecond pulse duration) is focused onto the surface of a material coated with a sacrificial protection layer (such as black paint or aluminum foil) and an overlying transparent confining layer such as water. Flash evaporation of the sacrificial layer creates a high-pressure plasma confined by the overlying water layer, generating a shock wave that causes plastic deformation of the material below the surface. This treatment creates deep and homogeneous compressive residual stresses, frequently to depths of a few millimeters—much deeper than other forms of shot peening.[15]

LSP is particularly beneficial for aerospace, nuclear, and biomedical applications where high precision and minimal surface damage are critical. Unlike mechanical

peening methods, LSP causes minimal surface roughness and can be precisely targeted using robotic systems, making it ideal for complex geometries and localized treatment [16]. Additionally, it offers superior fatigue life improvement and can delay crack initiation even in high-temperature environments. However, the process is relatively expensive and requires careful parameter optimization, including laser energy, pulse duration, spot size, and overlap rate.[17] Recent developments in Laser Shock Peening (LSP) have broadened its applications through innovative variants like femtosecond laser peening and warm laser shock peening, which help achieve improved control over residual stress distribution and enhanced surface integrity. The introduction of high-repetition-rate laser systems and integration of real-time monitoring technologies have made the LSP process more consistent and scalable for industrial applications. For example, LSP has been successfully adopted in the maintenance and enhancement of turbine blades, significantly extending their operational life by repairing micro-cracks and increasing resistance to foreign object damage (FOD). Additionally, the use of numerical modeling and simulation tools, such as finite element analysis (FEA), enables engineers to predict stress fields and optimize process parameters efficiently, thereby minimizing the need for experimental trial- and-error. Although the initial setup cost of LSP is relatively high, the technique provides exceptional benefits such as deep compressive stress penetration and minimal surface distortion, making it ideal for critical components exposed to cyclic loading and elevated temperatures—areas where conventional peening methods often fall short.

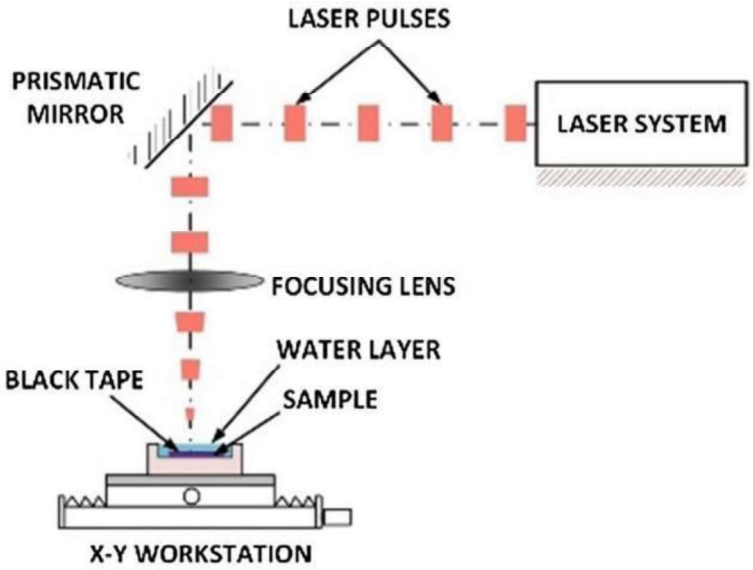

Fig 1.8 Schematic of laser shock peening

1.5 Literature Review

1.5.1 Current Status on DED of Titanium Alloys

Titanium alloys, particularly Ti-6Al-4V, have received significant attention for high-performance use in the aerospace, biomedical, and defense industries because of their superior mechanical properties, high corrosion resistance, and good biocompatibility. Conventional processes like forging and casting, however, tend to cause substantial wastage of material, high tooling expenses, and poor geometric freedom. To surpass these constraints, Direct Energy Deposition (DED), which is a laser-based additive manufacturing (AM) process, has become an effective method for the manufacturing and repairing of titanium parts [18], [19]. DED involves feeding material in powder or wire form into a melt pool created using a high-energy heat source, most commonly a laser, electron beam, or plasma arc. The capability of DED to deposit material layer by layer with accurate control of geometry makes it particularly well suited for near-net-shape production, functional repairs, and even material property tailoring in intricate parts [20].

Despite its advantages, DED of titanium alloys presents a set of process-related challenges, primarily due to the high reactivity of titanium at elevated temperatures and its strong affinity for oxygen and nitrogen. This necessitates a controlled environment, typically using argon shielding, to avoid oxidation and contamination during processing [21]. Moreover, the thermal behavior during DED is highly dynamic, with repeated heating and cooling cycles that lead to steep thermal gradients and the accumulation of residual stresses. These thermal cycles also have a strong influence on the microstructure of the deposited layers, making the optimization of process parameters a crucial step in ensuring part integrity and mechanical performance [22].

Process parameters like laser power, scan speed, powder or wire feed rate, standoff distance, and layer thickness control the energy input and cooling rates, which in turn influence melt pool dynamics and solidification behavior. Research has demonstrated that increased laser power deepens the melt pool and enhances fusion but also enhances the tendency to form keyhole and thermal distortion. Conversely, too high scan speeds lead to poor surface finish and inadequate bonding [23], [24]. Similarly, powder feed rate variations influence the dilution ratio and deposition efficiency; lack of fusion defects are caused by underfeeding, while overfeeding causes un-melted powder and high surface roughness [25].

Microstructural studies of DED-deposited Ti-6Al-4V reveal a typical columnar β-grain structure aligned with the build direction, with basketweave α+β phases within. The columnar grains result from directional solidification and epitaxial growth during deposition, leading to anisotropy in mechanical properties. This anisotropy is particularly pronounced in tensile and fatigue behavior, which has led researchers to explore various strategies for grain refinement and homogenization. Techniques such as beam oscillation, interlayer rolling, and in-situ heat treatment have been shown to significantly influence grain morphology and reduce microstructural anisotropy [26], [27]. Additionally, post-processing methods including annealing, stress-relieving, and hot isostatic pressing (HIP) are widely

used to modify the microstructure, relieve residual stress, and enhance ductility [28].

The mechanical performance of DED-processed titanium parts is largely influenced by the microstructure, defect distribution, and surface quality. When optimized process parameters are used, the tensile strength of DED-fabricated Ti-6Al-4V can be comparable to, or even exceed, that of wrought counterparts, often reaching values above 1000 MPa. However, fatigue properties remain a concern due to the presence of internal porosity and rough as-built surfaces. Several researchers have reported that fatigue cracks typically initiate from surface irregularities or sub-surface pores, indicating the importance of post-deposition surface finishing for fatigue-critical components [29], [30].

Residual stress buildup remains a significant issue in DED, particularly for titanium alloys, which tend to undergo thermal distortion due to their poor heat conductivity and considerable thermal expansion characteristics. These internal stresses result from rapid solidification and frequent thermal cycling during the layer-by-layer fabrication process. These stresses arise due to rapid solidification and repeated thermal cycling during the layer-by-layer build process. Techniques such as baseplate preheating, controlled scan strategies, and interlayer dwell times have been proposed to reduce thermal gradients and mitigate stress accumulation [31]. Finite element simulations and experimental stress measurements using X-ray diffraction and neutron diffraction methods have provided valuable insights into stress evolution, guiding the development of stress-relief strategies [32].

Recent advances in sensor-based monitoring and closed-loop control are helping address some of the reliability issues in DED. In-situ monitoring systems using infrared cameras, pyrometers, and laser displacement sensors have been employed to track melt pool temperature, height, and surface roughness in real time [33].

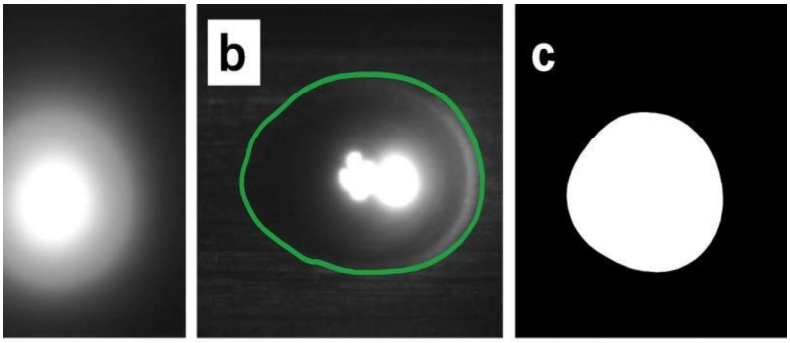

Figure 1.9: Image of Molten pool Capture by Infrared Camera [65].

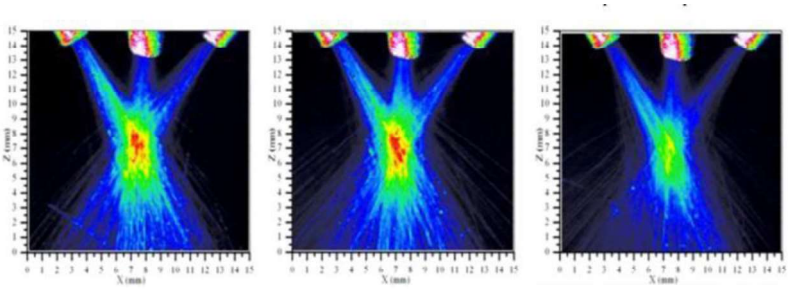

Fig 1.10 Above Images of different Catchment of powder stream [65]

These systems enable adaptive control of process parameters to maintain consistent deposition quality, especially in complex geometries. Furthermore, machine learning approaches are being integrated to predict defects and optimize build strategies based on historical process data [34].

In addition to component manufacturing, DED has shown great potential in the repair and remanufacturing of high-value titanium parts, such as aerospace turbine blades, biomedical implants, and defense equipment. Its ability to restore worn-out or damaged components without removing them from service environments offers significant economic and operational benefits. Moreover, multi-material and functionally graded structures using DED have opened new research directions, where tailored compositions and property gradients can be engineered across the part volume [35], [36].

In summary, the current research on DED of titanium alloys demonstrates a strong focus on process parameter optimization, microstructure control, real-time

monitoring, and mechanical property enhancement. While substantial progress has been made, challenges such as anisotropic properties, residual stress, and surface roughness remain areas of active investigation. Future work is likely to see a greater integration of intelligent control systems, advanced modeling, and hybrid manufacturing techniques to further expand the capabilities and industrial adoption of DED for titanium components.

1.5.2 Current Status of Tribological Studies on Additively Manufactured Parts and the Impact of Laser Shock Peening

Conventional manufacturing methods have been altered forever by additive manufacturing (AM) or 3D printing because of its precise capability to create intricate shapes while minimizing material waste. The alteration occurs by placing layers of materials, which allows for unparalleled created design templates and quicker prototypes to be made. Manufacturing Additive is greatly utilized in the aerospace, biomed, and automotive industries that heavily rely on customization and lightweight features [37].

However, as AM transitions from prototyping to functional component production, the tribological performance of AM parts—concerning friction, wear, and lubrication has gained significant attention.

The microstructural heterogeneity, anisotropic properties, and surface irregularities inherent to AM often degrade tribological performance compared to conventionally manufactured parts [38]. These issues arise from factors like poor layer adhesion, surface roughness, and residual stresses introduced during rapid solidification. To counteract these drawbacks, advanced surface engineering techniques such as Laser Shock Peening (LSP) have been investigated to enhance surface properties, improve wear resistance, and extend service life of AM parts [39].

AM components often face tribological challenges primarily due to surface imperfections and structural inconsistencies. One of the most significant issues is high surface roughness, which increases contact area and thus elevates the

coefficient of friction during sliding contact [40]. The partially fused powder particles and stair-step morphology result in non-uniform surfaces that accelerate abrasive wear and act as initiation sites for cracks. Additionally, the rapid cooling rates and directional solidification characteristics of AM lead to anisotropic mechanical properties and columnar grain structures. These structural features, along with residual tensile stresses, decrease fatigue resistance and make AM parts vulnerable to wear under cyclic loading [41]. Porosity is another critical issue, especially in powder-based AM techniques like Electron Beam Melting (EBM) or Selective Laser Melting (SLM). Pores reduce the effective contact area and act as stress concentrators, promoting micro-crack formation under repeated stress cycles [42].

These microstructural and surface challenges significantly influence tribological behavior, often leading to a trade-off between strength and wear resistance. Thus, optimizing surface properties through post-processing is crucial to ensure the functional performance of AM components.

Recent studies have investigated the tribological behavior of commonly used additively manufactured (AM) metals and alloys such as Ti-6Al-4V, Inconel 718, and 316L stainless steel. Ti-6Al-4V, a popular choice in aerospace and biomedical applications due to its high strength and low density, often exhibits different microstructural characteristics when processed through AM. Specifically, the rapid cooling rates associated with AM techniques can result in the formation of a martensitic α’ phase, which increases brittleness and negatively affects its wear resistance. [43]. Tribological tests such as pin-on-disk and reciprocating sliding have shown that as-built Ti-6Al-4V suffers from high wear rates and friction coefficients under dry conditions [44]. Similarly, 316L stainless steel fabricated via AM shows decreased wear resistance compared to its conventionally manufactured counterpart. The presence of porosity and surface oxides contributes to increased friction and wear, particularly under dry sliding conditions. However, improvements are possible through surface finishing or peening techniques [45]. Inconel 718, a nickel-based superalloy used in turbine blades and aerospace

applications, also exhibits poor tribological properties in its as-built state. Its wear resistance is hindered by internal porosity and microstructural anisotropy. However, post-processing techniques such as hot isostatic pressing (HIP) and LSP have demonstrated the potential to enhance its surface strength and wear performance [46].

To assess tribological behavior, standard laboratory tests are commonly employed. These include pin-on-disk, ball-on-flat, and reciprocating wear tests that measure wear volume, friction coefficient, and surface damage under controlled load and motion [47]. For more precise evaluations, nanoindentation and micro-scratch tests are used to analyze surface hardness, elastic modulus, and crack initiation at small scales [48]. Environmental conditions play a significant role in determining tribological responses. For instance, elevated temperature tests reveal that oxidative Oxide layer development on AM surfaces plays a key role in determining their wear performance, which can either protect or degrade the material depending on their adherence and brittleness [49]. Lubricated conditions, on the other hand, show better performance but are still affected by surface roughness and porosity.

Additionally, wear mechanisms can vary depending on the build orientation and laser scan strategy. Sliding parallel to the layer lines often results in higher wear rates due to weak interlayer bonding, whereas perpendicular orientations exhibit slightly better resistance [50]. Therefore, consistent post-processing and optimized AM parameters are essential for reliable tribological performance.

Laser shock peening (LSP) is a technique that has tuned in an attention as a more advanced AM surface treatment. It consists of directing a laser to a metal surface for a short pulse, and the resulting plasma causes shock waves to be generated. Such waves will propagate within the material resulting in enhanced fatigue life and wear resistance due to the elastic deformation and residual compressive stresses formed [51]. Compared to traditional methods such as shot peening, LSP has advantages. It has a greater compressive stress range of about 1-2 mm, minimal surface roughness, and reduced contaminant adhesion, all of which extend the life of

sensitive and precision components [52]. It also refines surface grain structures through dynamic recrystallization, reducing crack initiation sites. When applied to AM materials like Inconel 718 and Ti-6Al-4V, LSP has been shown to significantly reduce surface roughness, increase hardness, and enhance wear resistance. For example, studies show that the friction coefficient of LSP-treated AM Ti-6Al-4V dropped by up to 30% compared to the untreated condition [53]. Additionally, LSP improved the load-carrying capacity of AM SS components under reciprocating wear tests [54]. Moreover, LSP mitigates tensile residual stresses inherent to AM, transforming them into beneficial compressive stresses. This not only enhances tribological properties but also improves fatigue performance under cyclic loads, making it highly suitable for aerospace and automotive parts produced by AM [46].

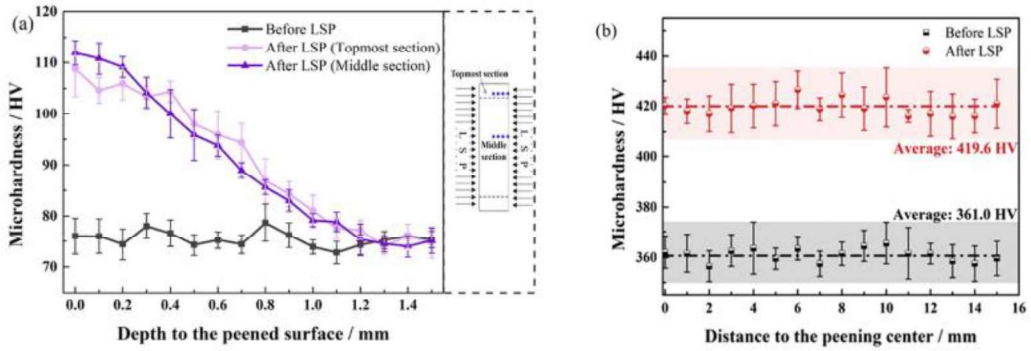

Fig 1.11 (a) and (b) Micro-hardness distributions of Al alloy

1.6 Motivation of the Present Study

The field of additive manufacturing (AM) has witnessed significant advancements in recent years, especially with the development and application of Directed Energy Deposition (DED) techniques. Among the various alloys used in this process, titanium alloys like Ti-6Al-4V are of particular interest due to their exceptional mechanical strength, corrosion resistance, and biocompatibility. These properties make them ideal candidates for critical applications in aerospace, biomedical, and energy sectors. However, the fabrication of thin-walled structures using DED techniques presents unique challenges in terms of defect control, microstructural

consistency, and mechanical performance. This has necessitated a critical need to maximize the process parameters and incorporate efficient post-processing methods for improving the overall integrity of the manufactured components. Therefore, this Present study deals with the experimental exploration into various process parameters and its influence on the output response as per the Box-Behnken design of experiment.

One of the key issues in the manufacturing of thin-walled Ti-6Al-4V parts using DED is the development of internal flaws like porosity, microcracks, and irregular surface morphology. These flaws not only lower the mechanical integrity and fatigue life of the parts but also decrease their reliability and working life. Though DED has been explored in depth, few studies have addressed thin-walled structures, which act differently than bulk or solid parts because of their lower ability to dissipate heat and higher sensitivity to thermal gradients. Therefore, studying the influence of the DED parameters on defect generation in such structures is necessary. By scientifically analyzing these parameters, one can create optimized conditions that reduce porosity and other imperfections to a great extent, thus improving the structural properties of the components. Another promising method to further enhance the performance of DED-produced parts is through post-processing methods such as Laser Shock Peening (LSP). LSP is a surface treatment technique based on the use of high-intensity laser pulses to create advantageous compressive residual stresses, improve microstructures, and enhance surface hardness and surface roughness. Although LSP benefits on traditionally produced Ti-6Al-4V components have been extensively reported, its application to additive manufactured components, particularly those with complex or thin-walled structures, is relatively unexplored. This provides a significant research opportunity to analyze the impact of LSP parameters on the surface integrity and internal microstructural transformation of DED parts. Additionally, as LSP interacts with AM parts differently owing to their layer-by-layer build approach and inherent residual stresses, its impact has to be examined comprehensively and systematically. A most critical gap in the literature is the scarcity of combined studies that investigate the correlation between process parameters, defect

generation, post-processing methods, and ultimate mechanical performance in thin-walled Ti-6Al-4V structures. While isolated efforts have been made to understand DED or LSP independently, there is minimal research connecting the two, particularly in the context of optimizing both processes to achieve the best possible outcomes. Understanding how DED-induced porosity affects the efficacy of LSP and how LSP can in turn mitigate such defects is crucial for developing a holistic manufacturing process chain. Moreover, this relationship becomes even more important for applications where dimensional accuracy, surface quality, and mechanical reliability are non-negotiable, such as in turbine blades or medical implants. To address these challenges, in this present study, a detailed paramedic investigation into the pulsed laser shock peening in an open atmosphere is performed using Nd: YAG laser. The changes in tribological, mechanical and surface properties by the laser shock peening are also studied.

1.7 Research Objectives

The present thesis focuses on optimizing parameters in the Directed Energy Deposition (DED) process for manufacturing Ti6Al4V alloy components. It aims to study the mechanical and tribological behavior of additively manufactured Ti6Al4V thin-walled structures, such as turbine blade profiles used in aerospace, marine, and biomedical applications. Additionally, the research investigates the role of laser shock peening (LSP) as a post-processing method to improve these properties. The primary objective of the thesis are as follows:

1) To carry out the parametric optimization of the Direct Energy deposition of the part Ti6Al4V profile turbine blade based on box Behnken design
2) Evaluate the effect of DED parameter on defects generation, during fabrication of thin wall. Further use the outcome of the study to optimize the DED parameters for minimizing porosity.
3) Evaluate the effect of LSP parameter on surface porosity generated during fabrication of thin wall using DED process. Further use the outcome of the study to optimize the LSP parameters for minimizing porosity.

4) Perform different characterizations on DED parts post processed with LSP at each stage to understand microstructures development and their mechanical properties.

This work comprehensively provides adequate insights into the DED additive manufacturing and its post processing by open atmosphere laser shock peening process. The experimental result obtained through investigation into hardness, roughness under different power densities and residual stress measurement can be useful for different marine and aerospace applications.

1.8 Outline of the Thesis

There are five chapters in the thesis, a synopsis of which is provided below.

Chapter 1: Introduction to Additive Manufacturing and its post processing by Laser shock peening

Chapter 2: Details of Experimental setup used for DED of Ti6Al4V and Laser shock peening of additively manufactured component

Chapter 3: Experimental Investigation into Laser based Direct Energy Deposition (LDED) of Ti6Al4v Turbine Profile Blade

Chapter 4: Experimental Investigation into Laser Shock Peening Process on Turbine Profile Blade

Chapter 5: Conclusions and Future scope of work

Chapter 2: Materials and Methods

2.1 Material Specification

Ti6Al4V, or Grade 5 titanium, is the most commonly used titanium alloy in high-tech engineering applications because of its higher strength-to-weight ratio, superior corrosion resistance, and sound mechanical integrity. This two-phase (alpha-beta) material generally contains approximately 90% titanium, 6% aluminum (which stabilizes the alpha phase), and 4% vanadium (which stabilizes the beta phase). The aluminum content also improves the strength and oxidation resistance of the material, while vanadium adds to ductility and allows for successful heat treatment. Having a tensile strength of usually between 900 and 1100 MPa and a relatively low weight of around 4.43 g/cm³, Ti6Al4V is greatly sought in industries where strong yet light materials are demanded. Its outstanding corrosion resistance, especially in sea and saline conditions, positions it for aerospace equipment, shipbuilding, and biomedical devices. In biomedical, Ti6Al4V is widely utilized for orthopedic implants, dental fixtures, and prosthetics because it is biocompatible and resistant to body fluids. Its microstructure ensures a combination of toughness, fatigue strength, and ductility so that it can withstand cyclic loading conditions. The alloy can be produced using different techniques, including forging, machining, and additive manufacturing routes like Direct Energy Deposition (DED) and Selective Laser Melting (SLM). Also, surface engineering methods like laser shock peening or nitriding are usually employed to enhance its fatigue life and wear resistance. While it has many advantages, Ti6Al4V has disadvantages such as its tough machinability and increased cost of production due to the more expensive metal compared to more traditionally used metals like aluminum or steel. It generally needs special equipment and welding with inert gas shielding to avoid oxidation. Generally speaking, Ti6Al4V is still a leading selection for mission-critical applications in aerospace, biomedical, and racing industries with a unique combination of mechanical strength, lightweight, and corrosion resistance.

Table 2.1 Composition of Ti6Al4V at 25°C [47]

Element	Ti	Al	V	Fe	O	C	N	H	Other
Weight %	~89–90	5.5 – 6.75	3.5 – 4.5	≤ 0.30	≤ 0.20	≤ 0.08	≤ 0.05	≤ 0.015	≤ 0.40 (total)

Table 2.2 Properties of Ti6Al4V at 25°C

Property	Values	Units
Density	4.43	g/cm³
Elastic Modulus (Young's Modulus)	113.8	GPa
Yield Strength (0.2% offset)	830 – 880	MPa
Elongation at Break	10 – 14	%
Hardness (Rockwell C)	36 – 41	HRC
Poisson's Ratio	0.31	–
Thermal Conductivity	6.7	W/m·K
Specific Heat Capacity	526	J/kg·K
Coefficient of Thermal Expansion	8.6	µm/m·°C
Electrical Resistivity	1.71×10^{-6}	Ω·m
Melting Point	1604 – 1660	°C
Modulus of Rigidity (Shear Modulus)	~43.7	GPa

2.2 Laser Direct Energy Deposition Setup Details

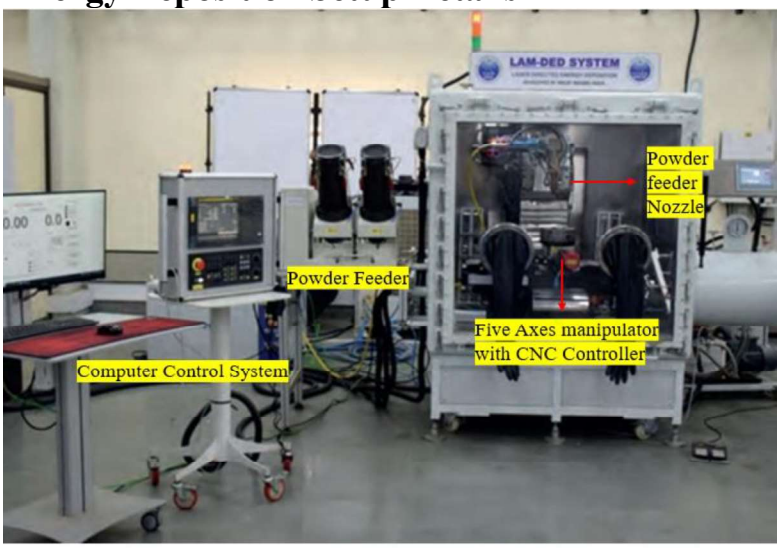

Fig. 2.1 Pictorial View of Laser DED setup

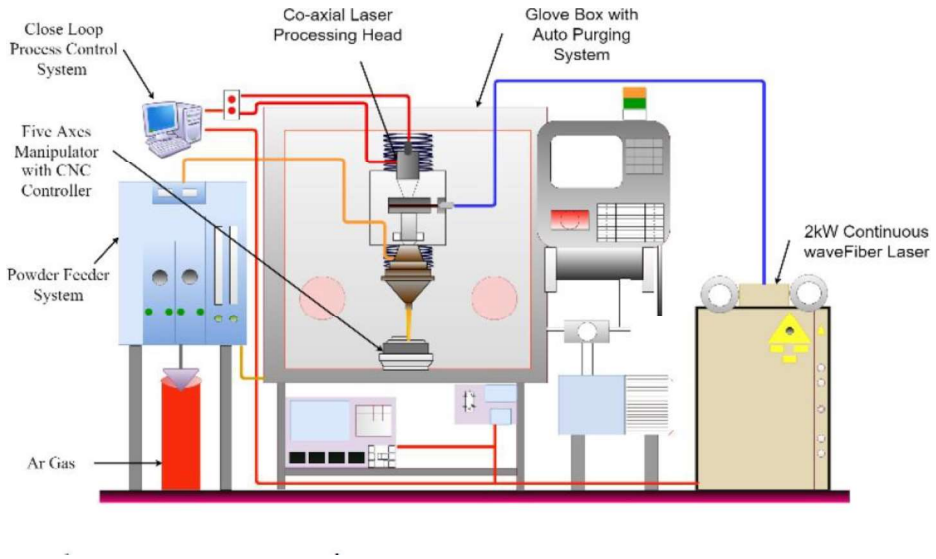

Fig.2.2 Schematic View of Laser DED setup

Laser Additive Manufacturing using the Directed Energy Deposition (L-DED) process allows for the creation of 3D metal components by melting the material as it is being added to the substrate. Unlike Powder Bed Fusion methods, which fuse layers of powder laid across a bed, L-DED introduces the feedstock—either in powder or wire form—directly into a high-power laser beam that melts it during deposition. The material is deposited in a controlled manner onto a substrate, building up the part layer by layer. In the L-DED setup, a focused laser beam heats and melts the feed material as it exits a specially designed deposition head. This head is engineered to simultaneously deliver both the laser and the feedstock to the targeted location. Typically, the laser is focused through the center of the nozzle, while the powder is injected using a carrier gas system that guides it to the melt pool. Shielding gases such as Argon, Helium, or Nitrogen are commonly used to protect the molten material from atmospheric contamination and oxidation.

The movement of the deposition head is synchronized with a computer-controlled system, allowing it to follow a predefined toolpath. As the feedstock melts and solidifies on the substrate, the head lifts after each layer, repeating the process until the complete part is formed. Components of the deposition head include laser optics, powder delivery nozzles, sensors, and inert gas tubing. The role of the carrier

gas is critical—it transports powder from the feeder to the deposition zone, while the shielding gas ensures a clean environment for high-quality layer formation.

2.3 Laser Shock Peening Setup Details

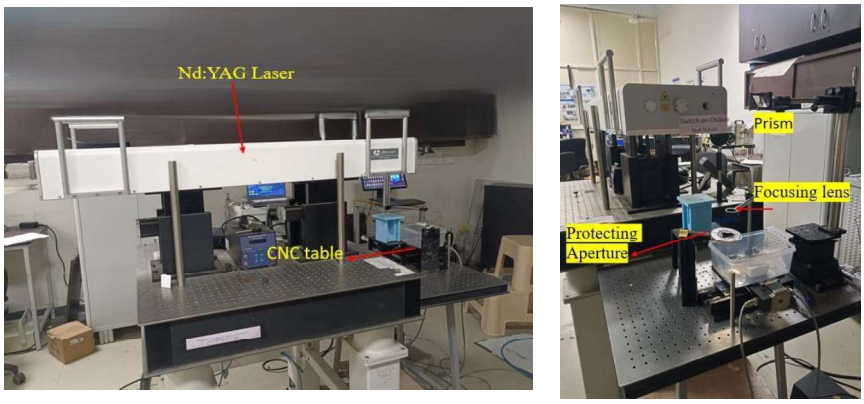

Fig. 2.3 Pictorial View of Laser Shock Peening setup

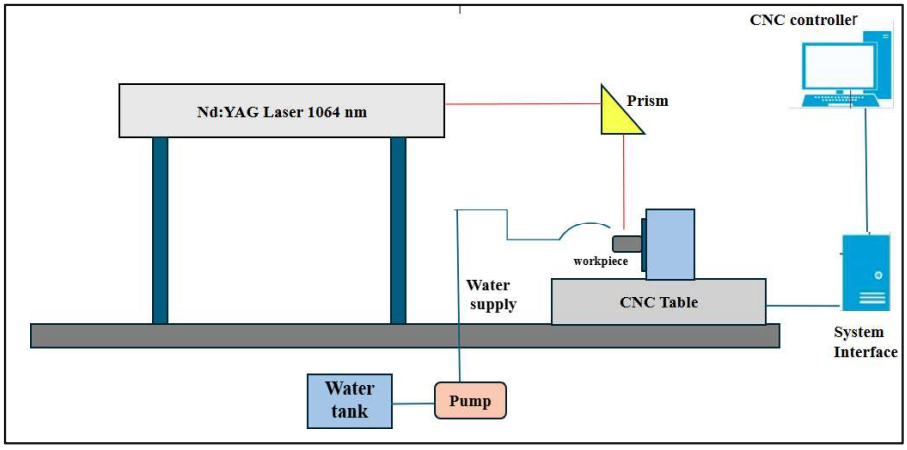

Fig. 2.4 Schematic view of Laser Shock Peening Setup

The laser shock peening was carried out by pulsed Nd3+: YAG laser (Litron laser model no. LPY764G-10) as show in Fig. 2.3 and Fig. 2.4 using the fundamental 1064 nm Wavelength, with the laser beam generated in a Q-Switch mode with a pulse duration of 9 nanoseconds and operating at a repetition rate of 10Hz. The 1064 nm wavelength provides strong energy absorption in metallic materials, while

the 532 nm wavelength offers shorter pulses, allowing for finer control over heat input and minimizing thermal damage to the surrounding area. The 9 ns pulse width was chosen as it balances high peak power with minimal heat diffusion, ensuring localized hardening without affecting the bulk material. The energy of the laser can be controlled by adjusting the oscillator drive, amplifier drive, and FL delay. After measuring the laser energy levels at various settings, the Laser Shock Peening (LSP) process was initiated. During this procedure, a continuous flow of water was directed over the turbine profile blade, which was securely mounted on a rotating holder attached to a CNC-controlled table. This configuration allowed precise control over the movement and orientation of the component throughout the peening process. A focusing lens with a focal length of 100 mm was employed to concentrate the laser beam onto the target surface. The distance between the focusing lens and the component was maintained at 105 mm, referred to as the Stand-Off Distance (SOD). With this optical setup, a laser spot diameter of approximately 0.987 mm (close to 1 mm) was achieved. Based on this diameter, the calculated spot area was approximately 0.767 mm^2. A high overlap ratio of 90% was maintained between successive laser spots to ensure uniform surface treatment and enhanced residual stress distribution. The LSP process parameters were carefully selected to study their effect on the mechanical properties of the treated surface. The laser fluence was varied within the range of 5 GW/cm^2 to 15 GW/cm^2, and the corresponding laser energy was adjusted from 0.326 J to 0.986 J. These parameters were systematically analyzed to optimize the microhardness of the turbine blade surface, which was considered the primary response variable.

Table 2.3 Machine Specification

Wavelength (nm)	1064,532,355
Max. Output (J)	1
Pulse duration (ns)	9
Class of laser	4
Laser Medium	Nd: YAG

Subsequently, the sample treated under optimal LSP conditions underwent further evaluation, including mechanical testing and tribological ,An evaluation is carried out to determine enhancements in surface quality, resistance to wear, and the overall functionality of the component.

2.4 Mechanical Testing

Different mechanical testing like Micro-Hardness test and surface measurement test are performed on the DED deposited sample and Laser shock peening sample and its effects are studied.

2.4.1 Micro-Hardness Measurement

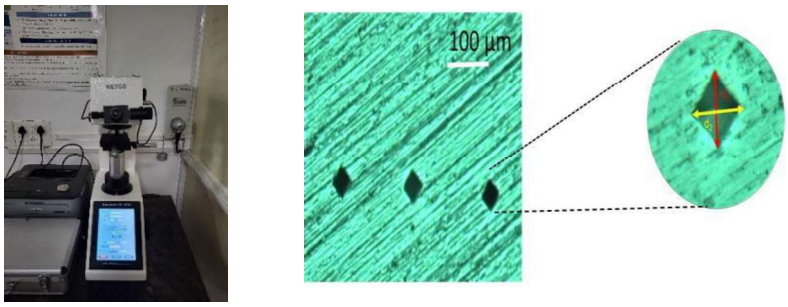

Fig 2.5 Vickers hardness setup and Microhardness indentations at 0.2 kg (1.96N) load with 10 sec dwell

Micro-hardness testing was performed using Micro-Vickers VH-1MDX (Economet VH-1MDX) with 200g load and 15 sec dwell time at the build direction section of each sample at different locations and the average of these value reported. Apart from that the micro-indentation for micro hardness measurement of DED deposited sample under optimal parametric setting, is observed along the deposition with 1 mm interval shown in the figure. To find out how laser shock peening affected the micro-hardness, a micro-hardness test was also run across the surface of cross section of build direction of sample.

P=load=0.2 kgf =1.96 N

D = d1+d2/2

HV = 1.854(P/D^2) (HV stands for Vickers Pyramid Number)

Where P denotes the value of load applied and D is the diagonal length calculated from the indentation made.

2.4.2 Compression Measurements Test

The compression testing setup consists of a Universal Testing Machine (UTM) configured for quasi-static testing. The UTM employed for the experiment is the CNC-controlled AGX-10KNVD model with a maximum load capacity of 10 kN. As shown in the schematic, the system includes two primary compression dies between which the test specimen (component) is positioned. These dies apply a uniform compressive force along the axial direction of the specimen. The entire assembly is mounted on a rigid workbench to ensure stability during the testing procedure. The UTM operates at a constant crosshead speed of 1 mm/min, resulting in an approximate strain rate of 0.003 s^{-1}. Data acquisition, including stress-strain response, is monitored and recorded in real-time through an integrated computer system linked to the testing machine.

Fig. 2.6 Pictorial View of Compressive Strength Measurement Setup

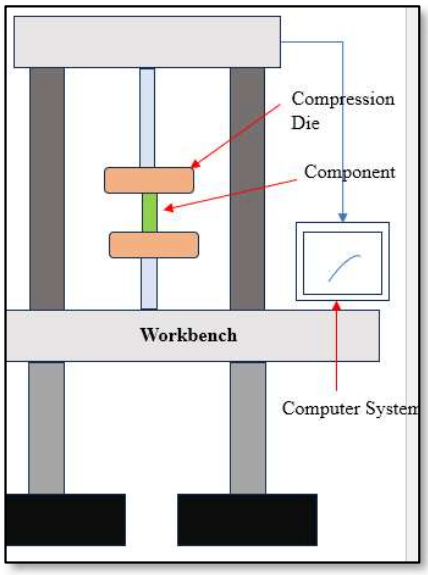

Fig. 2.7 Schematic View of Compressive Strength Measurement setup

2.5 Microstructure Analysis

To analyze the microstructure, cross-sectional samples were cut from the DED-fabricated part. These samples were subjected to careful metallographic preparation. They were first ground by 2000-grit silicon carbide paper to remove the surface imperfections. This was then followed by fine polishing with a 1 µm diamond suspension and polishing with a 0.25 µm diamond paste to get a mirror finish appropriate for microscopic examination. In etching, Keller's reagent was used to expose the grain boundaries and other microstructural characteristics. Polished samples were immersed in the etching reagent for about 25 seconds. The composition of the chemical etchant used is presented in Table 2.3 and involves the use of distilled water, nitric acid (HNO_3), and hydrofluoric acid (HF) in certain volumetric ratios. After etching, samples were investigated by an inverted optical microscope to assess the grain structure, dendritic morphology, and potential defects such as porosity or micro-cracks. The study sheds light on the solidification behavior and thermal history of the DED process.

Table 2.4 Etchant solution for Microstructure analysis

Ingredients	Distilled Water	Nitric Acid (HNO3)	Hydrofluoric Acid (HF)
Volume (ml)	100	5	2

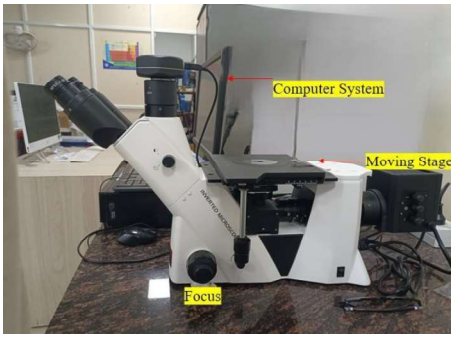

Fig 2.8 Optical Microscope

2.6 Characterization Techniques of Materials

The Directed Energy Deposition (DED) deposited sample and treated by Laser Shock Peening (LSP) sample were analyzed using multiple characterization methods to confirm their material properties. Morphological characteristics were examined through X-ray Diffraction (XRD) analysis to assess crystallographic changes. Additionally, the surface topography of the deposited samples was evaluated using 3D scanning techniques. Surface roughness measurements were conducted using a contact-type profilometer to quantify surface finish and texture.

2.6.1 X-Ray Diffraction

X-ray diffraction (XRD) is a common non-destructive method used to determine a material's crystal structure, crystallinity, and the existence of any second or impurity phases. The technique relies on the detection that upon interaction between high-energy X-ray beams and a crystalline material, energy is lost and electrons are excited from inner to outer, higher energy levels. These energetic electrons are unstable and migrate back to their initial, more stable energy levels, giving out X-rays in the process. Transitions of electrons from the M shell to the K shell produce Kβ radiation, while transitions from the L shell to the K shell produce

Kα radiation. The fundamental principle of analysis in XRD is Bragg's Law, which describes how X-rays are diffracted by the periodically repeating arrangement of atoms within a crystal structure. The law states that constructive interference results when the path difference between successive rays reflected off crystal planes is an integer multiple of the wavelength of the X-rays. Bragg's equation mathematically represents this condition:

$$n\lambda=2d\sin\theta$$

where:

- n is the order of diffraction (an integer),
- λ is the wavelength of the incident X-rays,
- d is the distance between adjacent crystal planes (interplanar spacing),
- θ is the angle of incidence (Bragg angle).

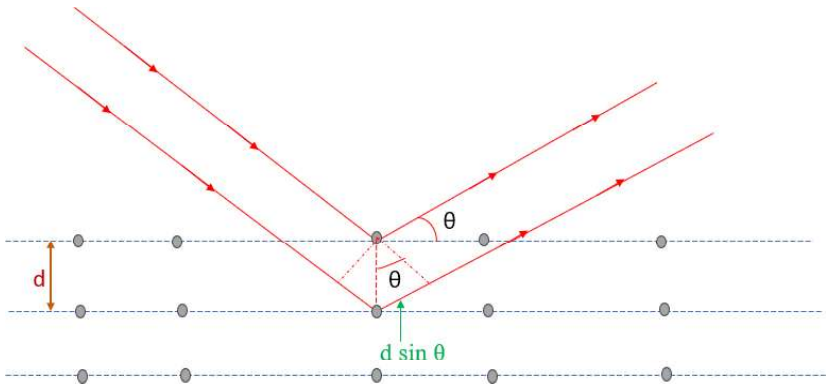

Fig 2.9 Bragg Diffraction Diagram

When this condition is satisfied, the reflected X-rays interfere constructively, producing a peak in the diffraction pattern. By analyzing these peaks, one can determine the crystallographic structure, lattice parameters, and phase composition of the material.

2.6.2 3-D Scanning test

The EinScan-SP V2 is a cutting-edge desktop 3D Scanner designed by Shining 3D, renowned for its precision and user-friendly operation. Utilizing Structured Light Scanning (SLS) technology, this scanner ensures high-quality scans with exceptional accuracy. It offers both Fixed Scan modes: with and without turntable, providing versatility to accommodate various scanning needs. With an impressive scan accuracy of up to 0.05 mm (0.002 in), the Ein Scan-SP V2 delivers detailed and precise 3D modes of objects.

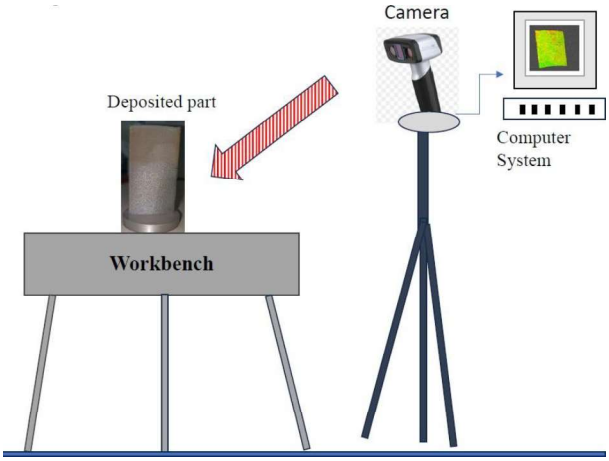

Fig 2.10 3D Scanning of DED deposited Sample

Despite its remarkable precision, it maintains a fast-scanning speed, capturing a single scan in just 4 seconds and completing an automatic scan mode in only 1 minute. This Scanner supports texture scanning and exports files in commonly used formats like STL, OBJ, and PLY. Its intuitive software simplifies the scanning process and offers comprehensive editing and processing capabilities. In this study, a EinScan-SPECS Desktop 3D Scanner is employed to study the overall geometry of DED deposited sample as shown in figure.

2.6.3 Contact Profilometer

2D Contact Profilometry (Mitutoyo SJ-410 model 178-397) is technique used to measure the surface profile and topography of a material or object in two

dimensions. This method involves physical contact between a stylus or probe and the surface being measured. In the present study 2 D contact profilometry as shown figure is used to measure DED deposited sample and Laser shock peening samples.

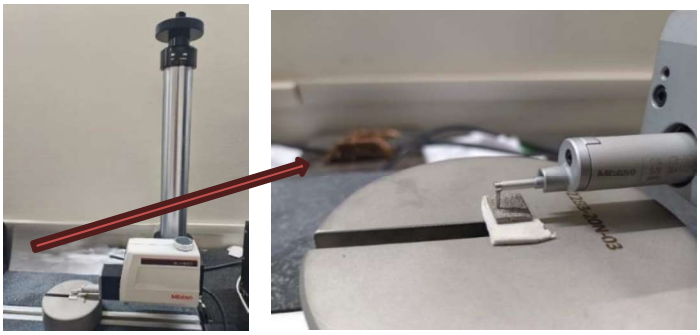

Fig 2.11 Pictorial View of Contact Profilometer

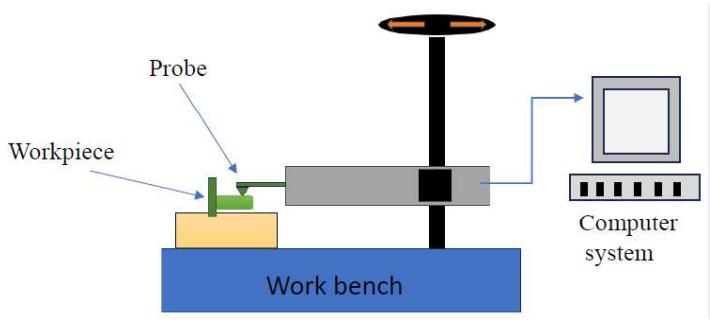

Fig 2.12 Schematic View of Contact Profilometer

2.6.4 Electro-chemical Polishing

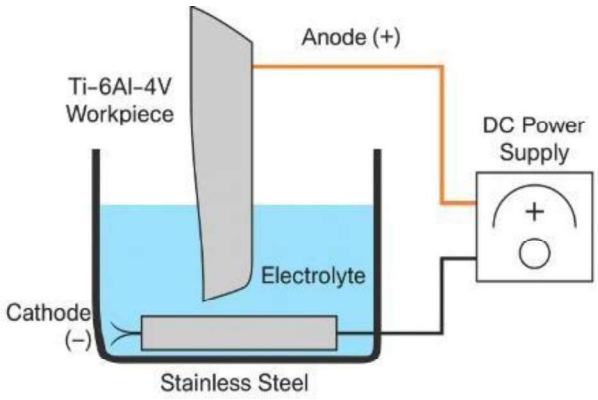

Fig 2.13 Schematic View of Electro-chemical Polishing Setup

Fig 2.14 Pictorial View of Electro-chemical Polishing

The electrochemical polishing (ECP) process for surface roughness improvement of a Ti6Al4V turbine profile blade fabricated using the Directed Energy Deposition (DED) method involves a carefully controlled setup designed to achieve uniform surface finish and minimize micro-defects on the blade's complex geometry. In this setup, the turbine blade serves as the anode, while stainless steel is employed as the cathode, both submerged in a specially prepared electrolyte solution. The electrolyte composition totals approximately 118.75 mL, consisting of 12.5 mL of perchloric acid ($HClO_4$), 100 mL of methanol (CH_3OH), and 6.25 mL of hydrofluoric acid (HF). This mixture is selected due to its efficacy in selectively dissolving the asperities on the surface of titanium alloys without introducing mechanical damage, enabling a smooth, bright, and defect-free finish. The methanol serves as a solvent and cooling medium, while the perchloric and hydrofluoric acids work synergistically to facilitate electrochemical dissolution of surface irregularities and passive layer breakdown on the Ti6Al4V alloy.

A constant current density of approximately 0.1 A/cm² is applied throughout the polishing process to ensure steady material removal while avoiding localized overheating or over-polishing that could compromise the integrity of the part. To maintain thermal stability and ensure safety, especially considering the volatility of perchloric acid and the aggressive nature of hydrofluoric acid, the electrolyte bath is kept at a controlled temperature between 10°C and 15°C using a refrigerated cooling system or ice bath. This low-temperature environment not only helps to suppress unwanted side reactions and vaporization of volatile components but also

contributes to a more uniform polishing effect across the complex surface contours of the turbine blade.

2.6.5 Polishing Machine

Fig 2.15 Pictorial View of Polishing Machine

The METCO BAINPOL grinding and polishing machine, as shown in the figure, was utilized for the metallographic preparation of specimens. This equipment is equipped with two independent polishing discs, each integrated with a water outlet to facilitate wet grinding and polishing processes. The machine includes an emergency stop button to ensure operator safety and features a digital control interface for adjusting parameters such as rotational speed and polishing duration. It is specifically designed to produce smooth and reflective surfaces on samples, which are essential for accurate microstructural examination. Additionally, a maintenance reminder is displayed on the front panel, emphasizing the importance of cleaning the machine after each use to maintain its efficiency and operational life.

Chapter 3: Experimental Investigation into Laser based Direct Energy Deposition (LDED) of Ti6Al4v Turbine Profile Blade

In this chapter, the parametric optimization of the Laser Based DED process parameters and its effect on the output response, like Micro-hardness, surface roughness measurement, and 3D scanning of deposited Ti6Al4V turbine profile blade, whose thin wall like structure is discussed. The mechanical and tribological performance of the DED deposited turbine profile blade part at optimal parametric conditions has also been discussed.

3.1 Factorial Design experiment for Process Parameter

Factorial Design experiments were conducted to understand the importance of the process parameters of DED to the quality of the produced part. According to the factorial Design experiments, the process parameters were chosen for the factorial Design of experiments model for the parametric optimization of the DED deposited Ti6Al4V Turbine Profile Blade.

3.1.1 Influence of Stand Of distance (SOD) on Ti6Al4V turbine profile blade

In the Directed Energy Deposition (DED) process, the stand-off distance (SOD)—the space between the nozzle and the workpiece—is a key parameter that significantly affects the efficiency of material delivery and the quality of the deposited layer. Especially when working with titanium alloys such as Ti6Al4V. In our study, we investigated the effect of varying the SOD from 9.5 cm to 10.5 cm during the deposition of Ti6Al4V tracks on a commercially pure titanium substrate. The results revealed a clear correlation between SOD and the morphology of the deposited tracks. Specifically, increasing the SOD led to a noticeable increase in the height of the deposited layers. At a higher SOD, the powder stream had a more diffused trajectory, allowing for better overlap and distribution on the substrate surface. This contributed to a more uniform track profile and a consistent layer

height, which is desirable for building multi-layer components with predictable geometry [56]. On the other hand, when the SOD was reduced to the lower end of the tested range, the deposition was less efficient. The powder particles, having less time to interact with the laser beam and melt zone, exhibited poor bonding and reduced layer height. In several instances, incomplete fusion and discontinuities were observed at lower SODs, resulting in inadequate track formation. This suggests that the interaction between the powder stream, laser beam, and substrate becomes less effective as the SOD decreases, likely due to improper focus and misalignment of the melt pool with the powder delivery zone.

Fig 3.1 Track deposition on Titanium Plate

The choice of SOD directly affects not only the geometric characteristics of the deposited track but also the quality and continuity of the layer. For Ti6Al4V deposition on a titanium substrate, maintaining an optimal SOD ensures a stable melt pool, efficient powder utilization, and enhanced track uniformity. Moreover, an appropriate stand-off distance minimizes spattering and material loss while promoting better metallurgical bonding between the layers and the substrate results underscore the significance of optimal process parameters in DED, especially when working with reactive and high-strength alloys such as Ti6Al4V. Optimizing the SOD results in successful dimensional accuracy and mechanical integrity of the finished part, which is essential for aerospace and biomedical uses where titanium alloys are widely utilized.

3.1.2 Influence of Power and Scan Speed on Ti6Al4V turbine profile blade

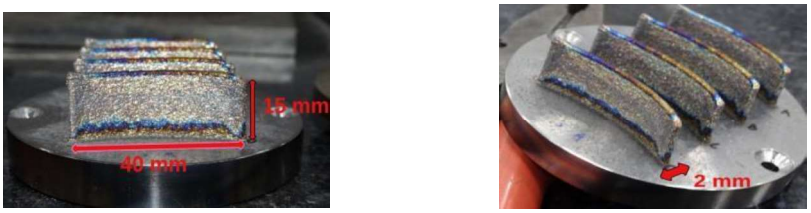

Fig 3.2 Deposition of blade height 15 mm with different power from 400 to 360 W

During the Directed Energy Deposition (DED) process using Ti6Al4V powder, I conducted a series of experiments to study how laser power and scan speed influence the quality of single-layer tracks deposited on a substrate with a defined target height. The deposition process began at lower laser powers and was progressively increased to examine the effects on track morphology and stability. At laser power levels below approximately 500 W, I observed that the energy supplied to the melt pool was inadequate to fully melt the incoming powder. This led to inconsistent melt pool formation and, in some cases, a failure to initiate deposition. In these conditions, some powder particles only partially melted and loosely adhered to the substrate, while others remained un-melted, creating a layer of loose powder that negatively impacted subsequent track formation. Post-process inspections confirmed the presence of scattered, un-melted particles around the deposited regions, contributing to surface defects and irregular track geometry. As I increased the laser power to a range between approximately 550 W and 800 W, the deposition behavior improved significantly. The powder particles were more consistently melted, and stable melt pools formed, allowing for more uniform and continuous track deposition. However, operating at the higher end of this power range (especially above 750 W) introduced new challenges. Localized overheating and excessive energy input caused not only full melting but also partial vaporization of powder near the laser interaction zone. In several instances, this led to reduced track height, powder blow-off, and occasional track disappearance due to melt pool instability. Additionally, visible spattering and surface imperfections indicated that excessive power, while improving melting, could induce secondary defects if not properly managed, to further understand the process, I also varied the scan speed in

conjunction with laser power. It became evident that scan speed played a crucial role in defining the energy input per unit length and the resulting track geometry. Increasing the scan speed reduced the interaction time between the laser and the substrate, leading to narrower, shallower melt pools. This often resulted in thinner tracks and, in some cases—particularly when combined with lower laser power—led to failed deposition due to insufficient melting. On the other hand, reducing the scan speed allowed the laser to dwell longer at each point, delivering more energy into the substrate. This increased energy input promoted deeper melt pools and enhanced powder capture, producing wider and thicker tracks. Nevertheless, extremely low scan speeds posed risks such as overheating, excessive dilution with the substrate material, and bead sagging due to prolonged thermal exposure. The figure above shows the multi-layer Ti6Al4V turbine blade profiles that I fabricated using the DED process. During the deposition, I noticed that when higher laser power or slower scan speeds were applied, overheating became a major issue. This was clearly visible through surface irregularities, oxidation-related discoloration, and uneven layer buildup along the blade height. In these cases, the excessive heat input caused the melt pool to grow too large, leading to distortion and sagging in the upper layers. As more layers were deposited, these effects became increasingly evident, emphasizing the need to fine-tune process parameters to ensure uniform geometry and high-quality builds throughout the process.

Table 3.1 Variation of power from 400 W to 360 W during the deposition of a 15 mm blade height

Power (w)	Scan Speed (mm/min)	Height (mm)	Thickness (mm)	Number of Layers
400	600	15	1.99	50
380			2.00	
370			2.05	
360			2.01	

After analyzing the results from multiple trials, I identified an optimal process window for producing consistent, high-quality single-layer tracks. This window was observed when using laser power levels between 500 W and 700 W, coupled with scan speeds ranging from 600 mm/min to 750 mm/min. Under these parameters, I achieved tracks with uniform height and width, good surface finish, and strong metallurgical bonding to the substrate. The tracks also displayed continuous geometry and minimal surface defects, the success of track formation in the DED process using Ti6Al4V powder strongly depends on a balanced combination of laser power and scan speed. Insufficient power results in poor melting and weak deposition, while excessive power leads to vaporization and surface flaws. Likewise, overly high scan speeds hinder energy delivery, while excessively slow speeds may cause overheating. The identified optimal window ensures reliable deposition and is critical for maintaining the quality and integrity of the turbine profile blade during fabrication.

3.1.3 Influence of Cooling time on Ti6Al4V of profile blade

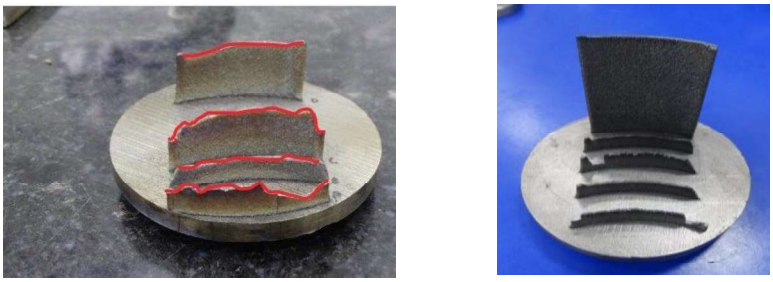

Fig 3.3 Photographic view of deposited Ti6Al4V turbine Profile Blade

During my experiments with the Directed Energy Deposition (DED) process for building Ti6Al4V turbine blade profiles, I started with simple single-layer depositions and gradually moved towards multi-layer structures. The main goal was to understand how laser power and inter-layer cooling time affect the quality of the final build. Throughout the process, I maintained a constant scan speed of 600 mm/min and a powder feed rate of around 1.1 rpm (approximately 3.5 grams per minute). Initially, I began deposition using a laser power of 400 W. With these

settings, I aimed to fabricate a multilayer structure having a width of 40 mm and a height of 15 mm. Based on a layer thickness of about 0.3 mm, the build required roughly 50 layers. However, I quickly ran into issues during this process. I observed problems such as overheating, surface irregularities, oxidation (visible through discoloration), and inconsistent layer buildup along the blade height. These issues were more noticeable in the upper regions of the build, where it became clear that the heat from each new layer wasn't dissipating fast enough, causing thermal accumulation. To try and fix this, I reduced the laser power step by step, from 400 W down to 360 W, while keeping the scan speed and powder feed rate the same. Unfortunately, the same problems persisted. Even at lower power, I noticed signs of overheating and non-uniform track formation. This made me realize that reducing power alone wasn't enough—the issue seemed to be related to the continuous deposition without giving the part enough time to cool down between layers. To tackle this, I decided to introduce cooling time (or dwell time) between the deposition of each layer. Initially, I wasn't using any cooling time—the laser would start the next layer immediately after finishing the previous one. So, I planned a series of trials where I kept the laser power fixed at 400 W and scan speed at 600 mm/min, but added inter-layer cooling times of 6, 10, and 12 seconds.

Table 3.2 Increases Dual time between the layer with constant Power and Scan Speed

Power (w)	Scan speed (mm/min)	Time between the layers (sec)
400	600	0 6 10 12

As I increased the cooling time, I observed a clear improvement in the quality of the deposited structure. The added pause between layers allowed the material and substrate to cool properly, which helped reduce heat buildup and improved heat

transfer balance. The melt pool became more stable, and the track geometry became more consistent. Among the three trials, the structure with a 12-second dwell time gave the best results. It had minimal surface roughness, reduced oxidation marks, and better bonding between the layers. The improvements achieved by increasing the cooling time can be clearly seen in the image above. The three structures shown represent deposition trials with cooling times of 0, 6, and 12 seconds (bottom to top, respectively). As indicated by the red contour lines, the bottom structure—fabricated without any cooling time—exhibits severe surface waviness, uneven layer buildup, and clear signs of thermal distortion. The middle structure, with a moderate cooling time of 6 seconds, shows some improvement but still lacks consistency in geometry. In contrast, the top structure, built with a 12-second inter-layer dwell time, displays the most uniform and stable profile. The layer boundaries appear smoother and more consistent, indicating better thermal control and layer bonding. From these results, it became clear that managing the heat during deposition is extremely important, especially for multilayer builds. Adding a cooling time between layers played a major role in avoiding common problems like overheating and distortion. I also realized that just adjusting the laser power isn't always enough—thermal control through dwell time can significantly improve the build quality, I found that overheating in multilayer Ti6Al4V DED builds can't be solved by power reduction alone. Introducing proper inter-layer cooling times helped stabilize the process, improve deposition quality, and achieve better structural integrity. These findings, along with the visual improvements shown in the image, highlight how critical it is to manage heat input in additive manufacturing, particularly when working with reactive materials like Ti6Al4V.

3.1.4 Design of Experiment

In this part of my study, I followed a structured Design of Experiments (DOE) approach, specifically using a full factorial design, to systematically investigate how laser power and scan speed affect the outcomes of the Directed Energy

Deposition (DED) process using Ti6Al4V powder. The primary goal was to examine the influence of these two critical parameters on the geometrical quality of the deposited tracks—namely the track height and width. These geometrical characteristics are crucial for ensuring dimensional accuracy, mechanical performance, and surface quality, especially in applications like turbine blades where precision is essential. For this experiment, I selected laser power as a variable with five different levels: 400 W, 500 W, 600 W, 700 W, and 800 W. This range allowed me to observe the effects of both low and high energy input on the melt pool behavior and the resulting track morphology. Scan speed, on the other hand, was set at two levels: 600 mm/min and 750 mm/min. These values were chosen based on prior knowledge and initial trial runs, as they represent realistic operating conditions under which the DED process can be performed with stability, avoiding major defects such as porosity or track deformation.

The combination of these two factors—five power levels and two scan speeds—formed a 5 × 2 full factorial design, resulting in 10 unique experimental runs. For each run, I deposited a single-layer track using a specific power-speed combination, and then I measured the resulting track height and width. This full factorial setup allowed me not only to assess the individual effect of each parameter but also to study any possible interaction between them, such as how scan speed might influence track geometry differently depending on the applied laser power. After conducting the experiments, I used statistical analysis tools—mainly MINITAB and Origin—for data processing and interpretation. I applied ANOVA (Analysis of Variance) to identify which factors significantly affected the track dimensions and to quantify the strength of those effects. I also used Origin to generate plots, visualize trends, and explore interaction effects through surface and interaction plots, helping me better understand the relationships between the input parameters and the observed outputs. Overall, this full factorial experiment gave me a comprehensive understanding of how laser power and scan speed interact to influence the deposition characteristics in the DED process. The findings from this phase not only highlight the optimal ranges for these parameters but also form the

basis for future optimization and process modeling in metal additive manufacturing, particularly for components requiring high geometrical accuracy such as turbine blade profiles.

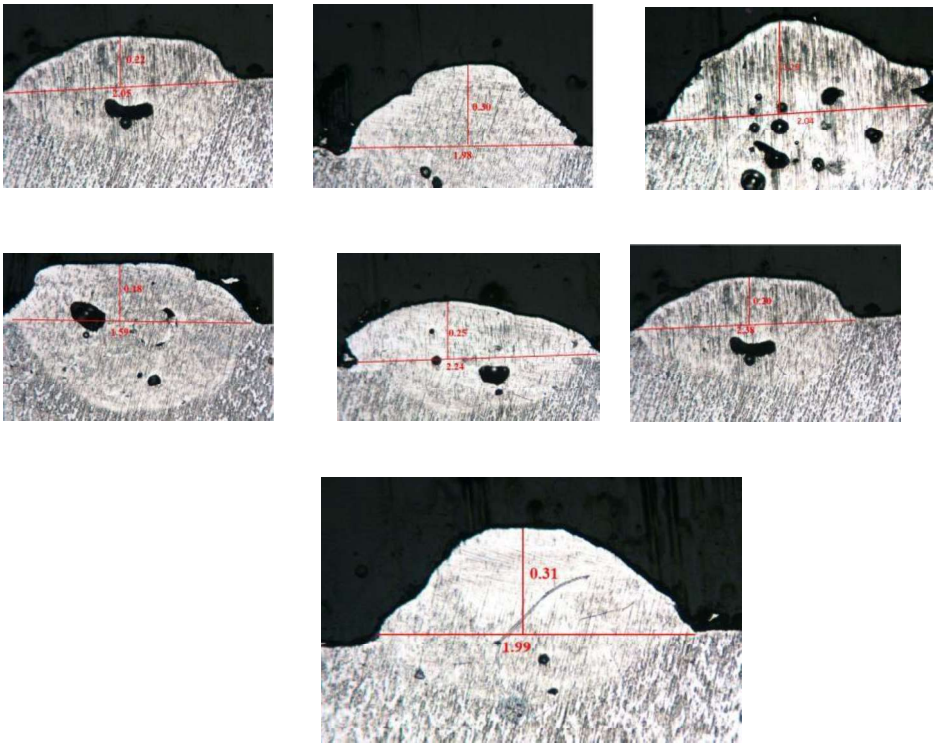

Fig 3.4 Track Dimensions Measured by LEICA Software

In this phase of the study, after the laser deposition process was completed on the titanium substrate, the deposited samples were sectioned using a wire-cut Electrical Discharge Machining (EDM) system to obtain precise cross-sectional cuts without inducing thermal damage or mechanical deformation. These cross-sections were then subjected to a standard metallographic polishing procedure using abrasive papers ranging from 320 to 2500 grit to achieve a mirror-like surface finish suitable for microstructural and dimensional analysis. Following the polishing, the cross-sectional geometry of each deposited track was examined under an optical microscope. High-resolution images were captured using a LEICA imaging system, which also enabled accurate measurement of the track dimensions. Both the track width (w) and height (h) were recorded in millimeters. These measurements were

essential for calculating two critical parameters: the aspect ratio and the deposition rate. The aspect ratio of each deposition track was calculated using the formula:

$$\text{Aspect Ratio} = h/w$$

where h is the height of the deposited bead and w is the width. This ratio provides insight into the shape stability and material flow during the deposition process. A higher aspect ratio typically indicates greater build height and improved vertical growth control.

To evaluate the efficiency of the material deposition process, the deposition rate was determined using the following formula:

$$\text{Deposition Rate (mm}^3\text{/min)} = (2/3) \times h \times w \times \text{Scan Speed}$$

where the scan speed is expressed in mm/min. This calculation helps quantify how much material is being deposited per unit time, which is critical for assessing the process productivity and optimizing manufacturing throughput. Through this procedure, I systematically evaluated the influence of different processing parameters on the geometry and build efficiency of the deposited tracks. All measured data and corresponding images were saved for further analysis and comparison in order to identify trends and establish optimal conditions for uniform, defect-free deposition.

Table 3.3: Experimental design and value of response based on Design of Experiment

Sr. NO.	Power (w)	Scan Speed (mm/min)	Height (mm)	Width (mm)
1	400	600	0.31	1.99
		750	0.29	2.04
2	500	600	0.30	1.98
		750	0.30	2.08
3	600	600	0.22	2.05
		750	0.31	2.34
4	700	600	0.29	2.29
		750	0.20	2.38
5	800	600	0.25	2.24
		750	0.18	1.59

3.2 Development of Mathematical Response based on Design of Experiment

```
Factor Information
Factor  Type   Levels  Values
A       Fixed       5  400, 500, 600, 700, 800
B       Fixed       2  600, 750


Analysis of Variance
Source  DF    Adj SS    Adj MS  F-Value  P-Value
  A      4  0.010700  0.002675     1.08    0.472
  B      1  0.000810  0.000810     0.33    0.599
Error    4  0.009940  0.002485
Total    9  0.021450
```

Model Summary

S	R-sq	R-sq(adj)	R-sq(pred)
0.0498498	53.66%	0.00%	0.00%

Coefficients

Term	Coef	SE Coef	T-Value	P-Value	VIF
Constant	0.2650	0.0158	16.81	0.000	
A					
400	0.0350	0.0315	1.11	0.329	1.60
500	0.0350	0.0315	1.11	0.329	1.60
600	0.0000	0.0315	0.00	1.000	1.60
700	-0.0200	0.0315	-0.63	0.560	1.60
B					
600	0.0090	0.0158	0.57	0.599	1.00

Regression Equation:

Height = 0.2650 + 0.0350 A_400 + 0.0350 A_500 + 0.0000 A_600 - 0.0200 A_700 - 0.0500 A_800
+ 0.0090 B_600 - 0.0090 B_750

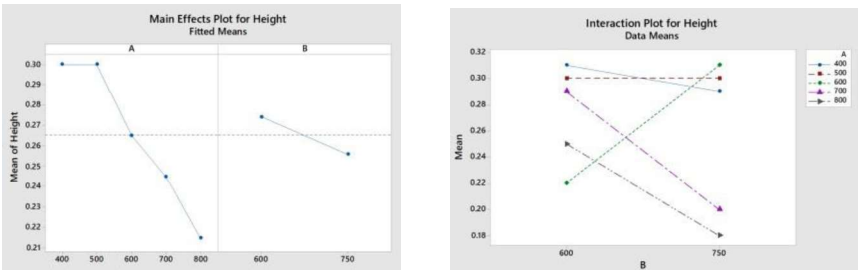

Fig 3.5 Graph 1and 2 height vs Power density and Scan speed (Interaction plot)

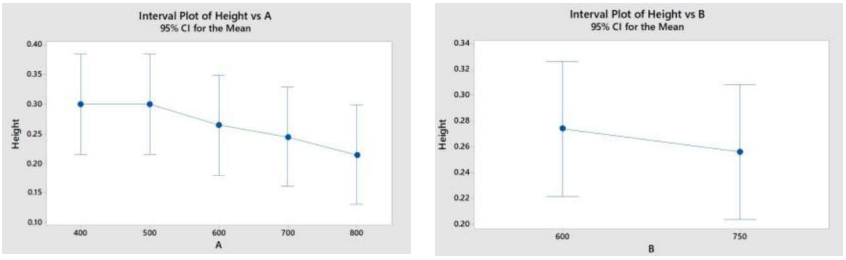

Fig 3.6 Graph 3 and 4 effect of factor A and B on Height of Track

While analyzing the **graph 1** of fitted means for height across different levels of factor A (laser power, ranging from 400 W to 800 W) with factor B (scan speed) held constant, I observed a slight increasing trend in the mean height values as the power increased. However, this increase gradually began to taper off. Beyond the mid-range power levels, the change in height became minimal, indicating that further increases in power did not significantly influence the track height. This behavior suggests that the height response may have reached a saturation point, and other external or process-related factors could be contributing to the variations observed at higher power levels. Upon examining the interaction plot (**Graph 2**), I observed how the mean height values varied with different combinations of factor A (laser power) and factor B (scan speed). Interestingly, the mean heights fluctuated as factor A increased, but there was no clear or consistent upward or downward trend. This irregular pattern suggests that the interaction between laser power and scan speed does not have a simple, linear effect on track height. Some combinations resulted in higher mean heights, while others did not show significant change, indicating a more complex relationship. It's likely that other variables—possibly environmental conditions or secondary process parameters—may also be influencing the deposition height. (**Graph 3)** While analyzing the graph displaying the 95% confidence intervals for the mean height across different levels of factor A (laser power), I noticed that some of the intervals overlapped, which suggests that the mean heights at those levels might be quite similar. However, there were also levels where the confidence intervals showed noticeable separation, indicating clearer differences in the mean heights. This observation implies that although there is a general trend of increasing height with higher power levels, the variation in confidence intervals also points to a degree of uncertainty in the measurements. These variations could be influenced by experimental inconsistencies or uncontrolled external factors affecting the deposition process. (**Graph 4**) In a similar manner to the previous plot, I examined the graph showing the 95% confidence intervals for mean height values corresponding to factor B (scan speed). I observed that the range of height values here was noticeably narrower compared to those associated with factor A (laser power). This suggests that the variation in

height due to changes in scan speed is more limited. From this, I inferred that while laser power has a stronger influence on the track height, scan speed appears to play a comparatively smaller role in affecting this particular output.

From my analysis, I observed that increasing the values of factor A (laser power) generally led to an increase in track height. However, this trend began to plateau at the higher power levels, indicating that beyond a certain point, further increases in power did not significantly affect the height. In contrast, factor B (scan speed) appeared to have a minimal effect on the height. The confidence intervals associated with factor B were much narrower, suggesting less variation in the measured height values across the different scan speeds. These observations point to the complexity of how laser power and scan speed interact to influence the deposition height. The trends are not entirely straightforward, and the presence of plateauing and limited variation suggests that other underlying factors may also be playing a role. This highlights the need for further investigation to better understand the dynamics of these parameters in the DED process.

Power (W)	400
Scanning Speed(mm/min)	600
Total Number of Layers	200
Layer Height (mm)	0.30
Carrier Gas or Flow rate (gram/min)	3
Feed Rate (rpm or Gram/min)	1.1 or 3.5
Cooling time between Succeeding Layers (Sec)	12

Fig 3.7 Deposited Profile Blade Ti6Al4V using DED

3.2.1 Analysis of Deposited Turbine Blade Through 3-D Scanning Test

In additive manufacturing, the dimensional accuracy and general quality of manufactured components are very important. 3D scanning is a great tool for determining these features through the creation of precise digital models of physical objects. In this research, we performed a 3D scanning test on turbine profile blades made by the Directed Energy Deposition (DED) process to determine the geometrical conformity and surface quality of the blades. or the 3D scanning operation, we utilized the Colin 3D software version 5.0.3, a full-fledged metrology software for accurate measurement and analysis of 3D scan data. The scanning setup involved a calibrated camera positioned at optimal angles to capture the intricate details of the turbine blades.

Scanning Process

1. **Camera Setup and Calibration**: The camera was carefully focused and calibrated to minimize distortion, ensuring high-quality data capture.
2. **Data Acquisition**: The scanning was conducted using a combination of static and rotational approaches to cover all surfaces of the turbine profile blades. Multiple scans from varying angles were implemented to obtain a comprehensive dataset.
3. **Model Generation**: The acquired scan data was processed to form a complete 3D model, which served as a virtual reference during quality assessment.
4. **Quality Control and Validation**: After generating the 3D model, it was compared against the original CAD data to evaluate dimensional accuracy, surface roughness, and any deviations from the intended design.

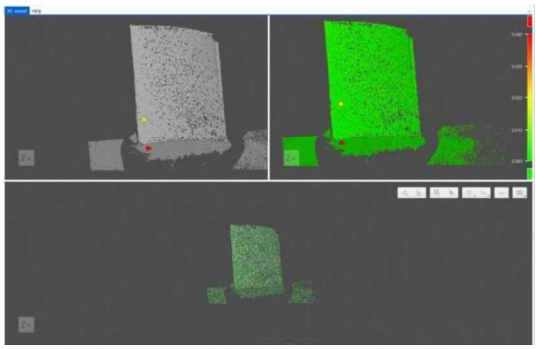

Fig 3.8 Scanning strategy

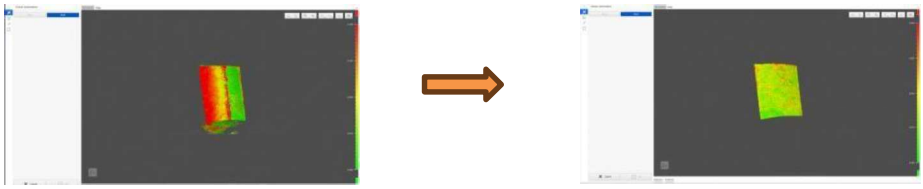

Fig 3.9 Combined All Planes

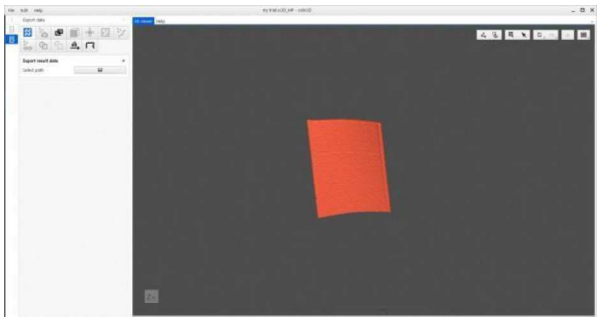

Fig 3.10 Fill Voids and errors and make perfect shape turbine profile blade

INSPECT Plus software is an advanced tool designed for the analysis and inspection of 3D models, particularly in the context of additive manufacturing. It enables users to conduct precise comparative evaluations between scanned parts and their original CAD designs, ensuring that manufactured components meet specified tolerances and quality standards. Upon importing STL files generated from 3D scans, INSPECT Plus utilizes sophisticated algorithms to align these models accurately, allowing for effective identification of any deviations from the desired specifications. One of the key features of INSPECT Plus is its color-mapping analysis, which visually represents discrepancies between the scanned

component and the reference model. This helps engineers easily identify areas needing attention, such as geometrical irregularities or excess material, which can significantly impact performance. Additionally, the software supports detailed measurement extraction, enabling users to quantify dimensions and assess conformity with design intent. By integrating INSPECT Plus into the quality control process, manufacturers can substantially enhance the reliability and accuracy of their additive manufacturing practices. This software not only aids in detecting potential defects but also facilitates continuous improvement efforts, ultimately contributing to higher standards of product quality and operational efficiency in modern manufacturing.

Comparison & Inspection Using INSPECT Plus Software:

1. Model Preparation & Import: The STL file generated from the scan is imported into INSPECT Plus software for detailed analysis. The original CAD model of the component is also loaded into the software to perform a comparative evaluation.
2. Alignment & Deviation Analysis: The scanned model and CAD model are aligned using best-fit algorithms to ensure accurate comparison. Colour-mapping analysis is performed to visualize deviations, highlighting areas where the manufactured part differs from the original design. Geometrical dimensions such as height, width, thickness, and curvature are inspected for variations.
3. Tolerance & Defect Detection: The software checks whether the manufactured component meets the specified tolerances. Surface defects such as distortion, unevenness, or dimensional changes resulting from the additive manufacturing process are detected and analyzed. Critical zones such as edges, holes, and complex geometries are examined for potential defects.
4. Measurement & Report Generation: Key dimensional measurements are extracted to verify conformance with the design requirements. The inspection report is generated, detailing deviations, tolerance limits, and any

necessary corrections. The results can be used for process optimization, rework decisions, or quality control documentation.

By integrating Colin 3D scanning with INSPECT Plus software, we achieve a comprehensive quality assessment of the additively manufactured turbine blade. This ensures that the final component meets design accuracy, functional requirements, and industry standards.

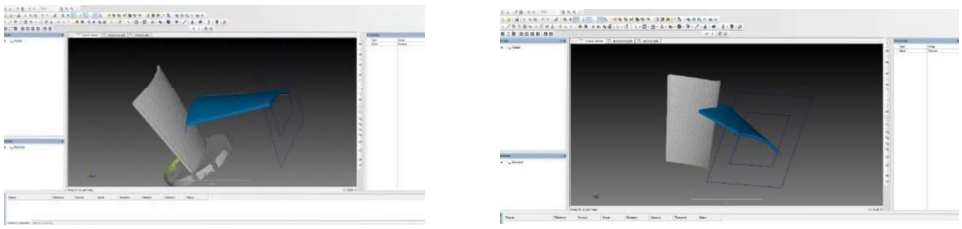

Fig 3.11 Actual (deposited) and Nominal part (CAD)

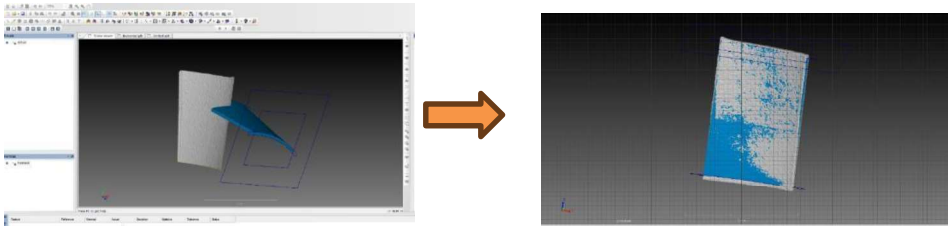

Fig 3.12 Alignment (best fit both part)

Analysis of Surface Comparison: Surface comparison plays a vital role in quality assurance by examining the geometric correlation between a manufactured part and its original CAD design. By using tools like INSPECT Plus, this process employs a color-mapping technique to highlight deviations, showcasing areas that align with the design and those that require adjustments. This analysis focuses on surface smoothness, dimensional precision, and tolerances, enabling the detection of issues such as surface irregularities or material inconsistencies. To conclude, conducting thorough surface comparisons is crucial for confirming that parts adhere to design standards. It allows for the swift identification of manufacturing flaws, enhances quality control, and fosters ongoing advancements in production methods.

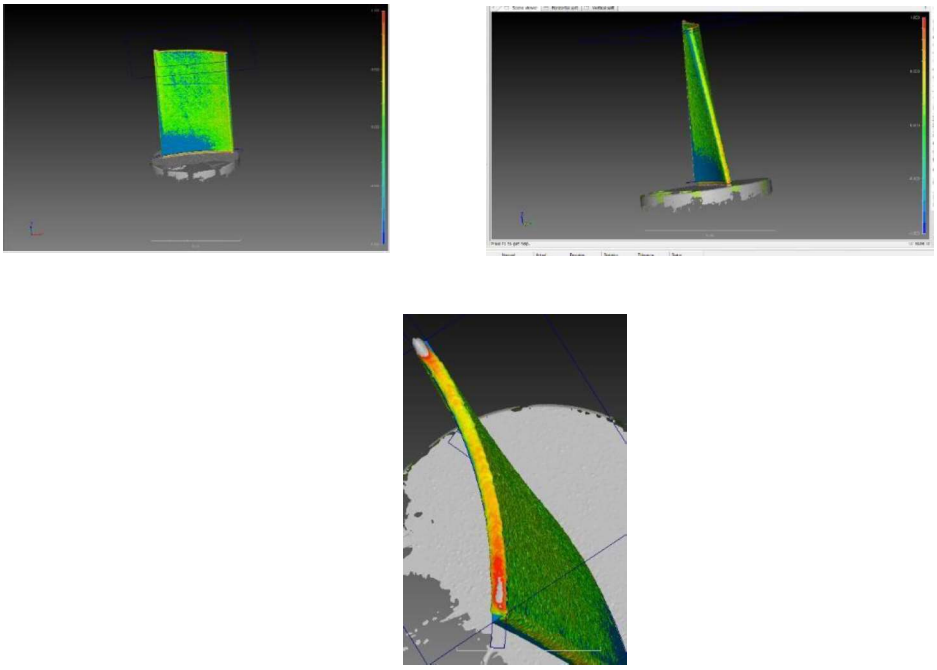

Fig 3.13 Surface Comparison

The visuals presented are from INSPECT Plus software, which is typically used for analyzing 3D scans of parts. These images compare the scanned surface of a component to a reference model, often a CAD design or another scan. The color map illustrates how much the scanned surface deviates from the reference.

- **Green areas** show that the surface closely matches the reference, falling within acceptable tolerance levels.
- **Yellow and orange tones** point to small discrepancies, which may be due to slight material build-up or surface imperfections.
- **Red zones**, found mostly along edges, often mean there's too much material or a noticeable raised area.
- **Blue regions** indicate the surface is lower than expected, suggesting possible material loss or wear.
- **White spots** could be anomalies, noise in the scan data, or regions that require further inspection.

Analysis of Section Comparison: Sectional comparison is an essential part of analyzing a manufactured component's accuracy by evaluating cross-sections between the actual part and its CAD model using INSPECT Plus software. Once the component is imported into the software, the relevant sections are extracted for comparison. This process allows for the calculation of absolute deviations, which quantifies the differences in dimensions between the manufactured part and the intended design. In this analysis, the average absolute deviation was found to be 0.11475 mm. A key reason behind these deviations often lies in the thermal behavior during the additive manufacturing process. Variations in heat distribution throughout the part can lead to differential cooling rates, causing discrepancies between the expected and actual dimensions of the manufactured component.

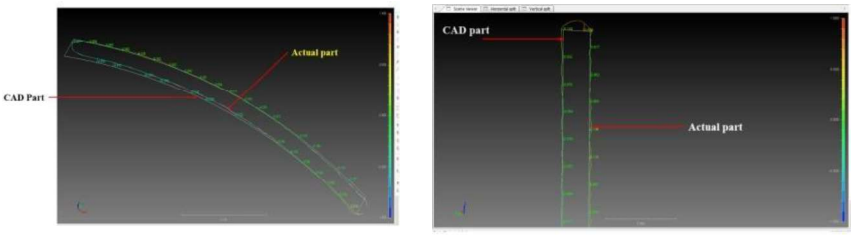

Fig 3.14 Scanning Direction and Built direction of Blade

The average absolute deviation between the actual part and the nominal CAD part is 0.11475 mm.

The maximum deviation is 0.132 mm.

The average absolute deviation is ~0.109 mm

Top region: ≈ 0.132 mm (positive deviation)

Middle region: ≈ 0.078 mm (negative deviation)

Lower region: ≈ 0.118 mm (positive deviation)

During the manufacturing process, heat distribution plays a crucial role in the deviation observed in the final part. At the initial stage of layer deposition, heat flows easily toward the substrate, resulting in better thermal dissipation. Similarly, at the final stage, heat is released into the atmosphere, leading to a positive deviation in these regions. However, in the middle portion, heat flow is interrupted, causing localized thermal accumulation. This results in differential cooling rates, leading to a negative deviation in this section. Additionally, factors such as material properties, deposition speed, and ambient conditions further influence the thermal behavior, contributing to the overall geometric variations in the part.

3.2.2 Analysis of Vicker's Hardness Test

The variation in Vickers hardness from top to bottom of the DED-manufactured turbine blade profile is mainly due to uneven heat distribution during the deposition process. The top and bottom sections show higher hardness values (around 480–485 HV) because they cool more rapidly— the bottom cools quickly due to contact with the cold substrate, while the top is exposed to ambient air without further heat input. In contrast, the middle section records lower hardness (around 460 HV) because it undergoes repeated thermal cycling from the layers deposited above and below, leading to heat accumulation. This sustained heat exposure can result in microstructural coarsening or partial annealing, reducing hardness slightly in this region. [57]

Table 3.4: Average Hardness Value as per Section of Blade

Section of Blade	Hardness Value (HV)
Top	480.13
Middle	460.92
Bottom	485.47

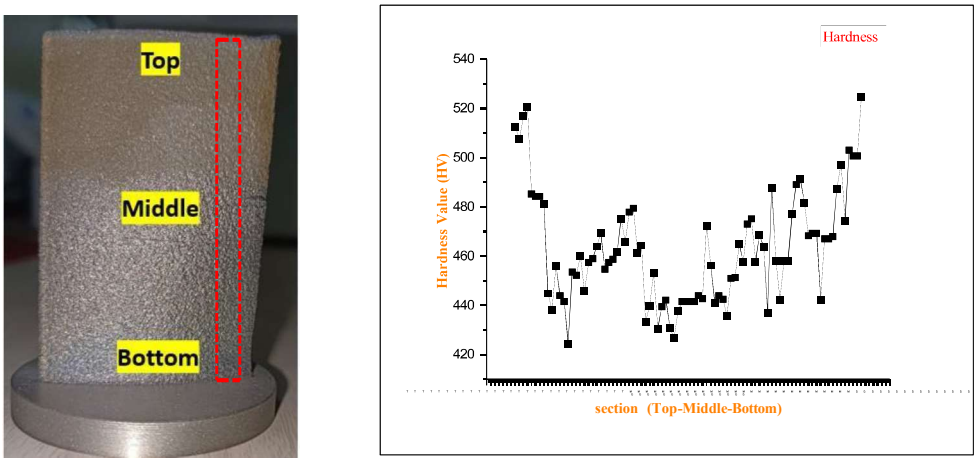

Fig 3.15 section of turbine profile blade and Graph of Profile of Turbine blade

3.2.3 Analysis of Compression load on the turbine profile blade

In this investigation, a thin wall of the Ti6Al4V material was utilized. The preparation of cylindrical samples was carried out using Wire EDM (Electrical Discharge Machining) in compliance with the ASTM E9 standard. Special attention was given to maintaining the recommended 1/d ratio of 1.5-2 during sample preparation, ensuring the attainment of precise and dependable test outcomes. Cylindrical samples were precisely cut from three distinct sections, namely top, middle and bottom surfaces. The cylindrical samples were carefully fabricated to possess a uniform diameter of 2 mm and a length of 4 mm, facilitating standardized testing conditions. The compression experiment has been carried out in a quasistatic manner at speed of 1 mm/min with a strain rate 0.003 $s^{-1}$by using the universal Testing Machine (UTM) (AGX-10KNVD) which is a CNC UTM of 10 KN capacity. The testing process was closely monitored using the system's digital interface, which recorded real-time load and displacement data. From the stress-strain curves obtained, I observed that the material demonstrated a high level of compressive strength, with the ultimate compressive strength measured at approximately 1012.69 N/mm^2. This value reflects the material's capacity to withstand high compressive loads, indicating excellent structural integrity of the

laser additively manufactured blade. The results also suggest that the additive manufacturing process used maintained sufficient bonding and density to support high-performance applications in load-bearing environments.

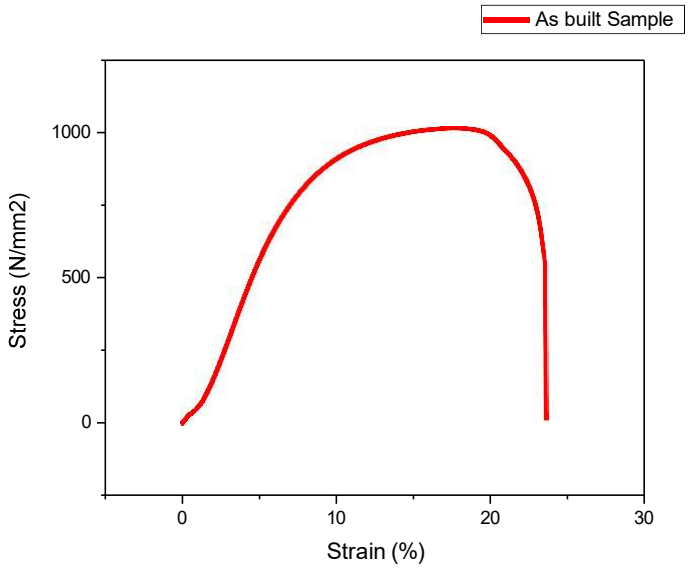

Fig 3.16 Compressive strength of as built sample

3.2.4 Analysis of Microstructure

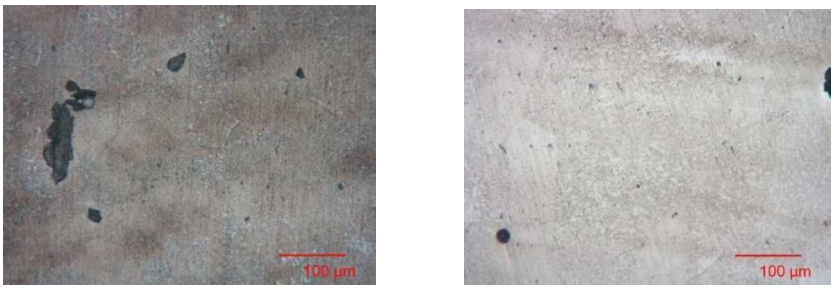

Fig 3.17 Microstructure of as built sample in built direction

When I looked at the microstructure of the Ti6Al4V turbine blade made using the DED process, I could see some important things about how good the material is and how well it might perform. In the image, there are some dark spots and uneven areas, which probably happened because the laser didn't fully melt the powder or the layers didn't fuse properly. This might be due to wrong settings like low laser

power or moving the laser too fast. These areas could cause weak points in the blade. There are also some small holes and particles, which might be oxides or trapped gas—these can lead to cracks or failure over time. The main part of the metal is usually made of alpha and beta phases, formed because the metal cools quickly and gets reheated again and again during printing. Normally, the grains grow in the same direction the blade was built, which might make the properties different in different directions. To clearly see the fine grain structure, higher magnification tools like SEM are needed. Also, because of changing heat during the process, the grain size or phases might not be uniform everywhere. To get detailed information, image analysis can help measure pores, grain shapes, and defects. These microstructural details are important because they affect the strength and durability of the part. To improve the quality, post-processing methods like heat treatment or HIP can be used. So overall, studying the microstructure helps me understand what went right or wrong during printing and how to make the blade better and more reliable.

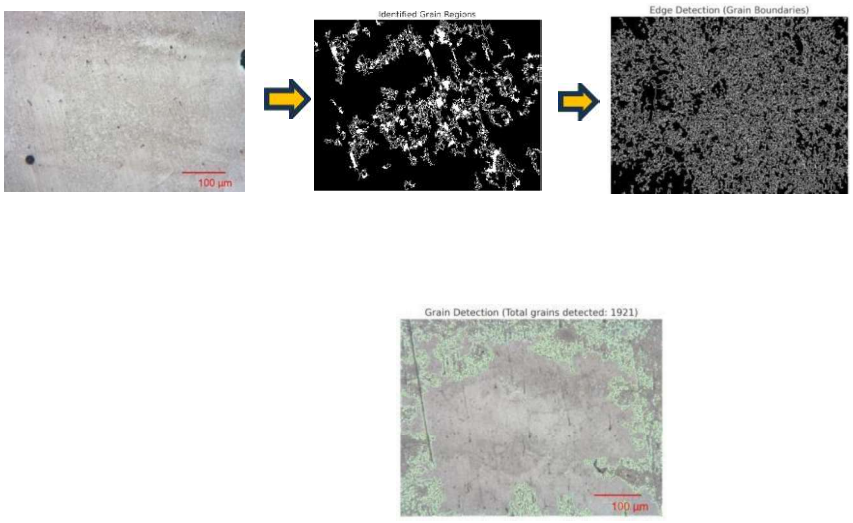

Fig 3.18 Grain size measurement procedure in Microanalysis software

In these above images, I analyzed the microstructure of the DED-manufactured Ti6Al4V blade step by step. First, in the identified grain regions image, I used image processing techniques to detect and highlight the grain areas in white against a black background. This helped me clearly see the shape, size, and distribution of

grains throughout the material. The grains appear irregular and scattered, showing how the material solidified during the additive manufacturing process. This image gives a detailed view of how the grains are spread and their boundaries, which is important for understanding the strength and structure of the blade. Then, in the second set of images, I used thresholding and segmentation to separate different features from the microstructure image. The left image shows the thresholder version where black and white contrast makes it easier to identify defects or different phases. Finally, in the grain boundary overlay image on the right, I added the detected grain outlines (in green) on top of the original microstructure. This makes it easier to compare the detected grain edges with real features like pores or un-melted particles. With the help of the above procedure, I was able to calculate the average grain size, which came out to be 380 μm^2. These steps help me understand how the grains are formed, their boundaries, and how they might affect the performance of the blade.

3.2.5 Analysis of Roughness Measurement

Additive manufacturing, especially of intricate parts such as turbine blades, is very influential on the surface properties—particularly on surface roughness. In this work, a turbine profile blade was manufactured by the Directed Energy Deposition (DED) process, and the surface roughness of the blade was analyzed using a contact-type surface profilometer. This instrument gauges roughness by scanning a thin probe over the surface, measuring differences in height. The starting roughness value measured was 23.728 μm, which is significantly greater than that of traditionally machined parts, which are usually significantly smoother in finish. High surface roughness can contribute to lower aerodynamic efficiency, greater fatigue wear, and greater corrosion risk, so post-processing is necessary for functional application. To enhance surface finish, methods such as sandblasting and laser shock peening (LSP) are commonly practiced. On applying sandblasting to the blade, roughness decreased to around 13.415μm, showing an appreciable reduction. Electrochemical polishing can be used for finer surface polishing. This process involves the controlled removal of material from the surface using an

electrochemical reaction, which smooths the surface without introducing mechanical stress or deformation. The choice of post-processing method depends on the specific requirements of the component, such as its shape, application, and performance expectations. Ultimately, enhancing the surface finish of additively manufactured parts is critical for achieving better durability, performance, and reliability in demanding environments.

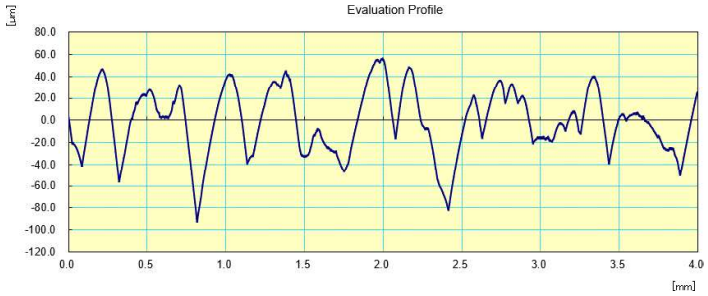

Ra	23.566 µm
Rq	28.564 µm
Rz	117.925 µm

Fig 3.19 Surface roughness measurement by contact profilometer

In my Electro-chemical Polishing experiment, I carried out electrochemical polishing on a DED-manufactured Ti6Al4V turbine blade using a specially prepared electrolyte solution totaling approximately 118.75 mL. The mixture consisted of 12.5 mL perchloric acid ($HClO_4$), 100 mL methanol (CH_3OH), and 6.25 mL hydrofluoric acid (HF). This specific combination was chosen for its effectiveness in removing surface asperities without causing mechanical damage, allowing for a smoother and brighter finish. In this process, methanol acted as both a solvent and a cooling medium, while perchloric acid and hydrofluoric acid worked together to dissolve the passive oxide layer and smoothen the surface through controlled electrochemical reactions. I applied a constant current density of 0.1 A/cm^2 to maintain a uniform material removal rate and avoid issues like localized overheating or over-polishing, which could affect part integrity. To ensure

both safety and performance consistency, I maintained the electrolyte bath temperature in the range of 10°C to 15°C using an ice bath setup. This low-temperature condition helped prevent rapid evaporation of volatile chemicals and suppressed unwanted side reactions, leading to a more controlled and even polishing outcome. After completing the polishing process under these conditions, I used a contact-type surface profilometer to measure the surface roughness. The probe made direct contact with the polished surface to capture the texture profile and quantify the roughness improvements. This step allowed me to compare the surface finish before and after polishing and evaluate the effectiveness of the parameters used in the electrochemical process. (un-electro-chemical polishing sample 23.728 µm)

Table A: surface roughness Balde after electrochemical Polishing

Sample No.	Voltage (V)	Time (min)	Surface Roughness (Ra, µm)	Observation
1	15	5	12.841	Partial smoothing
2	18	10	6.220	Good polishing
3	20	12	9.970	Over-polishing/pitting occurred
4	22	15	17.748	Mild over-polishing, surface stable

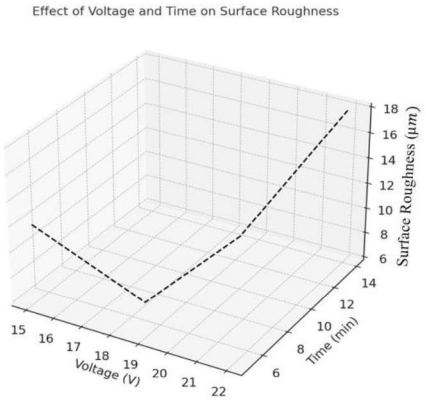

Fig 3.20 Effect of voltage and time on Surface Roughness

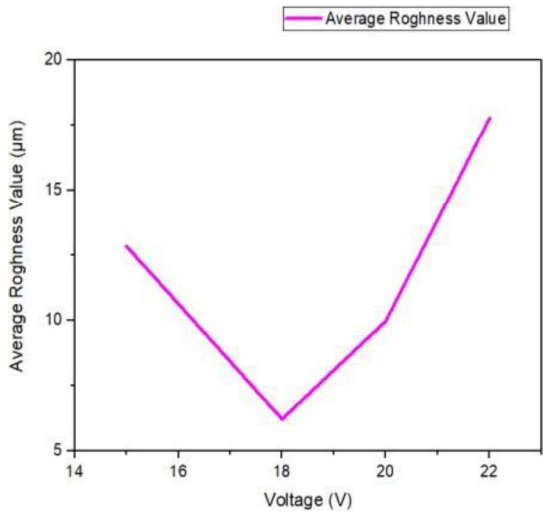

Fig 3.21 Average Roughness vs Voltage

As I observed from the graph showing the relationship between voltage, polishing time, and surface roughness during the electrochemical polishing of the DED-manufactured Ti6Al4V blade, I noticed a clear trend. When both the voltage and polishing time were increased gradually, the surface roughness started to reduce, which means the surface became smoother. The best result was seen at 18 volts and 10 minutes, where the roughness dropped to 6.220 µm—this point gave the smoothest finish. But when the voltage and time were increased beyond that, especially at 20 V and 22 V, the surface roughness started going up again, reaching 9.970 µm and 15.748 µm. This rise happened because of over-polishing and some pitting effects on the surface. So, from this, I understood that both voltage and polishing time are important, but going beyond the ideal values can damage the surface instead of improving it. It's really important to find the right balance to get the best polishing results.

Chapter 4: Experimental Investigation into Laser Shock Peening Process on Turbine Profile Blade

In this chapter the parametric optimization of the laser shock peening process parameters has been included and its effects on the output response like Micro-Hardness of the laser shock peening DED deposited Ti alloy have been analyzed. The mechanical and tribological performance of the laser shock penned DED deposited Ti6Al4V part at the optimal parametric condition have been discussed and also the effects of laser shock peening process on the surface of peened sample of the produce surface have been included.

4.1 Experimental plan of the laser shock peening process

On the basis of literature [58],[59],[60], it was observed that the most important process parameters of the laser shock peening were laser power density (laser beam per unit area per unit time), laser Spot charactertics (spot shape, Spot size, distance between adjacent spot) overlap ratio or percentage, Impact times where as the number of laser processing time, laser wavelength etc. Yet, literature on the combined effects of all the process parameters on the output responses is not found. In this research, the combined effects of the laser shock peening process parameters are investigated on output responses such as micro-hardness, compressive strength, and residual stress analysis through experiments.

4.2 Parametric study for Laser Shock Peening

In this research, I have concentrated on investigating major laser process parameters, including laser wavelength, spot size, overlapping ratio, and power density, and how they affect the quality and properties of the deposited material in the Direct Energy Deposition (DED) additive manufacturing process. These parameters play a key role in defining the thermal behavior, dynamics of the melt pool, and the final shape of the deposited Ti-6Al-4V alloy that is widely utilized for manufacturing intricate components such as turbine profile blades. Based on the desired output characteristics such as surface finish, dimensional accuracy, and material properties, I carried out a comprehensive parametric study to select and optimize these parameters. I discovered that laser wavelength is an important factor in energy absorption efficiency and that Ti-6Al-4V responded to the most efficiently at approximately 1070 nm. Spot size directly affects energy distribution,

which in turn influences the resolution of the deposition. Additionally, the overlapping ratio influences the uniformity and continuity of the deposited layers, which is critical for maintaining the structural integrity of the part. Power density, which is determined by the combination of laser power and spot size, governs the size of the melt pool and the cooling rate, both of which have a substantial effect on the microstructure and mechanical properties of the deposited material. By systematically varying these parameters and analyzing their effects on the deposition process, I have gained valuable insights into how to optimize the DED process for producing high-performance aerospace components.

4.2.1 Influence of Wavelength on laser in Laser shock Peening Process

Based on various studies, it is evident that the laser wavelength plays a major role in determining the effectiveness of the Laser Shock Peening (LSP) process, especially for metals like Ti6Al4V, which are widely used in aerospace components. In the LSP technique, a high-intensity laser pulse is directed onto the surface of the material, usually covered with a sacrificial layer and a transparent confinement medium such as water. The laser energy generates a plasma, and the rapid expansion of this plasma results in a high-pressure shock wave that travels into the material. This process introduces compressive residual stresses, which improve mechanical performance such as fatigue strength and crack resistance. The laser wavelength directly affects how efficiently the plasma is generated and how deep the stress wave penetrates the material [61].

Nd: YAG lasers generally operate at 1064 nm, but this wavelength can be converted to 532 nm using nonlinear optical processes. The green 532 nm wavelength tends to have higher absorption on metallic surfaces due to its shorter wavelength and higher photon energy. This leads to a stronger and more localized plasma, which is advantageous for improving surface-level properties like hardness and surface fatigue resistance. However, this strong surface interaction also increases the chances of thermal effects such as surface melting or ablation—especially risky when working with additively manufactured (AM) parts that already have surface

defects or are geometrically thin [62]. In contrast, the 1064 nm wavelength is absorbed less at the surface, resulting in reduced thermal load and less risk of damaging the part. This characteristic is particularly useful when processing thin-walled AM structures, such as turbine profile blades, where maintaining surface integrity is critical. The lower absorption allows the shock wave to penetrate more deeply into the material, promoting deeper residual stresses and improving subsurface mechanical properties. Additionally, using 1064 nm simplifies the laser system by avoiding the energy losses and complexity associated with wavelength conversion [61].

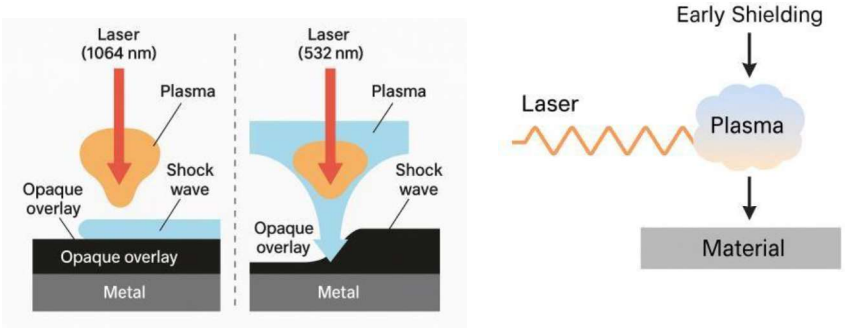

Fig 4.1 Influence of Wavelength on laser in Laser shock Peening Process and Plasma Shielding effect

Although 532 nm is effective for aggressive surface treatments, it may not be ideal for thin or complex AM geometries due to the higher risk of surface degradation. On the other hand, 1064 nm provides a safer and more balanced approach, especially for parts like Ti6Al4V AM turbine blades. Its moderate plasma intensity and deeper penetration support mechanical improvements without compromising the part's surface condition. The decision between the two wavelengths should therefore be guided by the geometry, material condition, and performance goals of the component undergoing LSP [63].

4.2.2 Influence of Power and Scan speed on Laser Shock Peening Process

Several studies have examined the combined influence of laser power and scan speed on the effectiveness of the Laser Shock Peening (LSP) process. According to literature, laser power directly affects the peak pressure generated by the plasma plume, which governs the intensity of shock waves induced in the material. Higher laser power typically results in greater compressive residual stresses and deeper plastic deformation, thereby improving fatigue life, hardness, and wear resistance. For instance, researchers have noted that increasing the laser power enhances the depth of the affected zone and the magnitude of compressive stresses, but excessive power may lead to surface melting or ablation if not controlled properly.

Scan speed, on the other hand, determines the interaction time between the laser pulse and the target surface. A slower scan speed allows more energy to be deposited per unit area, which can intensify the shock effect and increase the residual stress depth. However, too slow a scan speed can result in overlapping or overheating, which may negatively affect surface integrity. Conversely, very high scan speeds may reduce the peening effect due to insufficient energy delivery, leading to shallow plastic deformation and less effective strengthening. Some researchers emphasize that there is a critical balance between power and scan speed. For example, maintaining moderate laser power with an optimized scan speed ensures uniform stress distribution and avoids defects such as thermal damage or delamination. The literature also highlights the importance of process optimization tailored to specific materials and component geometries to achieve the best results. When both parameters are finely tuned, the LSP process can produce a well-refined microstructure with enhanced mechanical properties, particularly in aerospace and biomedical applications where fatigue strength is critical. In my own words, the influence of laser power and scan speed in LSP is interdependent and crucial for process efficiency. Power controls the strength of the shock, while scan speed regulates how that energy is applied across the surface. Optimizing both helps achieve deep, uniform compressive stresses without damaging the material, making it essential to tailor these parameters based on material type and desired application

outcomes. Based on the consideration of these parameters, I conducted Laser Shock Peening (LSP) on turbine profile blade samples that were fabricated using a laser-based additive manufacturing process. In my study, I varied the scan speed and laser power density (fluence) to investigate their combined influence on the material's surface and subsurface properties. These parameters were carefully selected based on insights from previous literature, which emphasize that laser power density governs the intensity of the shock wave, while scan speed influences the energy distribution and interaction time on the material surface. By adjusting these parameters, I aimed to optimize the LSP process to enhance the mechanical performance—particularly fatigue resistance and surface hardness—of the additively manufactured blades. The results helped to identify the optimal window where compressive residual stresses were maximized without causing thermal damage or surface degradation, confirming the importance of parameter optimization in LSP for complex geometries like turbine blades. By varying the laser power density, I was able to identify the optimal condition at which the maximum power enabled the highest number of effective impacts during the Laser Shock Peening process.

4.2.3 Influence of Overlap ratio and Impact times on Laser Shock Peening Process

Several literature studies have explored the effects of overlap ratio and number of impact times on the Laser Shock Peening (LSP) process, emphasizing their importance in enhancing surface integrity and mechanical properties. The overlap ratio refers to the degree of overlap between adjacent laser spots during the peening process. A higher overlap ratio generally leads to more uniform and deeper compressive residual stress distribution, as the laser pulses affect the material repeatedly in closely spaced areas. However, excessive overlap can result in energy accumulation, local heating, and potential surface damage, particularly in thermally sensitive materials. Studies suggest that an overlap ratio in the range of 50–75% is often optimal, as it balances coverage efficiency with controlled energy input. The number of impacts—or the number of times a single spot is subjected to repeated

laser pulses—also plays a critical role in influencing the microstructure and mechanical response of the treated surface. Increasing the number of impacts can intensify the compressive residual stress and enhance the depth of the plastically deformed layer. This contributes to improved fatigue resistance, hardness, and wear behavior. However, beyond a certain number of impacts, the benefits may plateau or even reverse due to saturation effects or excessive energy input leading to surface roughness and possible micro-cracks. Literature reports that two to three impacts often provide optimal results for many engineering alloys, though this can vary depending on material type and thickness. In my own words, the overlap ratio and number of impacts are key factors in the effectiveness of LSP. The overlap ratio ensures that the entire surface is treated uniformly, avoiding untreated gaps or overly stressed regions. When managed properly, it leads to consistent mechanical enhancement across the peened area. Similarly, repeating the laser impact at the same spot allows deeper and stronger compressive stress zones to form. However, there is a threshold—too much overlap or too many impacts can harm the surface instead of improving it. Therefore, fine-tuning these parameters based on the material and application requirements is essential to achieving the best outcomes in Laser Shock Peening. the beam spot size is a critical parameter that directly influences the overlap ratio in the Laser Shock Peening (LSP) process. The overlap ratio is calculated based on the spacing between adjacent laser spots relative to the diameter of the beam spot. A larger beam spot size allows for greater surface coverage per pulse, and when combined with proper spot spacing, it can help achieve a higher overlap ratio with fewer shots. Conversely, a smaller beam spot requires more pulses to cover the same area, which may reduce the overlap ratio unless spot spacing is tightly controlled.

Literature indicates that when the spot size is not appropriately matched with the selected overlap ratio, it can lead to either under-peening (gaps between treated areas) or over-peening (excessive energy concentration). For example, if the beam spot is small and the overlap ratio is high, the same area may receive multiple impacts unintentionally, increasing thermal accumulation and potentially degrading

the surface. On the other hand, a larger beam spot with a low overlap ratio might result in uneven stress distribution and insufficient mechanical improvement. The spot size of the laser beam plays a key role in determining how effectively the laser pulses cover the surface during LSP. If the spot is large, fewer pulses are needed, and a moderate overlap can still provide uniform coverage. But if the spot is small, precise control over pulse spacing is essential to maintain a good overlap ratio. So, when selecting overlap settings, it's important to consider the beam diameter to ensure efficient energy usage and consistent surface treatment without defects.

4.3 Process Parameter Optimization and Performance Evaluation of Laser Shock Peening on Additively Manufactured Components

In this study, I conducted laser shock peening (LSP) using a Q-switched Nd: YAG laser operating at a wavelength of 1064 nm. The laser system employed was a Class 4 device, capable of delivering pulses with a duration of 9 nanoseconds and a maximum energy output of 1 J (1000 mJ) per pulse. The experimental arrangement was such that the laser beam directly impacted the surface of the additively manufactured specimens without any intermediary optics or beam splitting. This direct interaction was essential to investigate the raw influence of laser parameters on the peening process. a major part of the experiment involved optimizing the laser output energy by adjusting key internal parameters accessible through the Litron laser control software—namely, the oscillator drive, amplifier drive, and flashlamp (FL) delay. Each of these variables plays a crucial role in shaping the characteristics of the laser pulse.

The oscillator drive regulates the power supplied to the oscillator unit, which is responsible for generating the seed pulse. During the trials, I noted that small changes in this parameter significantly influenced the consistency and sharpness of the initial pulse, affecting its coherence and beam profile. Following this, the amplifier drive governs the gain in the amplifier stages that boost the oscillator's pulse to the desired energy levels. I found that increasing this value led to higher pulse energies, but only up to a limit beyond which pulse stability started to

degrade, indicating the need for careful calibration. The flashlamp delay is a timing control that determines the delay between flashlamp excitation and Q-switch activation. Precise tuning of this delay was critical; I observed that improper synchronization could lead to suboptimal pulse energy or pulse distortion. An optimized FL delay ensured maximal energy extraction from the laser cavity,

enhancing both pulse efficiency and repeatability. By systematically varying these three parameters, I successfully generated a range of pulse energies from 0.326 J to 1.028 J. These results allowed me to tailor the laser parameters to meet the energy requirements for effective peening, ensuring adequate pressure wave generation without damaging the material. The insights gained from this parameter tuning were vital for establishing a robust LSP setup and achieving uniform surface treatment across the samples.

Table 4.1 Laser Output Energy vs Amplifier and Oscillator Drive Settings (FL Delay = 0)

Sr. no	Amplifier Drive	Oscillator Drive	FL Delay	Energy (J)
1	100	100	0	1.028
2	100	90	0	0.986
3	90	90	0	0.876
4	80	90	0	0.774
5	80	80	0	0.681
6	70	80	0	0.576
7	100	60	0	0.526
8	70	70	0	0.496
9	70	60	0	0.418
10	70	55	0	0.386
11	60	60	0	0.326

After establishing the optimal range of laser pulse energies—from 0.326 J to 0.986 J—through systematic adjustments of the oscillator drive, amplifier drive, and flashlamp delay settings in the Nd: YAG laser system, I finalized the remaining process parameters for laser shock peening (LSP) based on a detailed literature review and preliminary trials. The aim was to implement a controlled and effective peening strategy tailored to the surface treatment of additively manufactured components. During the experimental work, I fixed the pulse repetition frequency at 10 Hz, which proved to be an optimal choice for maintaining a balance between process throughput and thermal control. Higher frequencies were avoided to prevent excessive local heating, while lower frequencies were found to slow down the overall peening efficiency. The 10 Hz setting enabled stable laser operation and consistent pulse delivery with minimal thermal accumulation. The laser spot diameter at the target surface was measured to be 0.987 mm, which was achieved by setting a stand-off distance of 105 mm between the focusing lens and the component. This distance was carefully maintained considering the lens's focal length of 100 mm, ensuring a focused and nearly circular beam profile suitable for LSP. A sub-millimeter spot diameter was ideal to generate the required high-pressure shock waves for inducing localized plastic deformation while minimizing thermal effects.

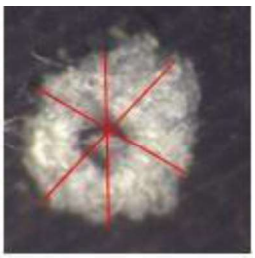

Fig 4.2 Spot diameter measurement LEICA software

Based on the spot diameter, the spot area was calculated using the relation

$$A = \frac{\Pi}{4} d^2$$

resulting in an approximate area of 0.765 mm². This spot area directly influenced the power density and peak pressure during the laser-material interaction, both of which are critical for effective peening. To achieve uniform surface coverage, I applied a 90% overlap ratio between adjacent laser spots, as recommended in several studies for enhancing surface hardening and ensuring complete coverage. The overlap ratio was calculated using the formula:

$$\text{Overlap Ratio} = 1 - \left(\frac{v}{f \times d}\right)$$

where v = 1 mm/s is the scan speed, f = 10 Hz is the pulse frequency, and d = 0.987 mm is the spot diameter. Substituting these values yielded an overlap ratio of approximately 89.8%, which closely approximates the desired 90% coverage. The scan speed of 1 mm/s was selected to match the pulse frequency and spot diameter, allowing sufficient overlap without missing areas or inducing over-peening. Additionally, the focal length of 100 mm provided a working distance that ensured a stable and consistent spot size on the component surface.

Table 4.2: Parameter setting on setup during Laser shock peening

Sr. No	Parameters	Values
1	Pulse Frequency (Hz)	10
2	Spot Diameter (SOD- 105mm) mm	0.987
3	Spot Area (mm^2)	0.765
4	Scan Speed (mm/sec)	1
5	Overlap Ratio (%)	90
6	Pulse Duration (ns)	9
7.	Focal length (focusing lens) mm	100

After finalizing the spot diameter and confirming the pulse duration, I proceeded to calculate the power density corresponding to the range of laser pulse energies

obtained during the experiment. The spot diameter was fixed at 0.987 mm, giving a spot area of approximately 0.765 mm² (or 7.65×10^{-7} m²), which served as a constant reference for all subsequent energy-based calculations. The laser pulse duration was maintained at 9 nanoseconds (9×10^{-9} seconds), as defined by the Nd: YAG laser system specifications. To estimate power from the energy values, I used the fundamental relation:

$$\text{Power (w)} = \frac{Energy\ (J)}{Pulse\ duration}$$

Applying this formula across the observed range of energies—from a minimum of 0.326 J to a maximum of 0.986 J , I obtained the corresponding instantaneous peak powers**:**

- For 0.326 J

$$P = \frac{0.326}{9\times10^{-9}} = 0.0362 \text{ Gw}$$

- For 0.386 J

$$P = \frac{0.386}{9\times10^{-9}} = 0.0429 \text{ Gw}$$

- For 0.480 J

$$P = \frac{0.480}{9\times10^{-9}} = 0.0533 \text{ Gw}$$

- For 0.569 J

$$P = \frac{0.569}{9\times10^{-9}} = 0.0633 \text{ Gw}$$

- For 0.986 J

$$P = \frac{0.986}{9\times10^{-9}} = 0.109 \text{ Gw}$$

These values represent the peak power delivered by the laser during each pulse within the nanosecond regime.

Subsequently, the power density (W/m²), a critical factor in determining the shock pressure induced during laser shock peening, was calculated using:

$$\text{Power Density} = \frac{Power}{Spot\ Area}$$

Using Constant spot area 0.007645 cm2

- For 0.326 J

$$\text{Power Density} = \frac{0.0362}{0.007645} \sim 5\ \text{GW/cm2}$$

- For 0.386 J

$$\text{Power Density} = \frac{0.0429}{0.007645} \sim 6\ \text{GW/cm2}$$

- For 0.480 J

$$\text{Power Density} = \frac{0.0533}{0.007645} \sim 7\ \text{GW/cm2}$$

- For 0.569 J

$$\text{Power Density} = \frac{0.0633}{0.007645} \sim 8\ \text{GW/cm2}$$

- For 0.986 J

$$\text{Power Density} = \frac{0.0633}{0.007645} \sim 15\ \text{GW/cm2}$$

Table 4.3: Laser Energy and Power Output at Different Power Densities

Sr. no	Power Density (GW/cm^ 2)	Energy (J)	Power (GW)
1	5 (min)	0.326	0.0362
2	6	0.386	0.0429
3	7	0.480	0.0533
4	8	0.526	0.0633
5	15(max)	0.986	0.109

Hence, the power densities for the laser shock peening process were calculated based on the output energy levels obtained from the laser system. After determining the range of laser energies (from 0.326 J to 0.986 J) and corresponding power densities (ranging from 5 GW/cm² to 15 GW/cm²), I structured the LSP trials into three main stages. The first stage involved applying multiple impacts at a constant high energy of 0.986 J (15 GW/cm²). This step was intended to induce deep compressive residual stresses and significantly improve the surface hardness of the component. Such multiple impacts at higher energy levels have been proven in literature to generate favorable stress profiles and microstructural refinement, which ultimately enhance fatigue resistance. In the second stage, single-impact trials were performed at a lower energy level of 0.569 J, yielding a power density of approximately 8 GW/cm². The reason for choosing this reduced energy was to understand how minimal energy inputs influence the surface condition, especially when applied on electrochemically polished surfaces. These surfaces provide a uniform base to study the isolated effects of LSP without interference from surface irregularities. Additionally, a scan speed of 1 mm/s was maintained to ensure consistent overlapping of laser spots and effective energy deposition. The final phase involved a detailed parametric study, where both power density and scan speed were varied to optimize the LSP conditions. This parametric investigation was essential to identify the balance between energy efficiency and surface improvement. By understanding how different combinations affect outcomes such as hardness, roughness, and residual stress, this study aims to propose a reliable processing window for effective LSP treatment of AM components. The ultimate goal is to develop a robust methodology that can be used in real-world manufacturing environments to enhance the service life of parts.

4.4 Result and Discussion

A parametric study on laser shock peening was conducted by varying both power density and scan speed. Based on this study, the most suitable combination of power density and scan speed was identified for experimental investigation focused on the number of impacts required to achieve the desired depth of compressive residual stress. Additionally, a separate set of experiments was carried out at a constant power density while varying the scan speed, with surface roughness considered as a critical factor in evaluating the outcomes. These analyses helped in finalizing the experimental parameters. Subsequently, a detailed characterization process was performed to validate the effectiveness of laser shock peening. The aim was to confirm whether the expected improvements in material properties were achieved as a result of the process.

4.4.1 Mechanical Testing

4.4.1.1 Vickers Hardness Test

It was observed that the hardness value of the material increased significantly with an increase in power density during laser shock peening (LSP), ranging from 5 GW/cm² to 15 GW/cm². Before the LSP process, the average hardness of the untreated material was measured at 376.3 HV. After applying LSP, the hardness rose from approximately 384.9 HV at 5 GW/cm² to 549.3 HV at 15 GW/cm². This consistent upward trend indicates that higher power density levels resulted in more energetic laser impacts, which generated stronger shock waves during the LSP process. The increased energy input from higher power densities induced greater plastic deformation and led to the development of deeper and more substantial compressive residual stresses within the surface layer of the material. These compressive stresses effectively inhibited dislocation movement and altered the microstructure in a way that enhanced the material's surface hardness. The improvement in hardness correlates with increased resistance to fatigue, wear, and crack propagation—critical factors in the performance and durability of

components such as turbine blades. Therefore, optimizing power density is essential for maximizing the hardening effect and ensuring long-term structural integrity.

Table 4.4 : Hardness value before and after LSP with different Power densities

Sr. No	Energy (J)	Power Density (GW/cm^2)	Hardness Value (HV)
1	Before- LSP	----------	376.3
2	0.326	5	384.9
3	0.386	6	441.0
4	0.480	7	472.8
5	0.569	8	515.5
6	0.986	15	549.3

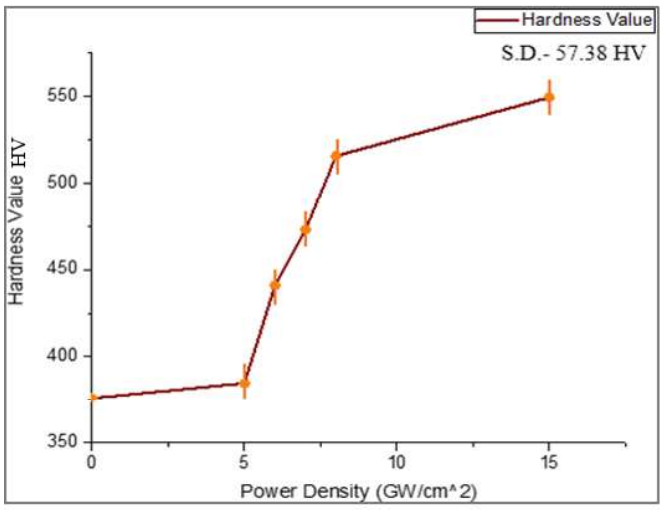

Fig 4.3 Power density Vs Hardness value

After performing laser shock peening (LSP), the blade profile was thoroughly examined to evaluate the distribution and uniformity of surface hardening achieved through the process. Hardness measurements were taken across different regions of the blade—specifically the top, middle, and bottom sections—to characterize the

effect of LSP. Prior to treatment, the average surface hardness was measured at approximately 475.54 HV. Following LSP, conducted at a power density of 6 GW/cm² (0.386 J), the average surface hardness increased to 482.3 HV. The hardness data was visualized in the form of a profile curve, clearly illustrating the improvement in hardness values along the blade's surface post-treatment. Notably, the previously identified low-hardness regions showed a significant enhancement, confirming that LSP effectively targeted and improved these zones. Furthermore, the hardness distribution became more uniform throughout the blade, which is critical for enhancing resistance to fatigue, wear, and crack initiation. The depth and consistency of the hardening layer, as observed in the hardness profile, provided valuable insights into the extent of the compressive residual stress zone induced by LSP. Overall, the profile analysis confirmed that the laser shock peening process, when applied with optimized parameters, successfully strengthened the blade surface and contributed to improved mechanical properties and structural integrity.

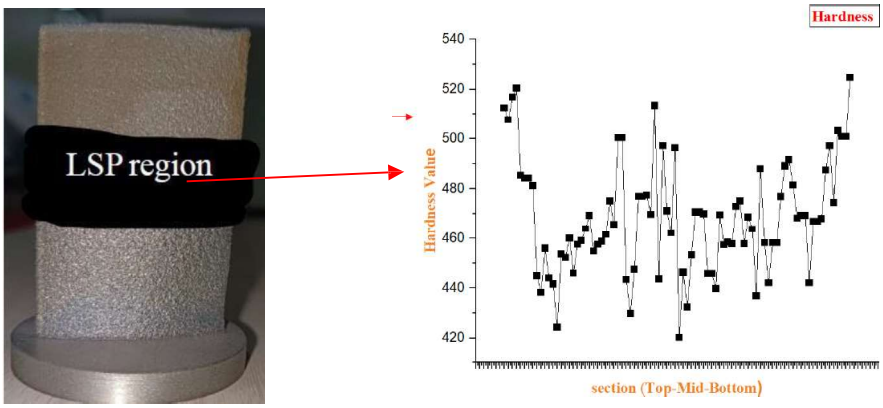

Fig 4.4 After LSP Measure Hardness value and plot profile of Blade

Table 4.5: after LSP on Blade Hardness Value per section

Section	Hardness Value
Top	480.13
Mid	481.80
Bottom	485.47

After optimizing the power density, I conducted a number of impact experiments on the profile blade using a power density of 0.986 J (15 GW/cm²) and a scan speed of 1 mm/sec. From the results, I observed that as the number of impacts increased during laser shock peening, the surface hardness also increased noticeably. This is mainly because each impact adds to the cumulative plastic deformation and enhances the level of residual compressive stress near the surface. These repeated impacts cause microstructural changes like grain refinement, which directly contributes to increased hardness. With every additional impact, the surface undergoes more work hardening, which results in a steady rise in hardness values. This clearly shows that increasing the number of LSP impacts not only improves residual stress profiles but also significantly strengthens the material by enhancing its surface hardness.

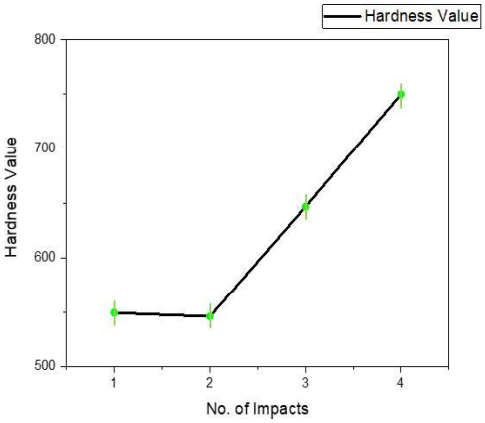

Fig 4.5 Number of impact Vs Hardness Value

Sr.no	Number Of Impact	Hardness Value (HV)
I	01	549.3
II	02	570.0
III	03	646.5
Iv	04	750.0

Table 4.6: hardness value per Impact

After conducting the laser surface treatment experiment by varying the scan speed (mm/sec) while keeping the power density constant at 8 GW/cm², I analyzed the resulting hardness values (HV) and plotted them accordingly, From the analysis, it is observed that the hardness value increases as the scan speed decreases. At a scan speed of 0.5 mm/sec, the maximum hardness of 543.5 HV was achieved, while at a higher scan speed of 1.2 mm/sec, the hardness dropped to 511 HV. This clearly shows an inverse relationship between scan speed and hardness value. The reason behind this trend is due to the higher energy input per unit area at lower scan speeds. When the laser moves slowly, it allows more energy to be absorbed by the material

surface, resulting in better melting, stronger metallurgical bonding, and more refined microstructures. This leads to an increase in surface hardness. On the other hand, higher scan speeds reduce the laser-material

interaction time, leading to **less** energy absorption and lower hardness. Thus, it can be concluded that reducing the scan speed enhances the surface hardness due to increased heat input and improved microstructural modifications during laser processing.

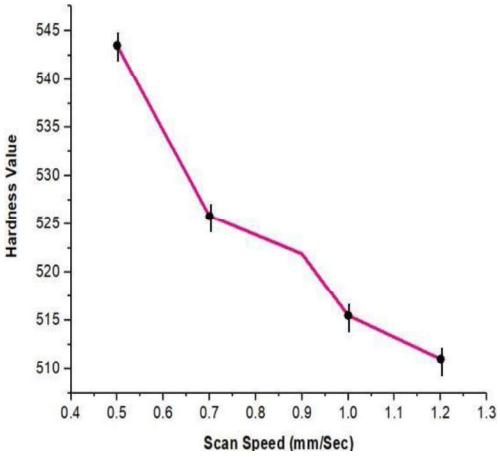

Fig 4.6 Scan Speed Vs Hardness Value

Sr. No.	Scan Speed (mm/sec)	Hardness Value (HV)
1	Untreated	376.3
2	1.2	511
3	1	515.5
4	0.9	521.9
5	0.7	525.8
6	0.5	543.5

Table 4.7: Various Scan speed represents Hardness Value

4.4.1.2 Ultimate Compressive Strength Measurement

Compressive strength measurements conducted before and after laser shock peening (LSP) demonstrated a distinct and progressive enhancement in the material's ultimate compressive strength with increasing power density. Initially, prior to the application of LSP, the untreated material exhibited an ultimate compressive strength of 1012.69 MPa. After implementing LSP, with power densities systematically varied from 5 GW/cm² to 15 GW/cm², the material showed a marked increase in strength, reaching a peak value of 1598.54 MPa at the highest power setting. This improvement is directly linked to the generation of intense

shock waves during LSP, which promote the development of deeper and more stable residual compressive stresses on the surface and sub-surface regions of the material. These compressive stresses effectively suppress dislocation activity and hinder crack initiation and propagation, resulting in an increase in the material's resistance to compressive loading. Additionally, the process induces plastic deformation and localized microstructural refinement, such as grain size reduction and work hardening, both of which contribute to the enhancement of mechanical properties. The test results validated that higher power densities significantly strengthen the treated surfaces by altering the stress state and microstructure. Moreover, no signs of surface damage or over-peening effects were observed at 15 GW/cm², indicating that the process was within the optimal range for the material system under investigation. Therefore, the findings confirmed that optimizing LSP parameters—especially power density—plays a critical role in tailoring surface mechanical properties and extending the service life of components exposed to high mechanical loads and fatigue-prone environments.

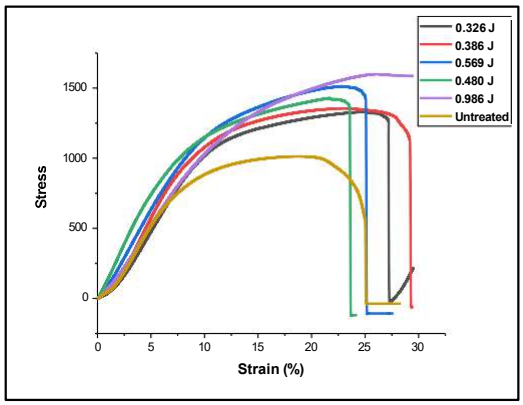

Fig 4.7 Stress Vs Strain

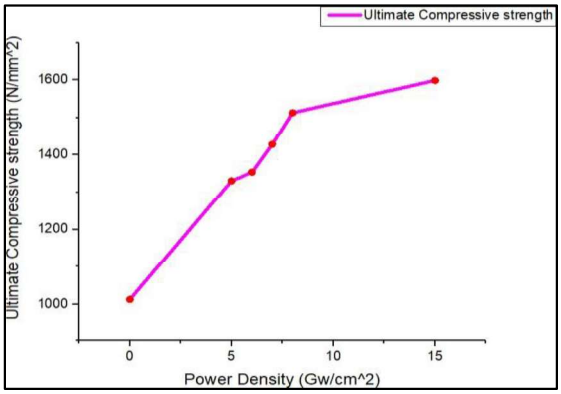

Fig 4.8 Ultimate Compressive strength vs Power density

4.4.2 Grain Size Measurement

a. Vary Power density with Constant Scan Speed 1 mm/sec



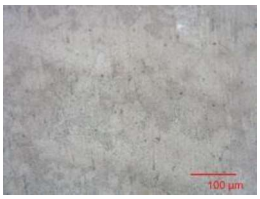

Untreated

5 Gw/cm^2 6 Gw/cm^2

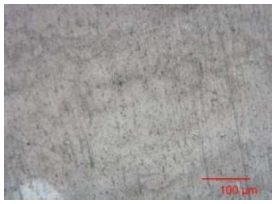

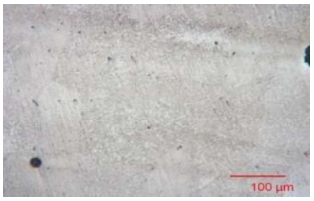

7 Gw/cm^2 8 Gw/cm^2 15 Gw/cm^2

Fig 4.9 Microstructure images of various power densities

While observing the optical microscope images of Ti6Al4V alloy, I first examined the untreated sample labeled "AM Deposited." The surface appeared rough with noticeable debris and irregularities, which I suspect are due to the additive

manufacturing process. As I moved to the sample treated at 5 GW/cm², I noticed a clear improvement — the surface had fewer contaminants and some early signs of deformation, likely from the initial effects of laser shock peening (LSP). When analyzing the 6 GW/cm² and 7 GW/cm² samples, I observed that the surfaces looked cleaner and more uniform. The LSP treatment seemed to enhance the consolidation of the material, smoothing out surface irregularities and initiating more visible plastic deformation. At 8 GW/cm², the texture of the surface became even finer and more consistent, with fewer scratches and a more refined look — a sign of deeper compressive stresses and grain refinement setting in. The 15 GW/cm² image showed the most dramatic change. The surface was highly uniform with very fine features, although I did notice a few dark spots, which might be due to localized overheating or ablation. Microstructurally, I could clearly see that the α and β phases became more defined as the LSP intensity increased. By 8 and 15 GW/cm², the α-phase appeared more dominant and the β-phase more evenly distributed, suggesting progressive grain refinement and better phase alignment.

Overall, these images clearly show how increasing LSP power density not only smooths the surface but also refines the microstructure — something that would likely enhance the alloy's mechanical performance.

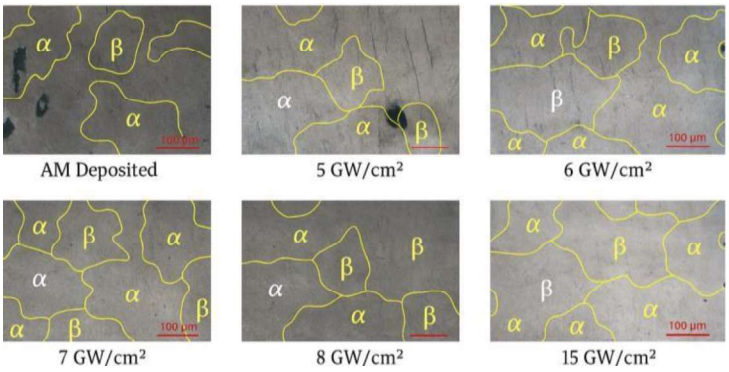

Fig 4.10 Microstructure images of various power densities represent α and β phases

While analyzing the grain size data at a constant scan speed of 1 mm/sec, I observed a clear trend — as the power density increases from 0 GW/cm² (un-LSP) to 15 GW/cm², the average grain size drops drastically, going from around 380.92

µm² to just 7.5 µm². This significant reduction clearly shows that higher power densities during the LSP process led to noticeable microstructural refinement. It's evident that the energy delivered by the laser shock peening causes the grains to break up and become more refined. The high-pressure impacts from the laser shocks seem to disrupt the original grain structure, encouraging dislocation movements and changes in the microstructure that result in smaller grains. From this, I can conclude that increasing the power density while keeping the scan speed constant is quite effective in reducing grain size. This refinement is beneficial because smaller grains usually mean improved material properties particularly in terms of hardness and strength.

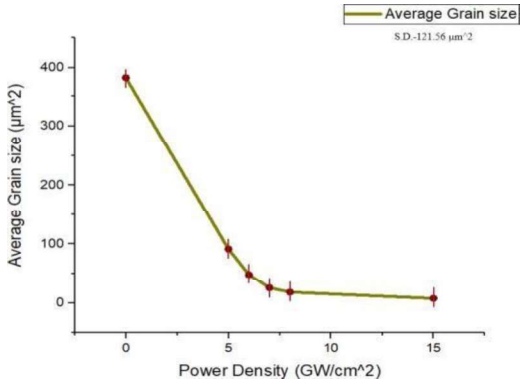

Fig 4.11 Average Grain Size Vs Power density

Table 4.8: various power densities show Average Grain size µm^2

Sr.no	Power Density (Gw/Cm^2)	Energy	Average Grain size (µm^2)
1	0	Un-LSP	380.92
2	5 (min)	0.326	91.35
3	6	0.386	48.20
4	7	0.480	25.44
5	8	0.569	18.05
6	15(max)	0.986	7.5

b. Vary Scan speed with constant Power density 8 Gw/Cm^2

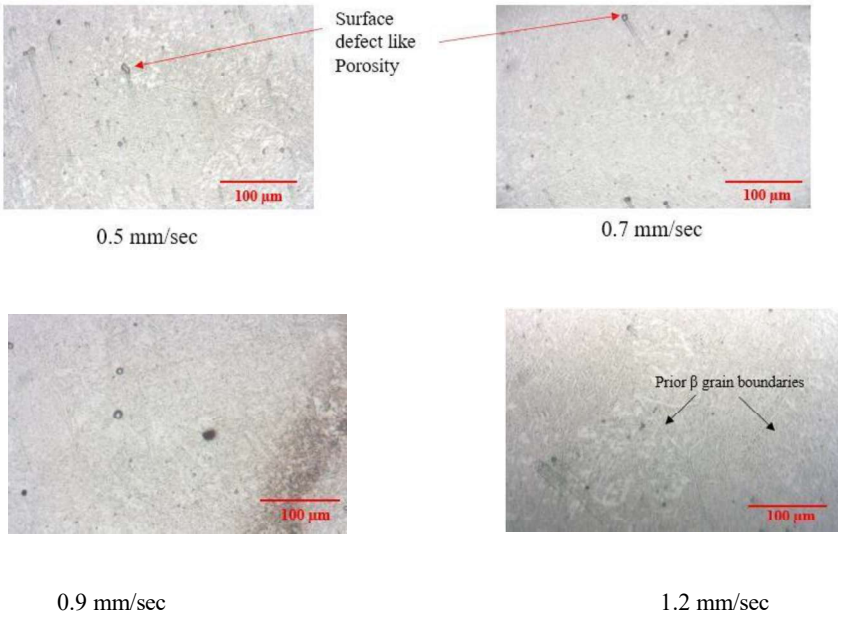

Fig 4.12 Microstructure images of various Scan speeds

The effects of varying scan speed during laser shock peening (LSP) on Ti6Al4V at a constant power density of 8 GW/cm². As the scan speed increases from 0.5 mm/sec to 1.2 mm/sec, noticeable changes occur in surface features and microstructural clarity. at the lowest scan speed of 0.5 mm/sec, the surface exhibits visible defects such as porosity and minor surface irregularities. These defects may be due to the prolonged exposure time allowing localized heating, which can enhance defect formation. Moving to 0.7 mm/sec, the surface still shows some porosity, but with a slightly more refined and uniform texture, suggesting improved shock impact balance and reduced thermal effects. As the scan speed increases to 0.9 mm/sec, the surface becomes cleaner with fewer visible defects, indicating that a moderate scan speed optimizes the shock energy distribution without causing overheating or surface damage. Finally, at the highest scan speed of 1.2 mm/sec, the prior β grain boundaries become more evident, suggesting that the LSP energy was not as deeply absorbed due to shorter interaction time. This might limit the extent of plastic deformation and microstructural refinement.

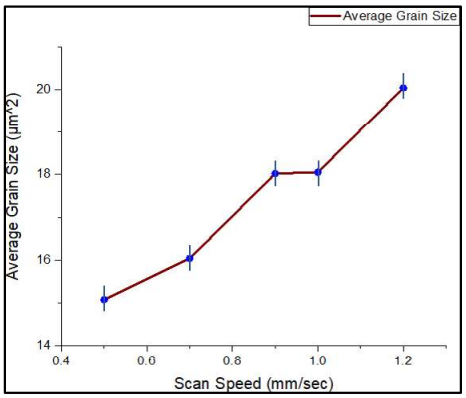

Sr. no	Scan Speed (mm/sec)	Average Grain size (µm^2)
1	0.5	15.08
2	0.7	16.04
3	0.9	18.02
4	1	18.05
5	1.2	20.04

Fig 4.13 Average Grain size Vs Scan Speed and table 4.9 represent its Value

At a constant power density of 8 GW/cm², the scan speed significantly affects the average grain size of the processed material. When the scan speed is low—specifically at 0.5 mm/s and 0.7 mm/s—the material develops smaller grains, with average grain areas around 15.08 µm² and 16.04 µm², respectively. As the scan speed increases to 0.9 mm/s, 1 mm/s, and 1.2 mm/s, the grain size also increases gradually, reaching up to approximately 20.04 µm². This trend occurs because scan speed influences the heat input per unit length during laser processing. At slower scan speeds, the laser beam stays longer over a particular spot, supplying more heat and forming a wider melt pool. This leads to slower cooling and gives more time for nucleation, which helps in forming a finer grain structure. In contrast, higher scan speeds reduce the laser's dwell time, delivering less energy to the surface. This causes the melt pool to solidify quickly, limiting the time for new grains to form and instead allowing existing grains to grow larger. Therefore, as the scan speed increases, the reduced interaction time between the laser and material leads to lower thermal energy input and rapid solidification. This results in coarser grains and less refined microstructures. This observation aligns with basic principles of solidification, which state that lower heat input and faster cooling tend to limit nucleation but promote grain growth.

4.4.3 Surface Roughness Measurement

I initially measured the surface roughness of the Ti6Al4V turbine blades in their as-built condition, finding an average Ra of 23.52 µm. We then carried out laser shock peening at a pulse energy of 0.326 J (5 GW/cm²) and immediately re-measured the surface, observing a drop in roughness to 19.39 µm a clear indication that the treatment had smoothed the surface. Next, we increased the pulse energy to 0.386 J (6 GW/cm²) and 0.480 J (7 GW/cm²). After each run, we performed the same surface profilometry: roughness crept back up to 21.58 µm and then to 22.87 µm, suggesting that at these intermediate energy levels, some localized melting or micro-defects were being introduced, counteracting the smoothing effect. Pushing the energy further to 0.569 J (8 GW/cm²), we again measured the Ra and found it had decreased to approximately 18 µm. This told us that at this particular setting, the laser shock peening was optimized producing enough plastic deformation and microstructural refinement to lower surface roughness without crossing into the regime where damage occurs. Finally, we extended the peening duration beyond this point ("over-polishing" for about 15 minutes) and observed new profilometry results showing pitting and increased roughness. From these measurements, it became clear that moderate pulse energies refine and smooth the surface, while excessive energy or prolonged exposure introduces microcracks, pits, and other defects that raise the roughness again. Thus, our data confirm 0.569 J as the optimal laser-shock-peening energy for minimizing surface roughness on our DED-manufactured Ti6Al4V blades.

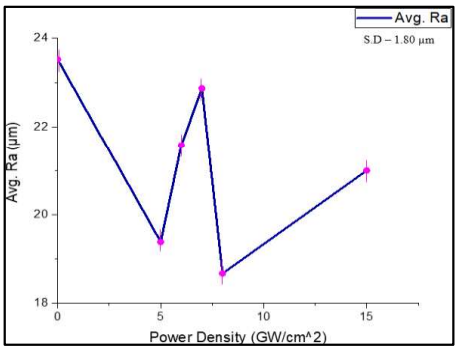

Fig 4.14 Power density Vs Average Surface Roughness

Table 4.10: various power densities represent Average Surface Roughness

Sr. No	Energy (J)	Power Density (GW/cm^2)	Avg. Ra (µm)
1	Before- LSP	----------	23.52
2	0.326	5	19.39
3	0.386	6	21.58
4	0.480	7	22.87
5	0.569	8	18.68
6	0.986	15	21.00

As the number of impacts increases during laser shock peening, the surface roughness shows an interesting trend. Initially, with an increase in impacts from 1 to 4, the surface roughness decreases—from about 21.00 µm to roughly 18.71 µm—indicating that the surface becomes smoother. This happens because repeated impacts help in uniformly plastically deforming the surface, filling in micro voids and leveling out surface irregularities. The continuous shockwave interaction modifies the microstructure and reduces surface asperities, leading to better surface smoothness. However, after reaching an optimal number of impacts, any further increase can cause slight roughness or keep it stable. This may be due to excessive energy input that can lead to surface damage such as microcracks or local roughening. So, it's important to carefully control and optimize the number of impacts during LSP to achieve the best surface finish while still enhancing the residual stress distribution.

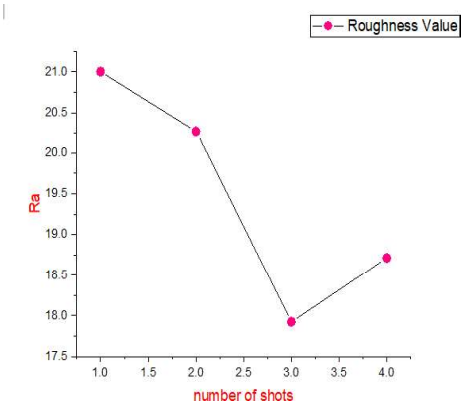

Sr.no	Number Of Impact	Roughness Value (µm)
I	01	21.002
II	02	20.270
III	03	17.923
Iv	04	18.712

Fig 4.15 Average surface roughness measurement per Number of impacts

After performing the laser processing experiment at a constant power density of 8 GW/cm², I measured the surface roughness of the treated samples at various scan speeds ranging from 0.5 mm/sec to 1.2 mm/sec. The results were then plotted, showing a clear trend between scan speed and roughness values. The analysis revealed that surface roughness decreases as scan speed increases. Specifically, the roughness value was 19.24 µm at the lowest scan speed of 0.5 mm/sec, while it reduced to 17.45 µm at the highest scan speed of 1.2 mm/sec. This inverse relationship is attributed to the fact that lower scan speeds allow more laser energy to interact with the surface, causing excessive melting and re-solidification, which increases surface irregularities. On the other hand, at higher scan speeds, the laser moves more quickly across the surface, reducing heat input per unit area and leading to less melting and a smoother, more uniform finish. Therefore, the experimental results confirm that increasing scan speed improves surface finish by lowering the roughness values.

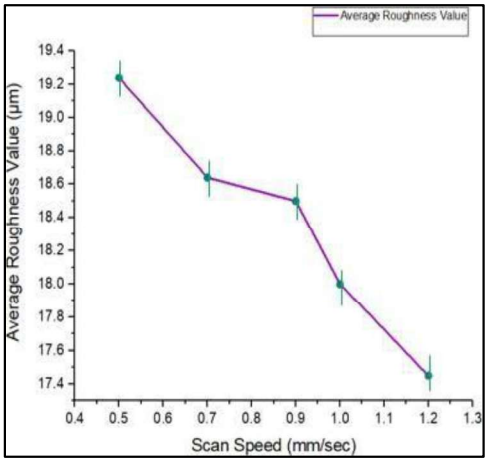

Fig 4.16 Scan speed Vs Avg. Ra values

Table 4.11: various Scan speed represents Avg. Ra values

Sr. No.	Scan Speed (mm/sec)	Roughness Value (µm)
1	Untreated	23.52
2	1.2	17.45
3	1	18
4	0.9	18.50
5	0.7	18.64
6	0.5	19.24

4.4.4 3-D Scanning Test

Corresponding Following image shows the results of a 3D scanning test carried out to study the surface variation of a Ti6Al4V turbine blade made using additive manufacturing. The scan was done both before and after applying Laser Shock Peening (LSP) to see how much the actual part differed from the CAD model and how LSP affected the surface finish. This high-precision scan helped compare the CAD design with the as-built part and evaluate the surface changes after LSP treatment. At first, when comparing the CAD model with the deposited part, an average deviation of about 0.109 mm was observed. This deviation is expected in DED processes due to factors like heat input, layer stacking, and process instability, which usually result in uneven surfaces and shape distortion. At this stage, the surface had noticeable fluctuations and didn't match the CAD geometry closely. After performing Laser Shock Peening, another 3D scan showed that the deviation between the as-built part and the LSP-treated surface increased slightly to around 0.153 mm. This increase indicates a small change in wall thickness, but it doesn't negatively impact the quality. In fact, LSP helps reduce surface roughness by flattening out peaks and introducing compressive stresses that improve surface smoothness and consistency, bringing the surface geometry closer to the CAD model. The comparison between the surface before and after LSP confirms that LSP improved the surface condition. The pre-LSP surface had high variation, while the post-LSP surface was smoother and more uniform. Although there was a slight increase in thickness after LSP, it was minor and doesn't affect the final part's performance. Hence, LSP can be applied safely to any part of the blade to enhance surface quality without compromising dimensional accuracy.

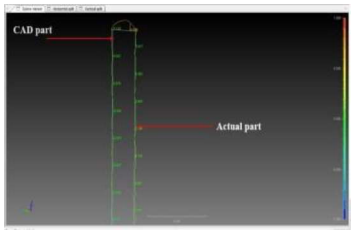

Fig 4.17 CAD Model Vs As Built Sample

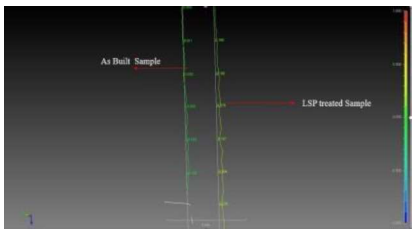

Fig 4.18 As Built Sample Vs LSP treated

Table 4.12: comparison part between both cases before and After LSP

Comparison	Avg. Absolute Deviation	Observation
CAD vs. Deposited Part	~0.109 mm	Initial surface deviation from nominal CAD
Deposited Part vs. LSP-Treated	~0.153 mm	LSP modifies surface, reducing roughness peaks
Pre-LSP Surface	—	Fluctuating, high deviations
Post-LSP Surface	—	More uniform, smoother, closer to CAD geometry
Conclusion	—	After LSP, a slight deviation in wall thickness is observed, but it is not significant; therefore, LSP can be applied to any section of the blade.

5/9/2025

4.4.5 Residual Stress Analysis

The X-ray Diffraction (XRD) plots shown above illustrate the phase structure and crystallographic changes in Ti6Al4V samples before and after Laser Shock Peening (LSP) at different energy levels. In the as-built condition (top left), the XRD pattern shows relatively broad and low-intensity peaks corresponding to the α-Ti (hexagonal close-packed) and β-Ti (body-centered cubic) phases. These broad peaks are typical for DED-manufactured components, indicating the presence of residual tensile stress, microstructural defects, and potentially finer grains or partial amorphization due to rapid solidification during the additive manufacturing process. As the samples underwent LSP treatment at increasing laser energies (0.386 J, 0.480 J, and 0.569 J), noticeable improvements in the XRD patterns were observed. The diffraction peaks became sharper and more intense, especially at the (100), (101), and (102) planes. This increase in intensity suggests enhanced crystallinity and a reduction in internal stresses. The high-pressure plasma shock waves generated during LSP cause plastic deformation at the surface, leading to dislocation movement, grain boundary rearrangement, and eventually microstructural refinement. This effect enhances the definition of existing α and β phase peaks without inducing any phase transformation, confirming that LSP modifies the surface structure through mechanical effects, not thermal ones, at 0.386 J and 0.480 J, the peaks become more defined, indicating partial alignment or ordering of the crystal lattice. However, it is at 0.569 J where the most significant improvements are seen, with the (101) peak reaching its maximum intensity. This suggests that this energy level is optimal for inducing beneficial compressive

residual stresses and improving phase clarity, without causing surface damage or introducing defects.[64] The consistent appearance of both α and β phase peaks across all treated samples confirms that LSP enhances the material's structural integrity by refining the existing phase structure rather than changing it, contributing to better fatigue resistance and mechanical performance in service.

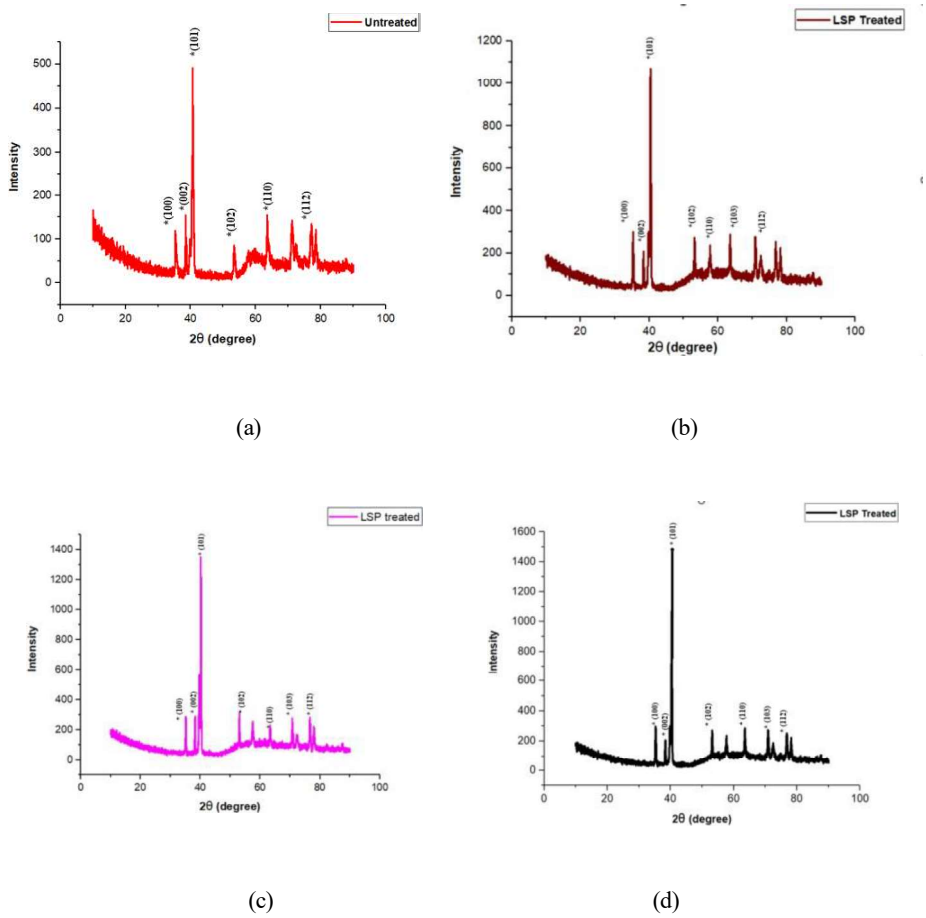

Fig 4.19. XRD graphs of (a) 0.386 J (b) 0.480 J (c) 0.569 J (d) 0.986 J

To calculate residual stress using XRD, I started by performing scans at different tilt angles (ψ) such as 0°, 7°, 10°, 15°, 30°, 45°, 60°, and 75°, focusing on a specific diffraction peak with maximum intensity. From each tilt, I noted the corresponding 2θ values and used Bragg's Law to calculate the d-spacing. Then, I calculated the $\sin^2\psi$ values for each tilt angle and plotted d-spacing versus $\sin^2\psi$. The slope of this linear plot indicates the strain, and using that slope, I calculated the residual stress using the equation:

$$\sigma = \frac{E}{1+\nu} \cdot \frac{Slope}{d_0}$$

Here, E is the Young's modulus, ν is Poisson's ratio, and d_0 is the reference d-spacing. A positive slope gave tensile stress, while a negative slope showed compressive stress. This process helped me determine how the residual stress changed after processes like Laser Shock Peening (LSP). Based on the residual XRD analysis, I obtained tilt angle (ψ) and corresponding d-spacing values from the diffraction peaks at each angle. Using these values, I plotted a graph of $\sin^2\psi$ versus d-spacing, which is the standard method for residual stress evaluation. From the plotted graph, I performed a linear regression to determine the slope, which reflects the elastic strain in the material.

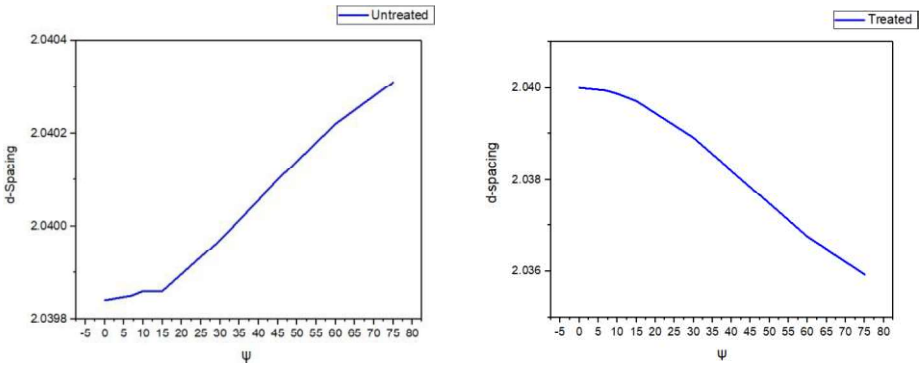

Fig 4.20 Graph represent d- spacing Vs tilt angle where Positive (tensile)Untreated and Negative Slope (compressive) Treated LSP

- For Untreated

$$\sigma = \frac{114 \times 10^{10}}{1.33} \cdot \frac{1}{2.040} \cdot (0.00244) = 102.34\ MPa$$

- For 0.386 J (minimum)

$$\sigma = \frac{114 \times 10^{10}}{1.33} \cdot \frac{1}{2.040} \cdot (-0.00348) = -146.05\ MPa$$

- For 0.480 J

$$\sigma = \frac{114 \times 10^{10}}{1.33} \cdot \frac{1}{2.040} \cdot (-0.00434) = -182.\ MPa$$

- For 0.569 J

$$\sigma = \frac{114 \times 10^{10}}{1.33} \cdot \frac{1}{2.040} \cdot (-0.00782) = -328.65\ MPa$$

- For 0.986 J (maximum)

$$\sigma = \frac{114 \times 10^{10}}{1.33} \cdot \frac{1}{2.040} \cdot (-0.00976) = -410.04\ MPa$$

Table 4.13: various Power density represents residual stress

Energy (J)	Power Density (GW/Cm^2)	Residual stress (MPa)
0.386	6	-146.05
0.480	7	-182.54
0.569	8	-328.65
0.980	15	-410.04

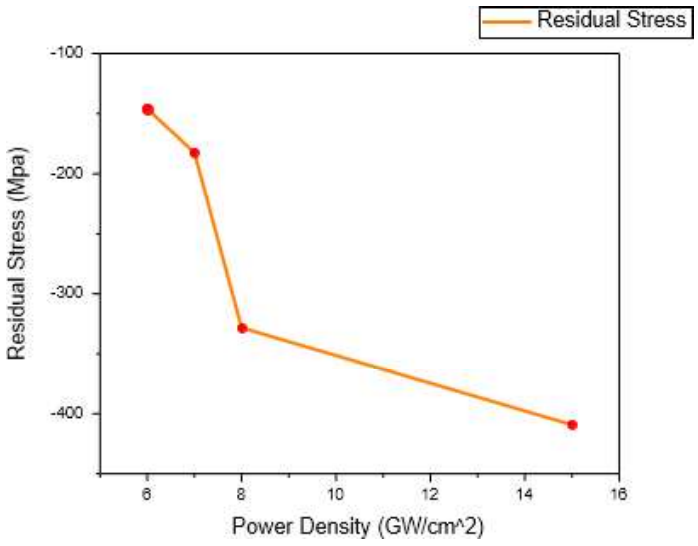

Fig 4.21 Power density Vs Residual Stress

From the graph, it's clear that as the power density increases, the residual stress in the material becomes more compressive. This compressive stress reaches its peak value of around -410 MPa at a power density of 15 GW/cm². This indicates that

higher power densities during laser shock peening deliver more energy to the material, which results in deeper penetration of compressive stresses into the surface and subsurface regions. These compressive residual stresses are beneficial, as they help improve the material's fatigue strength and overall mechanical performance. However, the trend also suggests that if the power density continues to increase beyond this optimal point, the surface may start to experience damage or microstructural changes. These adverse effects could reduce the positive impact of the compressive stresses, indicating that there's a threshold beyond which further increases in power density are counterproductive.

In this case study, I aim to investigate how surface roughness—specifically rough versus smooth surfaces—affects the development of residual stresses after laser shock peening (LSP). To explore this, LSP was performed using a power density of 8 GW/cm² (corresponding to 0.569 J of laser energy) with a scan speed of 1 mm/sec. These parameters were applied to electrochemically polished samples, which provide a smooth surface finish. The goal is to measure and compare the resulting residual stresses to understand whether smoother surfaces promote more favorable compressive stress profiles compared to rougher ones. This study will help clarify the role of surface condition in optimizing LSP outcomes.

Table 4.14: Represent various surface roughness values gives residual stress and hardness value

Sr .no	Surface Roughness (µm)	Residual stress Analysis (MPa)	Hardness Value (HV)
1	18.68	-328.65	515.5
2	17.74	-337.78	520.16
3	12.84	-476.24	590.81

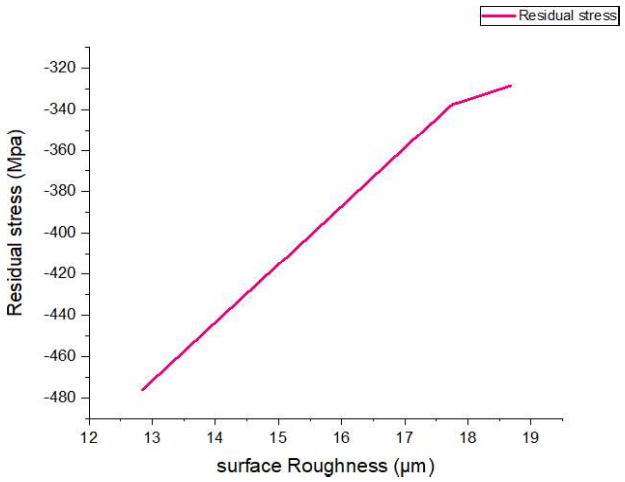

Fig 4.22 Graph represent Residual stress vs Surface roughness

From the results, it's observed that as the surface roughness decreases, the residual compressive stress tends to increase. This is likely because a smoother surface allows the laser-induced shockwaves to spread more evenly across the material during the LSP process. With fewer surface irregularities, the shock energy is transferred more efficiently into the material, leading to better and more uniform plastic deformation. This results in stronger and more consistent compressive residual stresses being developed in the treated area. In turn, this improves the material's mechanical properties, especially its fatigue resistance. So, having a smoother surface before LSP can be beneficial for achieving better results.

Table 4.15: Represent residual Stress per Impact

No. of shots	Residual Stress MPa
2	-470
3	-500
4	-530

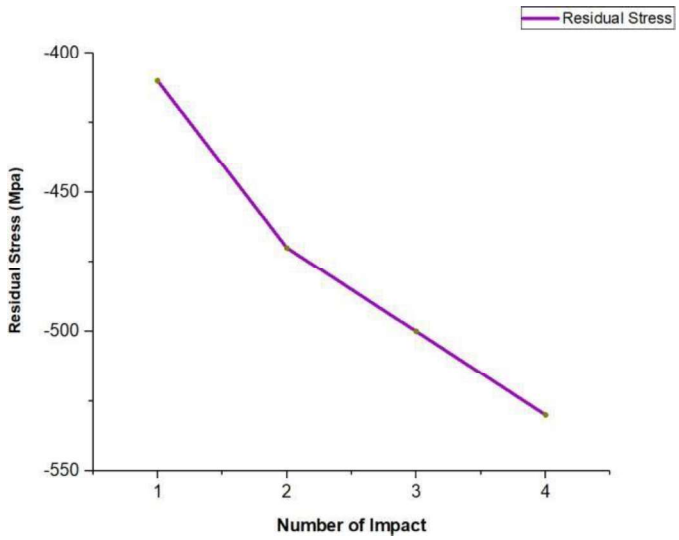

Fig 4.23 Graph Represent residual stress per impact

In Next experiment, I investigated how the number of laser shock peening (LSP) impacts influences the resulting residual stresses. I performed LSP using a maximum laser energy of 0.986 J, which corresponds to a power density of 15 GW/cm². After applying multiple impacts at this energy level, I carried out X-ray diffraction (XRD) analysis to measure the residual stresses generated in the material. Based on the graph of number of impacts versus residual stress, I observed a clear trend: as the number of impacts increased, the compressive residual stress also increased. This indicates that repeated shock loading enhances plastic deformation and promotes the formation of deeper and more consistent compressive stress layers beneath the surface. I also noticed that the depth of stress penetration increased with more impacts, which suggests improved energy absorption and stronger shockwave propagation through the material. These results highlight that increasing the number of LSP impacts can significantly enhance the effectiveness of the process, leading to better mechanical performance, especially in terms of fatigue resistance and structural durability.

Chapter 5: Conclusions and Future scope of work

5.1 Conclusion

Based on the experimental results, parametric analysis and mechanical and tribological studies on DED of Ti6Al4V part and its post processing by Laser Shock Peening, the following conclusions are drawn:

1) Based on one factor at a time (OFAT) experimentation, it is observed that the process variables such as standoff distance, power and Scan Speed , cooling time and feed rate have a significant effect on Turbine Profile Blade of Height-Width and micro-hardness of Titanium alloy deposition layer by DED process.
2) The investigation on the effect of Stand-Off Distance (SOD) in the deposition of Ti6Al4V turbine blades demonstrates that maintaining an optimal SOD in the range of 10.0 to 10.5 cm significantly enhances deposition quality. An increase in SOD from 9.5 cm to 10.5 cm resulted in improved layer height, surface uniformity, and a 12–18% increase in deposition efficiency. This improvement is attributed to better powder distribution and melt pool stability, which lead to reduced defects, improved layer bonding, and consistent geometrical features. In contrast, lower SOD values caused poor fusion, increased porosity, and incomplete layers. Thus, optimizing SOD is critical for achieving defect-free, structurally sound, and high-quality Ti6Al4V components in additive manufacturing.
3) The study on the influence of laser power and scan speed in the additive manufacturing of Ti6Al4V turbine blades highlights the importance of process parameter optimization. It was observed that insufficient laser power or excessively high scan speeds led to poor melting, weak interlayer bonding, and incomplete track formation. Conversely, overly high laser power or very slow scan speeds caused overheating, resulting in distortion and surface defects. Therefore, achieving a proper balance between laser power and scan speed is

critical for producing consistent, defect-free layers with accurate geometry, smooth surface finish, and strong structural integrity. This underscores the necessity of optimizing process parameters to ensure reliable and high-quality fabrication of Ti6Al4V turbine blades.

4) The application of the Design of Experiments (DOE) methodology was crucial in systematically analyzing the impact of key process parameters on the quality of Ti6Al4V deposits. Through a full factorial design, the study effectively captured the interactive effects of laser power and scan speed on critical geometrical features such as track height and width. This structured approach facilitated the identification of optimal parameter ranges that promote consistent layer deposition and reduce the likelihood of defects. Overall, DOE proved to be an effective and reliable tool for optimizing process variables and enhancing the overall efficiency and quality of the additive manufacturing process.
5) The analysis of layer height in relation to process parameters revealed that laser power has a significant impact on the deposition height of Ti6Al4V, with higher power levels increasing track height up to a saturation limit. Confidence interval analysis indicated overlapping regions at certain power levels, reflecting some variability and measurement uncertainty. In contrast, scan speed showed a comparatively limited effect on layer height, as evidenced by narrower confidence intervals and reduced variation across different speeds. Interaction plots further demonstrated the complexity of the combined influence of laser power and scan speed, highlighting the necessity for precise control and optimization of both parameters to ensure consistent and high-quality deposition in additive manufacturing.
6) 3D scanning analysis of the deposited Ti6Al4V turbine blade revealed that Laser Shock Peening (LSP) treatment led to a slight increase in surface deviation from the original CAD model; however, it significantly enhanced surface uniformity and smoothness. The as-built component exhibited notable surface fluctuations, whereas post-LSP treatment resulted in reduced surface roughness and improved surface integrity. These results confirm that LSP is

effective in refining surface quality without compromising the dimensional accuracy or structural performance of the component, making it a valuable post-processing technique in additive manufacturing.

7) Vickers hardness analysis of the DED-manufactured Ti6Al4V turbine blade revealed noticeable variation in hardness across different regions. The top and bottom sections exhibited higher hardness values (~480–485 HV), likely due to rapid cooling rates, whereas the middle region showed slightly lower hardness (~460 HV), attributed to the effects of thermal cycling during deposition. This variation highlights the influence of non-uniform heat distribution on microstructural evolution, emphasizing the need for controlled thermal management to ensure consistent mechanical properties throughout the component.
8) Compression load analysis of the laser additively manufactured Ti6Al4V turbine profile blade demonstrated excellent mechanical performance, with an ultimate compressive strength of approximately 1012.69 N/mm². This high load-bearing capacity confirms the structural integrity of the fabricated blade and its suitability for demanding applications where resistance to compressive stresses is critical. These findings reinforce the effectiveness of the additive manufacturing process in producing high-performance components for structural and aerospace applications.
9) Microstructure analysis showed that the as-deposited Ti6Al4V sample had an average grain size of approximately 380.92 μm², with noticeable defects such as porosity and uneven regions resulting from inadequate melting and fusion during the DED process. These microstructural imperfections can negatively affect the mechanical performance and reliability of the component. Therefore, this emphasizes the critical need for precise optimization of process parameters to enhance material quality, reduce defects, and ensure structural integrity in additive manufacturing applications.
10) Surface roughness measurements demonstrated that laser shock peening (LSP) effectively reduces surface roughness, with the Ra value decreasing from approximately 23.52 μm in the as-built condition to around 18 μm at the optimal

energy setting of 0.569 J. Moderate pulse energies contributed to surface refinement and smoothness, while excessive energy or prolonged treatment led to the formation of micro-defects, which increased roughness. These findings highlight the importance of carefully optimizing LSP parameters to achieve the desired surface finish and improve the overall quality of the component. And The electrochemical polishing process proved highly effective in improving the surface roughness of Ti6Al4V turbine blades produced via Directed Energy Deposition (DED). Initially, the roughness value was 23.728 μm, which was significantly reduced to 6.220 μm through precise control of voltage and polishing time. This surface enhancement is crucial for optimizing aerodynamic efficiency, reducing fatigue wear, and minimizing corrosion risks, thereby improving the performance and longevity of the turbine blades in demanding applications.

11) The choice of laser wavelength plays a critical role in the effectiveness of the Laser Shock Peening (LSP) process, particularly for materials like Ti6Al4V. The 1064 nm wavelength offers deeper penetration, providing a balanced approach to improving mechanical properties while maintaining surface integrity. In contrast, the 532 nm wavelength offers higher absorption but poses a risk of surface degradation, particularly in complex geometries. Thus, selecting the appropriate wavelength is crucial for optimizing the LSP process to meet specific material and performance requirements.
12) The interaction between laser power and scan speed is crucial for optimizing the Laser Shock Peening (LSP) process. Both parameters significantly influence the intensity of shock waves and energy distribution on the material surface. Higher laser power enhances the development of compressive residual stresses and improves mechanical properties, while an optimized scan speed ensures efficient energy delivery without inducing thermal damage. Balancing these factors is vital for achieving deep, uniform compressive stresses and maximizing the mechanical performance of components subjected to LSP treatment.
13) Optimizing overlap ratio and the number of impacts is essential for achieving

effective Laser Shock Peening (LSP) outcomes. An overlap ratio in the range of 50–75% promotes uniform surface treatment while avoiding excessive energy accumulation that may cause surface damage. Similarly, performing two to three impacts per spot was found to significantly enhance hardness and fatigue resistance. These findings underscore the importance of precisely controlling these parameters to improve surface integrity and mechanical performance in LSP-treated components.

14) Optimization of Laser Shock Peening (LSP) parameters—such as laser power, scan speed, overlap ratio, and number of impacts—is vital for improving the mechanical performance of Ti6Al4V turbine blades produced via additive manufacturing. Through controlled parameter adjustment, notable enhancements in surface hardness and fatigue resistance were observed, validating LSP's role in reducing surface defects and improving durability. These findings emphasize the necessity of tailored LSP parameter settings to ensure structural integrity and long-term reliability in high-performance applications.

15) Experimental results demonstrate that both power density and scan speed are critical parameters influencing the surface hardness of Ti6Al4V components during Laser Shock Peening (LSP). An increase in power density from 5 GW/cm² to 15 GW/cm² led to a significant rise in Vickers hardness from 376.3 HV to 549.3 HV, indicating enhanced material strength. Similarly, decreasing the scan speed from 1.2 mm/sec to 0.5 mm/sec resulted in an increase in hardness from 511 HV to 543.5 HV, due to improved energy input and thermal interaction. These findings highlight the importance of optimizing LSP parameters to improve the mechanical performance and durability of additively manufactured components, making them more suitable for demanding engineering applications.

16) The Ultimate Compressive Strength (UCS) analysis revealed a significant improvement in the material's load-bearing capacity after Laser Shock Peening (LSP). The compressive strength increased from 1012.69 MPa to 1598.54 MPa with power density rising from 5 GW/cm² to 15 GW/cm². This enhancement is

attributed to the development of deep and stable residual compressive stresses induced by intense shock waves. These stresses effectively reduce dislocation movement and crack propagation, thereby increasing structural integrity and mechanical performance of the Ti6Al4V component.

17) Grain size analysis confirmed a substantial refinement in microstructure with increasing power density during the Laser Shock Peening (LSP) process, where the average grain size was reduced from 380.92 μm^2 to as low as 7.5 μm^2. Scan speed also played a vital role—slower speeds enabled finer grains due to extended thermal interaction, while faster speeds produced relatively coarser grains. These results highlight the importance of optimizing both power density and scan speed to achieve desirable grain refinement, leading to improved mechanical performance of the Ti6Al4V components.
18) The surface roughness analysis demonstrated a significant enhancement in surface finish after Laser Shock Peening (LSP), with the roughness reducing from an average of 23.52 μm to 18.68 μm. This improvement is primarily due to plastic deformation and grain refinement caused by repeated laser impacts, which effectively smooth out surface irregularities. These findings confirm the capability of LSP to improve surface quality, contributing to better functional performance. The experiment confirms that increasing scan speed during laser processing significantly improves surface finish by reducing roughness, with the lowest roughness value of 17.45 μm achieved at the highest scan speed of 1.2 mm/sec. This is due to reduced heat input and minimized surface melting, leading to a more uniform and smoother surface.
19) The 3D scanning analysis of the Ti6Al4V turbine blade revealed an average surface deviation of 0.109 mm from the CAD model in the as-built condition, primarily due to thermal effects and layer accumulation during the DED process. Following Laser Shock Peening (LSP), a noticeable improvement in surface finish and dimensional accuracy was observed. This confirms the effectiveness of LSP in refining surface quality and reducing geometric deviations, thereby enhancing the overall precision and reliability of additively manufactured components.

20) The Residual Stress Analysis demonstrated that Laser Shock Peening (LSP) effectively enhances compressive residual stresses in Ti6Al4V components, with a higher number of impacts leading to deeper and more uniform stress layers. This repeated shock loading promoted substantial plastic deformation, contributing to improved material performance. Additionally, electrochemical polishing further optimized the residual stress profile, indicating its dual role in refining surface finish and enhancing mechanical strength. These findings confirm the combined benefits of LSP and post-processing in strengthening additively manufactured parts.

5.2 Future Scope of Work

Based on the present study, further research can develop into broader aspects of laser shock peening combined with DED. The future scope of this work includes:

1) **In-situ Monitoring and Data Analytics**:

Implementing real-time monitoring of additive manufacturing process parameters and developing a closed-loop feedback system based on data analytics. This approach aims to achieve better deposition with enhanced geometric and mechanical properties.

2) **Simulation and Validation:**

Conducting simulations of laser nitriding process parameters and validating the results with experimental data. This will help in understanding the process better and optimizing the parameters for improved outcomes.

3) **Effective of additive Manufacturing (AM) Defects on LSP Performance**:

Component Produced DED often contain inherent defects such as porosity, microcrack and residual stress. The interaction of these defects with shock waves

generated during LSP is not fully understood. Investigation the influence of these AM specific defects on the effective of LSP is essential.

4) **Hybrid Post-Processing Technique**

Combining LSP with other surface treatment methods, such as heat treatment, laser polishing or mechanical finishing could be explored to further enhance the mechanical properties and surface finish Ti6Al4V component.

5) **Computational Modeling:**

Developing advanced computational models to simulate the effects of LSP on residual stress distribution and microstructural changes will enhance the understanding of the process and facilitate better design and manufacturing practices in additive manufacturing.

References:

[1] DebRoy, T., Wei, H. L., Zuback, J. S., Mukherjee, T., Elmer, J. W., Milewski, J. O., ... & Zhang, W. (2018). Additive manufacturing of metallic components – Process, structure and properties. *Progress in Materials Science*, 92, 112-224.

[2] Frazier, W. E. (2014). Metal additive manufacturing: a review. *Journal of Materials Engineering and Performance*, 23(6), 1917–1928.

[3] Herzog, D., Seyda, V., Wycisk, E., & Emmelmann, C. (2016). Additive manufacturing of metals. *Acta Materialia*, 117, 371-392.

[4] King, W. E., Anderson, A. T., Ferencz, R. M., Hodge, N. E., Kamath, C., & Khairallah, S. A. (2015). Overview of modeling and simulation of metal powder bed fusion process at Lawrence Livermore National Laboratory. *Materials Science and Technology*, 31(8), 957–968.

[5] King, W. E., Anderson, A. T., Ferencz, R. M., Hodge, N. E., Kamath, C., & Khairallah, S. A. (2015). Overview of modeling and simulation of metal powder bed fusion process at Lawrence Livermore National Laboratory. *Materials Science and Technology*, 31(8), 957–968.

[6] Zhang, Y., Ren, X., Zhang, X., & Liu, J. (2020). Laser shock peening on additive manufactured metallic materials: a review. *Journal of Materials Science & Technology*, 45, 270–286.

[7] Li, C., Liu, Z. Y., Fang, X. Y., & Guo, Y. B. (2017). Residual stress in metal additive manufacturing. *Procedia CIRP*, 71, 348–353.

[8] Kumar, M., Ramachandran, C. S., & Singh, S. (2021). Surface modification of additive manufactured aluminum alloy by laser nitriding. *Surface and Coatings Technology*, 409, 126899.

[9] John, Merbin, et al. "Peening techniques for surface modification: Processes, properties, and applications." *Materials* 14.14 (2021): 3841.

[10] Kumar, R., et al. (2021). *Hammer peening technology—the past, present, and future*. The International Journal of Advanced Manufacturing Technology.

[11] Lu, J., & Xu, W. (2015). Surface Modification by Ultrasonic Impact Treatment. In Lu, J. (Ed.), Laser Shock Peening (pp. 325–350). Woodhead Publishing. https://doi.org/10.1016/B978-0-85709-263-4.00011-9.

[12] Kondo, M., Takahashi, H., & Sano, Y. (2006). *Development of water jet peening technique for stress corrosion cracking mitigation*. Nuclear Engineering and Design, 236(19-21), 2194–2201.

[13] Rajak, D. K., Linul, E., & Sharma, S. (2021). Surface modification techniques for titanium and its alloys for biomedical applications: A review. Journal of Manufacturing Processes, 64, 1186–1205.

[14] Chakkravarthy, V., et al. "Effect of abrasive water jet peening on NaCl-induced hot corrosion behavior of Ti–6Al–4V." *Vacuum* 210 (2023): 111872. (water Jet Peening)

[15] Montross, C. S., Wei, T., Ye, L., Clark, G., & Mai, Y.-W. (2002). *Laser shock processing and its effects on microstructure and properties of metal alloys: a review*. International Journal of Fatigue, 24(10), 1021–1036.

[16] Zhou, L., Li, X., & Wang, Z. (2012). *Laser shock peening and its application in surface treatment of metallic materials*. Journal of Materials Science & Technology, 28(8), 693–701.

[17] Clauer, A. H. (2009). *Laser shock peening: process evolution and advances in control and quality*. Metalworking Technology, ASM Handbook, Vol.

[18] D. Herzog et al., “Additive manufacturing of metals,” *Acta Materialia*, vol. 117, pp. 371–392, 2016.

[19] Y. Kok et al., “Anisotropy and heterogeneity of microstructure and mechanical properties in metal additive manufacturing,” *Materials & Design*, vol. 139, pp. 565–586, 2018.

[20] W. E. Frazier, “Metal additive manufacturing: A review,” *J. Mater. Eng. Perform.*, vol. 23, pp. 1917–1928, 2014.

[21] M. P. Miles et al., “Shielding gas flow effects on laser additive manufactured Ti-6Al-4V,” *JOM*, vol. 70, no.3,pp.276–282,2018.
[22] T. DebRoy et al., “Additive manufacturing of metallic components–Process, structure and properties,” *Progress in Materials Science*, vol. 92, pp. 112–224, 2018.

[23] L. Xue et al., “Effect of interlayer delay on thermal history and microstructure in laser metal deposition,” *J. Mater. Process. Technol.*, vol. 293, p. 117094, 2021.
[24] F. Liu et al., “Influence of process parameters on the characteristics of Ti–6Al–4V during laser metal deposition,” *Additive Manufacturing*, vol. 5, pp. 8–19, 2015.
[25] M. Gouge and T. A. Palmer, *Laser Metal Deposition Process of Metals, Alloys, and Composite Materials*. Elsevier, 2018.

[26] D. Qian et al., “Grain refinement of titanium alloy by interlayer deformation during additive manufacturing,” *Acta Materialia*, vol. 162, pp. 56–69, 2019.
[27] E. Liverani et al., “Grain size and orientation in additive manufactured Ti6Al4V parts,” *J. Alloys Compd.*, vol. 695, pp. 1897–1905, 2017.
[28] F. Wang et al., “Microstructure and mechanical properties of wire and arc additive manufactured Ti-6Al-4V,” *Mater. Sci. Eng. A*, vol. 555, pp. 263–271, 2018.

[29] Z. Ali et al., “Fatigue behavior of additive manufactured Ti-6Al-4V,” *Int. J. Fatigue*, vol. 120, pp. 188–204, 2019.
[30] M. Attarilar et al., “Review on additive manufacturing of titanium-based materials: Powder characteristics, microstructure, mechanical performance, and future prospects,” *J. Mater. Res. Technol.*, vol. 9, no. 6, pp. 11649–11684, 2020.
[31] M. H. Farshidianfar et al., “Process optimization of laser additive manufacturing of Ti6Al4V,” *Optics & Laser Technology*, vol. 103, pp. 351–364, 2018.

[32] M. M. Kirka et al., “Strategy for structure and property optimization in directed energy additive manufacturing,” *Acta Materialia*, vol. 132, pp. 122–135, 2017.

[33] Z. Li et al., “Real-time monitoring and control of the direct energy deposition process for titanium alloys: A review,” *J. Manuf. Process.*, vol. 76, pp. 202–214, 2022.

[34] A. Khanzadeh et al., “Data-driven prediction of porosity in laser powder bed fusion of titanium,” *Addit. Manuf.*, vol. 30, p. 100827, 2019.

[35] S. A. Khairallah et al., “Laser powder bed fusion additive manufacturing: Physics of complex melt flow and formation mechanisms of pores, spatter, and denudation zones,” *Acta Materialia*, vol. 108, pp. 36–45, 2016.

[36] A. F. Gokuldoss et al., “Additive manufacturing processes: Selective laser melting, electron beam melting and binder jetting—Selection guidelines,” *Materials*, vol. 10, no. 6, p. 672, 2017.

[37] Herzog, D., Seyda, V., Wycisk, E., & Emmelmann, C. (2016). Additive manufacturing of metals. *Acta Materialia*, 117, 371–392.

[38] Gibson, I., Rosen, D. W., & Stucker, B. (2010). *Additive Manufacturing Technologies: Rapid Prototyping to Direct Digital Manufacturing*. Springer.

[39] Peyre, P., Fabbro, R., Berthe, L., & Coste, F. (2000). Laser-shock processing of materials. *Journal of Laser Applications*, 12(4), 175–183.

[40] Gu, D., Meiners, W., Wissenbach, K., & Poprawe, R. (2012). Laser additive manufacturing of metallic components. *International Materials Reviews*, 57(3), 133–164.

[41] Yadroitsev, I., & Smurov, I. (2010). Surface morphology in selective laser melting of metal powders. *Physics Procedia*, 5, 533–542.

[42] Zhang, Y., Wu, L., Guo, X., Kane, S., Deng, Y., Jung, Y. G., & Zhang, J. (2018). Additive manufacturing of metallic materials: A review. *Journal of Materials Engineering and Performance*, 27(1), 1–13.

[43] antos, E. C., Shiomi, M., Osakada, K., & Laoui, T. (2016). Rapid manufacturing of metal components by laser forming. *International Journal of Machine Tools and Manufacture*, 46(12–13), 1459–1468.

[44] Thijs, L., Verhaeghe, F., Craeghs, T., Humbeeck, J. V., & Kruth, J. P. (2010). A study of the microstructural evolution during selective laser melting of Ti–6Al–4V. *Acta Materialia*, 58(9), 3303–3312.

[45] Beretta, S., & Romano, S. (2017). A comparison of fatigue strength sensitivity to defects for AM and traditional materials. *International Journal of Fatigue*, 94, 178–191.

[46] Liu, C., Zhang, Y., Yao, H., Luo, Y., & Zhang, Y. (2020). Effects of laser shock peening on additive manufactured Inconel 718. *Surface and Coatings Technology*, 384, 125263.

[47] ASTM G99-17. (2017). *Standard Test Method for Wear Testing with a Pin-on-Disk Apparatus*. ASTM International.

[48] Vilaro, T., Colin, C., & Bartout, J. D. (2012). Heat-treated microstructures of Ti-6Al-4V processed by SLM. *Metallurgical and Materials Transactions A*, 42(10), 3190–3199.

[49] Li, Y., Gu, D., Dai, D., & Chen, H. (2019). Optimization of tribological performance of AM AlSi10Mg through burnishing. *Surface and Coatings Technology*, 357, 270–280.

[50] Hussein, A., Hao, L., Yan, C., Everson, R. M., & Young, P. (2013). Advanced lattice support structures for AM. *Journal of Materials Processing Technology*, 213(7), 1019–1026.

[51] Montross, C. S., Wei, T., Ye, L., Clark, G., & Mai, Y. W. (2002). Laser shock processing review. *International Journal of Fatigue*, 24(10), 1021–1036.

[52] Clauer, A. H., & Holbrook, J. H. (1981). Effects of laser-induced shock waves on metals. *Shock Waves and High-Strain-Rate Phenomena in Metals*, 675–702.

[53] Masood, M., Kumar, P., & Sharma, A. (2021). Enhancing tribological performance of AM Ti-6Al-4V by LSP. *Wear*, 474–475, 203844.

[54] Sankaranarayanan, S., Kuppan, P., & Suresh, S. (2020). Influence of LSP on tribology of AM 316L stainless steel. *Materials Research Express*, 7(11), 116543.

[55] C. P. Paul, S. Yadav, A. K. Rai, and J. A. Narayanan, “Laser Directed Energy Deposition based additive manufacturing of metallic multi-material : A Review

Laser Directed Energy Deposition based additive manufacturing of metallic multi-material : A Review," no. June, 2021.

[56] Shin, Yung C., et al. "Predictive modeling capabilities from incident powder and laser to mechanical properties for laser directed energy deposition." *Computational Mechanics* 61 (2018): 617-636.

[57] Liu, R. et al., 2017. "Microstructure and mechanical properties of laser metal deposition of Ti-6Al-4V with different heat input." *Materials Science and Engineering: A* 684, pp.605–616

[58] Cao, Yunfeng, Yung C. Shin, and Benxin Wu. "Parametric study on single shot and overlapping laser shock peening on various metals via modeling and experiments." (2010): 061010.

[59] Singh, Gulshan, Ramana V. Grandhi, and David S. Stargel. "Modeling and parameter design of a laser shock peening process." *International Journal for Computational Methods in Engineering Science and Mechanics* 12.5 (2011): 233-253.

[60] Gupta, Ram Kishor, et al. "Laser shock peening and its applications: a review." *Lasers in Manufacturing and Materials Processing* 6.4 (2019): 424-463.

[61] Clauer, A. H., & Fairand, B. P. (1979). *Laser shock processing as a surface enhancement process*. In Treatise on Materials Science and Technology, Vol. 18, pp. 99–138

[62] Montross, C. S., Wei, T., Ye, L., Clark, G., & Mai, Y. W. (2002). *Laser shock processing and its effects on microstructure and properties of metal alloys: a review*. International Journal of Fatigue, 24(10), 1021–1036.

[63] Peyre, P., & Fabbro, R. (1995). *Laser shock processing: a review of the physics and applications*. Optics and Laser Technology, 26(6), 397–402.

[64] Madapana, D., Ramadas, H., Nath, A. K., & Majumdar, J. D. (2024). Structure-Property-Process Parameters Correlation of Laser Shock-Peened Titanium Alloy (Ti6Al4V) Without Protective Layer. *Journal of Materials Engineering and Performance*, *33*(11), 5380-5387.

[65] Tang, Z. J., Liu, W. W., Wang, Y. W., Saleheen, K. M., Liu, Z. C., Peng, S. T., ... & Zhang, H. C. (2020). A review on in situ monitoring technology for directed energy deposition of metals. *The International Journal of Advanced Manufacturing Technology*, *108*, 3437-3463.